Title
KINETIC ENERGY AND MASS DISTRIBUTIONS FOR NUCLEAR FISSION AT MODERATE EXCITATION ENERGY

Author
Burnett, Donald S.

Publication Date
1963-10-07

UCRL-11006
c.2

University of California

Ernest O. Lawrence Radiation Laboratory

KINETIC ENERGY AND MASS DISTRIBUTIONS FOR NUCLEAR FISSION AT MODERATE EXCITATION ENERGY

Donald S. Burnett

Ph. D. Thesis

October 7, 1963

Berkeley, California

UCRL-11006
c.2

DISCLAIMER

Research and Development

UCRL-11006
UC-4 Chemistry
TID-4500 (19th Ed.)

UNIVERSITY OF CALIFORNIA
Lawrence Radiation Laboratory
Berkeley, California

Contract No. W-7405-eng-48

KINETIC ENERGY AND MASS DISTRIBUTIONS FOR NUCLEAR FISSION AT MODERATE EXCITATION ENERGY

Donald S. Burnett

(Ph.D. Thesis)

October 7, 1963

Printed in USA. Price $2.25. Available from the
Office of Technical Services
U. S. Department of Commerce
Washington 25, D.C.

CONTENTS

KINETIC ENERGY AND MASS DISTRIBUTIONS FOR NUCLEAR FISSION AT MODERATE EXCITATION ENERGY

Donald S. Burnett

Lawrence Radiation Laboratory
University of California
Berkeley, California

October 7, 1963

ABSTRACT

Fission fragment kinetic energy measurements using semiconductor detectors have been made for the alpha-induced fission of: (a) Au^{197} + 65.0 MeV α, (b) Bi^{209} + 65.0 MeV α, (c) Th^{232} + 21.4, 25.7, 33.0, and 65.0 MeV α, and (d) U^{238} + 25.7, 33.0, and 65.0 MeV α. The data were recorded as the number of events at fragment energies E_1 and E_2, $N(E_1, E_2)$. The data were then transformed into mass - total kinetic energy maps and anlyzed by means of moments. The Bi and Au data are in good agreement with quantitative theoretical predictions from the liquid drop model available for the lighter elements. The U and Th data are discussed in terms of qualitative ideas which have been proposed to explain the properties of the fission process for the heavier elements. The changes in the U and Th mass and total kinetic energy distributions with excitation energy are emphasized. Pulse-height energy relations for the detectors used were obtained by a detailed comparison of detector and time-of-flight results for the spontaneous fission of Cf^{252}.

I. INTRODUCTION

Nuclear fission is a complex process. The vast amount of literature is ample evidence for this point; and, further, the large number of papers on fission which are still appearing at the present time indicates that much remains to be understood. This complexity is due to the large number of observable quantities which must be known in order to define what happens in a given fission event. Considering only binary fission (a significant simplification!), a partial list of these would include

(1) the mass split of the initial fissioning nucleus
(2) the charge split of the initial fissioning nucleus
(3) the total kinetic energy of the two fragments
(4) the numbers and kinetic energies of the neutrons from each fragment
(5) the numbers and energies of gamma rays from each of the fragments
(6) the angular momenta of the fragments

In addition to all this one must also consider the effect of changing the charge, the mass, and the total excitation energy or nuclear temperature of the initial fissioning nucleus.

In recent years technological progress, in particular the refinement of high-speed computers and the development of the multi-dimensional pulse-height analyzer, has resulted in considerably more experimental knowledge on all of the above variables. An n-dimensional analyzer can analyze and individually store n correlated pulse heights, (V_1, V_2, ... V_n) which thus allows measurement of an n-dimensional pulse-height distribution function, $N(V_1, V_2 \ldots V_n)$. The simultaneous development of time-of-flight techniques and, in particular, semiconductor detectors have made items (1) and (3) the subject of considerable research in the past few years. These items are also the scope of the present work; however, the above list indicates that such experiments only provide a partial description of the fission process; and typically, will pose more questions than will be answered.

Generally speaking, the development of fission theory has not kept pace with a accumulation of experimental information. Many different models have been formulated which were successful in explaining some limited aspect of fission phenomena; nevertheless, at the present time, a comprehensive fission theory does not exist. Recent work on the liquid drop model, however, has indicated that the broad features of such a theory may be emerging, at least for nuclides in the region of $x \lesssim .67$*.[1,2] However, a theory of fission must be completely compatible with a general theory of complex nuclei. The question then arises how the liquid drop model can meet this requirement. The answer appears to be that one must view the liquid drop as an approximation to the unified model. In the final analysis single particle effects must be included in fission theory just as it appears necessary to introduce collective effects into the discussion of the ground state properties of nuclei. The problem at the present time is to determine the extent to which the liquid drop model describes fission, i.e. at what point will it be necessary to take shell effects into account. It may also be necessary to consider the influence of the density of states in the final fragments.[4]

The purpose of this work was to provide experimental data to compare with the liquid drop predictions. Two-dimensional fission-fragment kinetic energy measurements have been carried out for the alpha-induced fission of Au^{197}, Bi^{209}, Th^{232}, and U^{238} using semiconductor detectors. At the present time only the Au^{197} and Bi^{209} results are subject to theoretical interpretation. At an earlier stage it was thought that at least the symmetric fission of Th^{232} and U^{238} would be within the scope of the theory and that qualitative predictions of the relation between asymmetric and symmetric fission would be possible.[3] To attempt

---

*x, the fissionability parameter, is $(Z^2/A)/(Z^2/A)_o$ where $(Z^2/A)_o = 50.13$ is the critical value at which a spherical nucleus is unstable against any deformation. Its significance is that many quantities calculated by the liquid drop model are functions of x only.

this seems premature at present. The Th^{232} and U^{238} data are of considerable interest for their own sake since they exhibit many interesting features. The most important of these are (1) the transition from asymmetric to symmetric fission with increasing excitation energy, and (2) the lower total kinetic energy of the symmetric relative to the asymmetric fission. Item (1) was established by radiochemical work many years ago but a satisfactory explanation is yet to be found.[5] Thus it seems important to have more detailed information on this transition. This is obtained from the experiments to be described here. The existence of item (2) was indicated by work on fission at low excitation energy.[6,7] and has now been well established by experiments similar to those reported here.[8,9,10] In the present work this effect has been studied over a wide range of bombardment energy from 21 to 65 MeV.

The exact nature of the pulse-height energy relations for semiconductor detectors is not known; consequently studies were made in order to find an adequate approximate calibration scheme and to be able to estimate errors due to this uncertainty. A separate section following the usual experimental section and prior to the discussion of the results will present the results of these studies.

II. EXPERIMENTAL

A. Mechanical

1. Beam

Alpha particles of 33.0 and 65.0 MeV were obtained from the Lawrence Radiation Laboratory 88-inch variable-energy AVF (azimuthally-varying-field) cyclotron. The 33 MeV beam was degraded with absorbers to obtain lower energies. The external beam was made approximately parallel by a quadrupole magnet, deflected 20 deg. by a steering magnet, and focused on the target with a second quadrupole. Beam levels were typically 20-50 mμamp; but for the lighter elements beams up to 200 mμamp were used. No noticeable shifts or loss of resolution resulted from the use of these beam levels as determined by (a) the position and width of the spectrum of pulses produced by a pulse generator and (b) comparison of Cf^{252} spontaneous fission spectra taken in and out of the beam.

2. Apparatus

The chamber used for this work is a direct copy of another already in use at this laboratory and has been described elsewhere.[11] The beam was collimated by a single 3/16 inch collimator placed about 2 inches from the target. A cylindrical shield was placed around this collimator to protect the detector from the scattered beam. One detector was collimated to subtend an angle of about 5 deg. in order to define one angle as required by the center-of-mass correction.[16] In order to maximize the fraction of events in coincidence: (a) the second detector was set to subtend the maximum possible angle (about 15 deg), and (b) its angle was adjusted to maximize the coincidence counting rate. The collimated detector was set at 80 deg to make the counting rates in the two detectors more nearly equal. Magnets of about 1800 Gauss were placed in front of the detector to prevent low energy electrons from entering the detector.

3. Targets

The Bi and Au targets were prepared by vaporization from the elements; U and Th were vaporized as the tetrafluorides. The nominal thicknesses were determined by alpha-counting the latter and by weighing the former. In all cases the targets were vaporized onto commercial thin Ni foils. Table I lists the nominal target and backing thicknesses for the targets used in these experiments.

B. Electronics

The detectors and detector biases used in these experiments are listed in Table I. A complete discussion of the detectors and their calibrations will be given in Section III.

The electronic equipment consisted of a linear system (two linear amplifiers and preamplifiers)[12] and a coincidence system (two variable delay and gates and a slow coincidence unit).[13] Whenever both fragments of a fission event were caught by the two detector, the coincidence system provided a trigger pulse which activated the multi-dimensional analyzer causing the corresponding linear pulses to be analyzed and eventually recorded on magnetic tape.[14] Further details on the electronic system and multi-dimensional analyzer are given in Appendix A. The analyzer was operated such that either two or three simultaneous pulse heights could be recorded; the third dimension was reserved for a tally mark which identified events produced by a pulse generator and fed into the linear system at a slow rate (20 per minute) in order to check stability. The singles pulse-height spectra in each of the dimensions were monitored with two multi-channel pulse height analyzers. Comparison of monitor spectra obtained by internal triggering with those triggered by the coincidence system allowed a check for any bias due to the coincidence system or due to an error in detector angle.

A Tetronix Type Z oscilloscope plug-in unit was used to measure the pulse height of Cf^{252} alpha particles and the pulse generator directly in volts. This gave a value for the energy per channel at the same am-

Table I. Summary of experimental conditions.

Target	E_α (MeV)	Number of events ($\times 10^{-3}$)	Target thickness ($\mu g/cm^2$)	Nominal backing thickness ($\mu g/cm^2$)	Detector resistivity* (ohm-cm)	Detector bias (volts)
Au^{197}	70.0	43.4	~ 200	90	200	124
Bi^{209}	65.0	100.7	~ 150	113	1700	92
Th^{232}	65.0	122.2	40	90	1700	92
Th^{232}	33.0	96.6	80	90	200	124
Th^{232}	25.7	96.0	80	90	200	124
Th^{232}	21.4	43.0	80	90	200	124
U^{238}	65.0	72.4	80	113	1700	92
U^{238}	33.0	70.0	80	113	200	124
U^{238}	25.7	68.4	80	113	200	124

*All detectors were phosphorus-diffused with guard-rings.

plifier gain as used for the fission fragments and a valuable check on the stability of the linear system apart from the multi-dimensional analyzer.

The above method for measuring the energy per channel using Cf^{252} alpha particles was checked by comparison with a method which consisted of:

(a) recording the pulse heights from four different alpha sources and a Cf^{252} spontaneous fission source on a multi-channel analyzer, and

(b) measuring the required gain change with a pulse generator and the Type Z plug-in unit.

The values obtained by the two methods agreed to about 1%. The Type Z unit was also used to monitor the output directly from the pulse generator as a check on its stability.

Two-dimensional Cf^{252} calibration runs were made before and after each experiment. These data, recorded on magnetic tapes, were processed to obtain a calibration equation for the detectors according to methods described in Section III.

C. Data Processing

1. Corrections to the Measured Energies

(a) Thickness Correction

The correction used for the energy loss, ΔE_t, in the target and nickel backing for a fragment of energy, E, was of the form:

$$\Delta E_t = c\, E^{1/3} \qquad (1)$$

where c is a constant. The origin of this equation is the fission fragment range measurements of Alexander and Gazdik who found that the initial part of the fragment's range could be described by $R = K E^{2/3}$, where the dependence of K on fragment mass is not large.[15] A value of c for the target was obtained experimentally by measuring the shift in the fission

fragment energy spectrum when the target orientation was changed by 45 deg. If the detector is set at 120 deg, a change in target orientation from 0 deg to 45 deg with respect to the beam changes the effective thickness from which the fragments emerge by a factor of two. Rotation of the target by 180 deg allows c to be measured for the backing foil. The correction can be measured to about ± 5% which means an error in the measured energy of up to ± 0.3 MeV since $\Delta E_t \lesssim 5$ MeV.

(b) Center-of-Mass Correction

The difference between the laboratory and center-of-mass fragment energies is small for the fissioning nuclei considered in this work. The difference is typically 0 - 1.5 MeV. Correction was made by an iteration method described in detail by Haines.[16]

(c) Electronic Drift

In some of the longer experiments gain shifts in the linear system of up to 3% over a 24 hour period were encountered; however, the maximum shift between a measurement and a calibration was 1.5%. The drift within a given measurement was negligible and was followed from measurement to measurement by means of the pulse generator. It was thus possible to correct the calibration equation obtained from Cf^{252} to compensate for the observed pulser shift. Since the correction is small and is thought to be well understood, errors from this source should be negligible.

2. Calculations

Two-dimensional pulse height distributions may be transformed into several possible co-ordinate systems. The final data from these experiments were transformed using a random number method into a fragment mass, A_2, and total kinetic energy, E_T^*, distribution, $N(A_1, E_T^*)$.[10,17] E_T^* is defined:

$$E_T^* = E_1^* + E_2^* \qquad (2a)$$

E_1^* and E_2^* are the measured fragment energies. Mass may be calculated using momentum conservation:

$$A_2 \cong \frac{E_1^*}{E_1^* + E_2^*} A \qquad (2b)$$

where A is the mass of the original fissioning nucleus. Equation 2b is approximate because the measured energies are of the final fragments after neutron emission. The equation is strictly true only for the energies of the initial fragments, prior to neutron emission.

The two dimensional data will be presented in the form of moments of the distributions in one independent variable taken as a function of the other independent variable. The first moment of a distribution in a variable x is the mean, $\langle x \rangle$; the second moment, μ_2, is the variance which is a measure of the width of a distribution.*

$$\mu_2(x) = \langle x^2 \rangle - \langle x \rangle^2 \qquad (3)$$

Only the first and second moments will be considered in this work. The higher moments are not significant due to their sensitivity to both statistical and systematic error. The fourth moment, μ_4, is useful, however, in estimating the statistical standard errors, ϵ_1 and ϵ_2, in the first and second moments:[16]

$$\epsilon_1 = \sqrt{\mu_2}/N_T$$

$$\epsilon_2 = (\mu_4 - \mu_2^2)/N_T \qquad (4)$$

where N_T is the total number of events in the distribution being considered.

---

*The relation between the full-width at half-maximum, FWHM, and the variance for a Gaussian distribution is: $\mathrm{FWHM} = 2.36\sqrt{\mu_2}$

In order to minimize statistical erros and still process the data in a relatively fine grid without having to fold the data, 10^5 was set as the desired number of events although this was not attained in several runs (see Table I). Here "unfolded" means that the necessary symmetry of many of the distributions is not forced but must really be present in the data, i.e., an event (E_a, E_b) is considered distinct from an event (E_b, E_a). Leaving the data unfolded allows an important check on a large body of systematic error. Although the importance of symmetry properties is generally recognized by workers in the field, it has never been explicitly stated; consequently Appendix B has been included in which a more detailed discussion is presented. Unless otherwise specifically mentioned, all data will be shown unfolded.

The physically significant quantities are the masses and energies of the initial fragments prior to neutron emission; whereas a detector measures the fragment energy after neutron emission. The mass calculated by Eq. (2b) is a good approximation (within ~1 mass unit) to the true initial mass; thus, in the absence of sufficient knowledge of neutron emission for the systems studied, no correction to the mass has been attempted. However, the corrections to the average total kinetic energy and to the variances of the mass and total kinetic energy distributions, $\mu_2(A_2)$ and $\mu_2(E_T)$ respectively, were felt to be large enough to justify an attempt. The argument for this is simply that, with any type of reasonable correction, the corrected value will be a better approximation to the true value than the uncorrected. In order to write down explicit expressions for the corrected moments it was necessary to neglect any correlation between the number of neutrons from a given fragment, ν_1, and the fragment mass or total kinetic energy, i.e., $\nu_1 = \nu_2 = \nu_T/2$ was assumed, where ν_T is the total number of neutrons averaged over all fission events. ν_T was estimated from energy balance considerations (see Appendix C). The relations between the corrected (without stars) and uncorrected moments (with stars) are:

$$\langle E_T \rangle \cong \langle E_T^* \rangle \left(1 + \frac{\nu_T}{2A}\left(\frac{A_1}{A_2} + \frac{A_2}{A_1}\right)\right) + - - - \qquad (5a)$$

$$\mu_2(E_T) \cong$$

$$\left[\mu_2(E_T^*) - \frac{4}{3}\frac{m}{A}\langle E_T \rangle \langle E_n \rangle \frac{\nu_T}{2}\left(\frac{A_1}{A_2} + \frac{A_2}{A_1}\right)\right]\left[1 - \frac{\nu_T}{2A}\left(\frac{A_1}{A_2} + \frac{A_2}{A_1}\right)\right]^{-2} + - - - \qquad (5b)$$

$$\mu_2(A_2) \cong \left(\mu_2^*(A_2) - \nu_T\, m\, A \frac{\langle E_n \rangle}{E_T^*}\right)\left(1 - \frac{2\nu_T}{A}\right)^{-1} + - - - \qquad (5c)$$

where $\langle E_T \rangle$ is the average total kinetic energy for a given omit and $\langle E_n \rangle$ is the average neutron kinetic energy, and m is the neutron mass. The method for estimating $\langle E_n \rangle$ is given in Appendix C. Note that x in $\mu_2(x)$ stands for the variable averaged over, not the variable held constant; thus (a) and (b) are functions of mass, and (c) is a function of E_T. The expression for $\mu_2(A_2)$ is derived assuming that mass averages are taken over all masses, not for individual mass peaks. The derivation for these equations is outlined in Appendix D. Analogous equations were assumed to hold for the overall moments calculated by averaging over all fission events.

III. CALIBRATION OF SEMICONDUCTOR DETECTORS FOR FISSION FRAGMENTS

When a fission fragment strikes a semiconductor detector, the resulting pulse height is not proportional to energy in the sense that the pulse height depends on the mass or charge of the fragment as well as the energy. (This phenomenon will hereafter be referred to as "the non-proportionality".) Since the exact nature of the pulse-height-energy relation, V(E), is not known at present, the purpose of this section will be to describe attempts to find an adequate calibration equation with which to process the charged-particle-induced fission data. This will be preceded by a brief introduction concerning the evidence for the existence of the non-proportionality. Still later, in Section IV, the magnitude and significance of the errors introduced due to an incomplete understanding of V(E) will also be considered.

A. Evidence for the Non-Proportionality in the Pulse-Height - Energy Relationship

The simplest indication that pulse height is not directly proportional to energy is that the ratio of the pulse height of the most probable light fragment to that of the most probable heavy fragment for Cf^{252} is typically about 1.4 rather than the 1.3 expected from the ratio of energies,[7,18,19] i.e., if these two pulse heights and the known energies are used to define a calibration line, this line will not pass through zero but will have some positive intercept. If one further compares these pulse height peaks with a calibration line extrapolated from alpha particle measurements, both peaks are found to have less pulse height than would be expected on the basis of alpha particles with the heavy fragment being more deficient than the light (see Fig. 1).

The most recent development has been the work of Schmitt et al. who studied the response of a variety of detectors to Br^{79-81} and I^{127} ions accelerated in a tandem Van de Graaff accelerator.[20] A typical plot of their results is shown in Fig. 2.

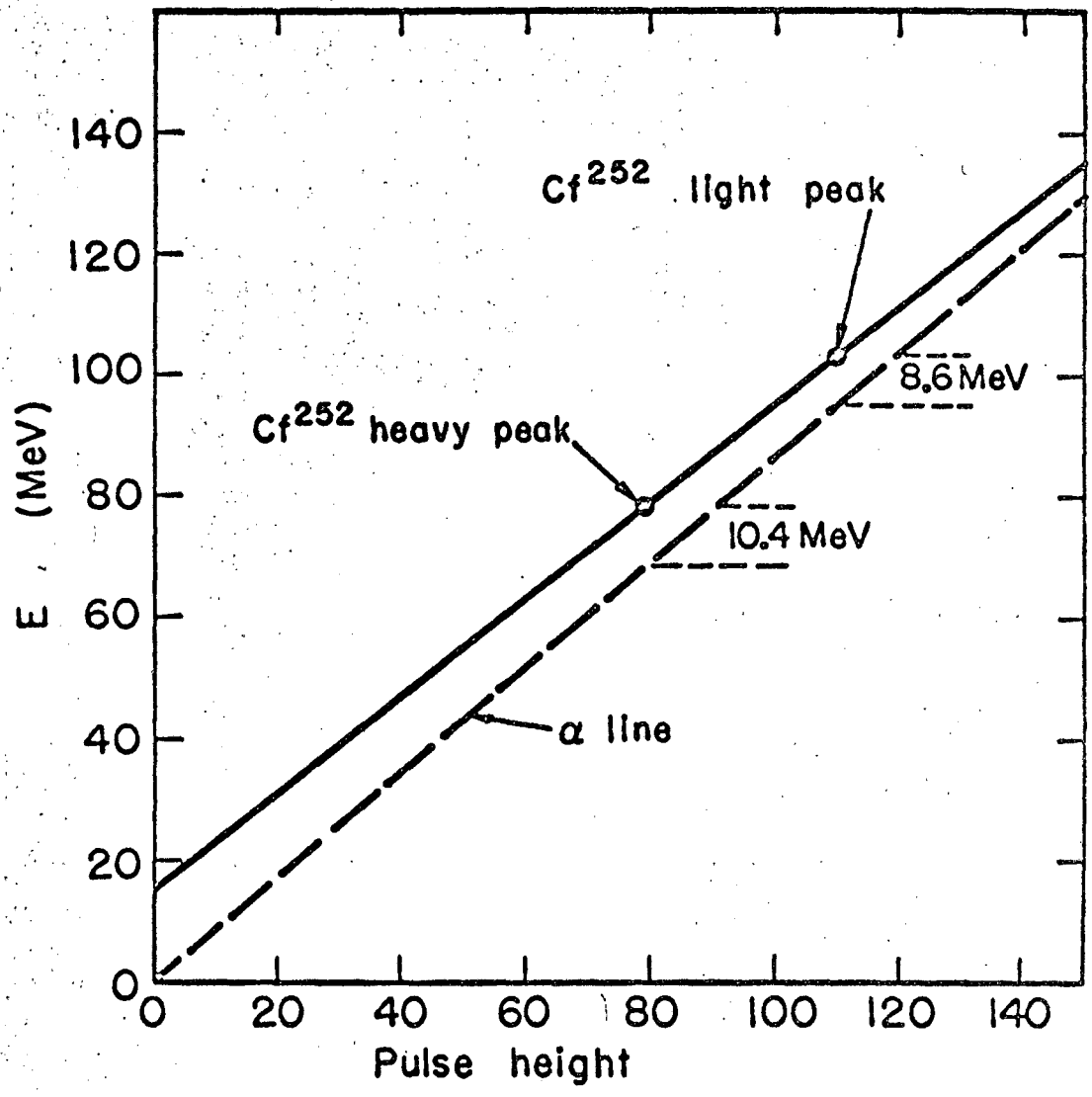

Figure 1. Typical pulse-height energy curve for a semiconductor detector showing positions of the heavy and light peaks of Cf^{252} relative to a calibration line extrapolated from α-particle measurements.

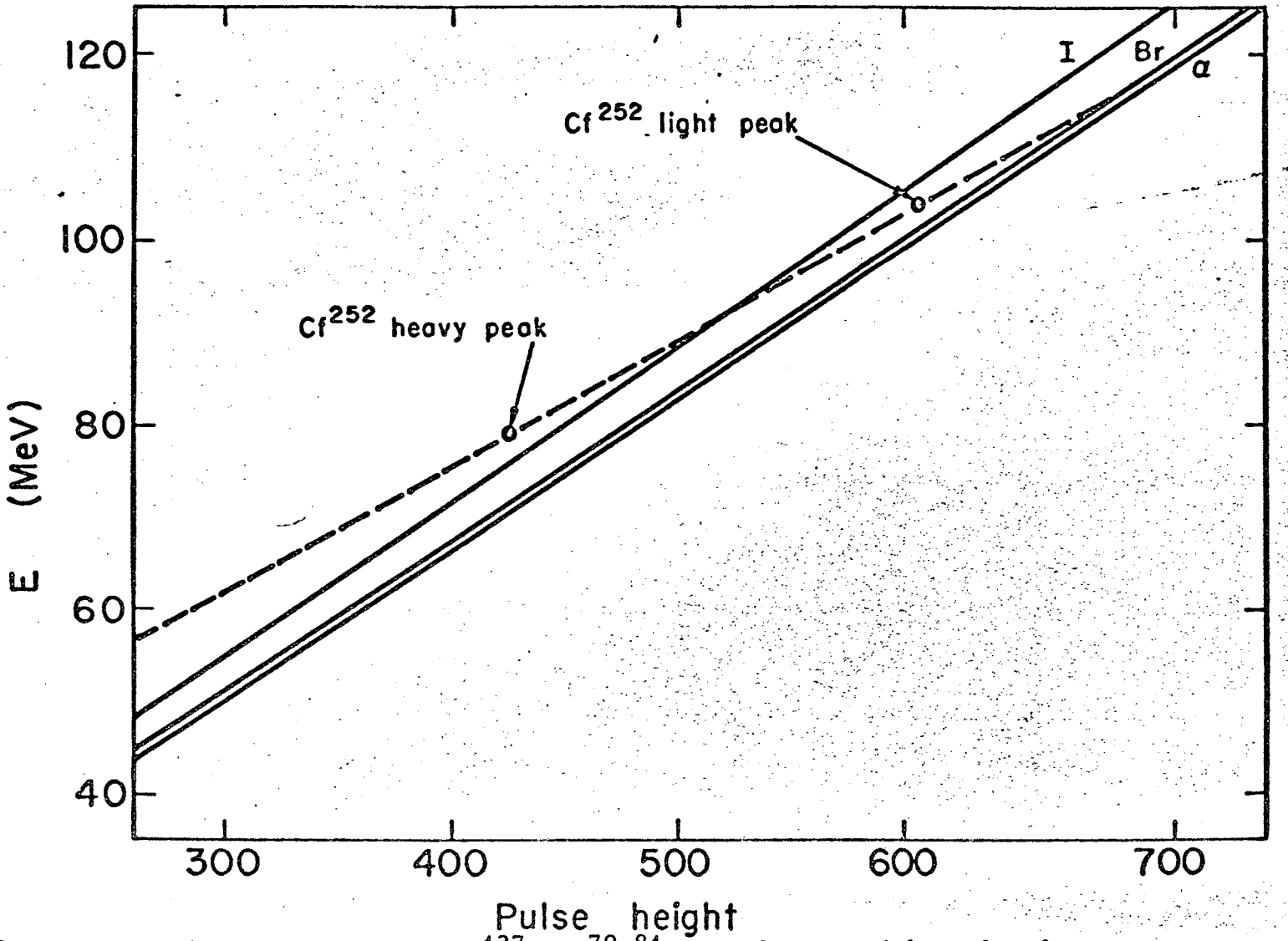

Fig. 2. Energy-pulse height curve for I^{127}, Br^{79-81}, and alpha particles taken from work of Schmitt et al.[20] Similar results were obtained for all detectors as long as data was taken on plateau of pulse-height bias curve.

MU-32153

These results indicate that there is no deviation from the alpha line until just before mass 80; but, for heavier masses, the deviation from the alpha line occurs rather rapidly. The Br line is quite parallel to the alpha line; whereas the I line shows a slightly greater slope. The pulse heights from the peaks of Cf^{252} fall on the diagram at points consistent with average masses of 106 and 142. Thus Br, I, and Cf points form a consistent picture. However, if the peaks for the thermal neutron fission of U^{235} and Pu^{239} are entered on the diagram in the same manner as Cf^{252}, they do not fit into the above pattern; so, at the present time, completely self-consistent results have not emerged from these experiments.

B. Choice of Detectors

The charged-particle-induced fission data to be reported were taken with two sets of detectors. The data for 65 MeV alphas were taken with 1700 ohm-cm. diffused-junction guard-ring detectors obtained from W. L. Hansen of this laboratory.[49] The remainder of the data were taken with 200 ohm-cm. detectors of the same type (see Table I). The properties of and the choice of operating conditions for these and other detectors are discussed in detail in Appendix E.

C. Detailed Comparison of Detector and Time-of-Flight Results for Cf^{252}

This section will describe attempts to find an adequate calibration equation with which to process the charged-particle-induced fission data. This was done by means of a comparison of detector and time-of-flight energy measurements for Cf^{252} spontaneous fission. There is nothing new in this; however, it is surprising that a detailed comparison using all the available time-of-flight data has yet to appear in the literature. The most complete work to date has been the work of Britt, Wegner, and Whetstone.[21] They discuss primarily the total mass distribution and the average total kinetic energy as a function of mass and conclude that, when corrections

for the emission of neutrons are properly made, good agreement is obtained between the time-of-flight and detector results. This section will show that it is necessary to make a more detailed comparison in order to see the effect of the non-proportionality. Further, recent time-of-flight remeasurements by Milton and Fraser[19] and by Whetstone[18] have made it appropriate to repeat the comparison in general.

It should be emphasized again at this point that an exact solution to the calibration problem is yet to be found and that, at present, this problem remains a serious limitation to precision measurements of fission-fragment kinetic energies.

Appendix F gives a suggestion for an exact solution of the detector calibration problem. Such an exact solution would seem to be prerequisite for high precision fragment energy measurements which may be necessary to gain information on some of the finer details of the fission process.

1. Calibration Schemes

a. Constraints on the nature of the calibration equation

Neither time-of-flight nor detector measurements give any information on the fragment charge; consequently the inclusion of charge as a variable in a calibration equation would have to be done via some correlation of the most probable charge with mass. Thus, for the purposes of data processing, the general calibration equation — possibly a function of energy, charge, and mass — reduces to one involving energy and mass only. Therefore no attempt to introduce a charge dependence has been made, either implicitly or explicitly, and only calibration equations which depend on energy and mass will be considered.

From the discussion thus far and, in particular, from the work of Schmitt et al.[20] four empirical constraints on the nature of the mass dependence emerge:

(1) For a given mass the pulse-height energy equation is linear, at least for the energy range corresponding to fission fragments i.e., $E_1 \gtrsim 20$ MeV.

(2) At a given energy the pulse height decreases with increasing mass.

(3) The mass dependence only becomes appreciable for masses above about 70-80, i.e., it exhibits a threshold effect.

(4) The mass 80 curve is parallel but displaced from the alpha line; the mass 127 curve has a slightly more positive slope.

What has been done is to formulate various physically reasonable calibration equations based on the above empirical constraints, calculate fragment energies from detector pulse heights using these equations, and finally to compare the results with the time-of-flight data. The approach is strictly empirical; no attempt has been made to deduce equations on the basis of any proposed mechanism.

b. Mathematical formulation

From constraint (1), for a given mass, A_1, the energy, E_1, is related to pulse height, V, by a linear equation:

$$E_1 = a(A_1) + b(A_1) \cdot V \qquad (6)$$

where the coefficients, a and b, are functions of mass. Constraints (2), (3), (4), and Fig. 2 suggest that the dependence of a and b on A_1 is schematically as shown in Fig. 3. The slope b is plotted as a ratio to the alpha slope, b_α. Figure 3 has no quantitative significance whatsoever. In practice the variations in E_1 for a given V introduced by the mass dependence amounts to less than 10%, so a and b could be expanded about some typical fission fragment mass, say 106.

$$a(A_1) = a_o(106) + a_1(A_1 - 106) + a_2(A_1 - 106)^2 + \ldots$$

$$b(A_1) = b_o(106) + b_1(A_1 - 106) + \ldots \qquad (7)$$

where the results of Schmitt et al.[20] suggest that second order terms may be necessary, at least in $a(A_1)$.

Results will be reported from three types of calibration schemes. Two have been chosen because they represent the extreme cases rather than

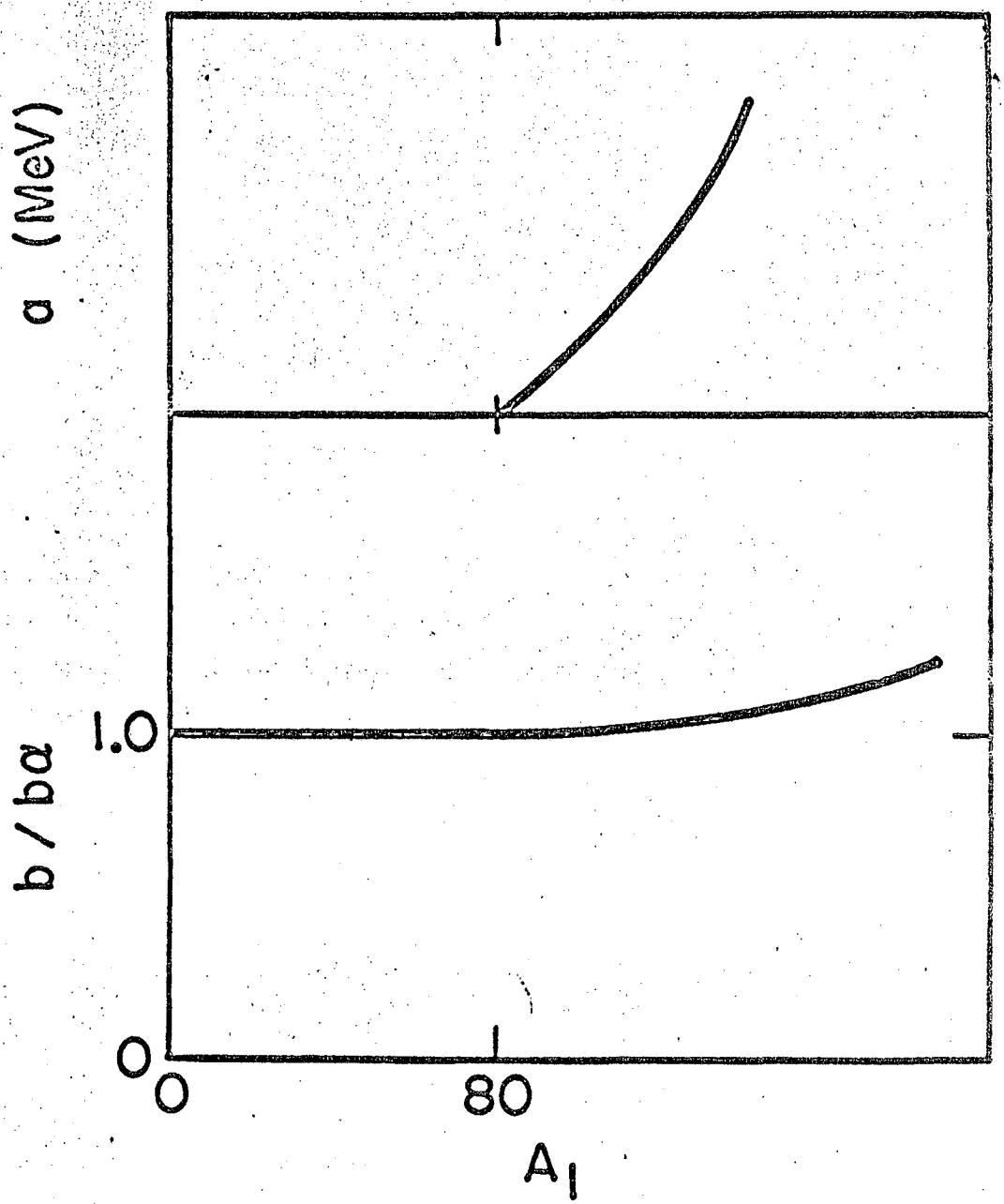

Figure 3. Schematic illustration of dependence of coefficients of calibration equation on mass.

because they adhere closely to the constraints mentioned above. The third is an attempt to formulate a scheme which has the most physical significance and meets the requirements of the above constraints.

(1) Two Peak Calibration Scheme

(hereafter referred to as the TP scheme)

This scheme is an extreme in the sense that all mass dependence is neglected, i.e., $a(A_1) = a_o$, and $b(A_1) = b_o$ in Eq. (7). The coefficients, a and b, are evaluated from the average energies and pulse heights for the heavy and light peaks of the Cf^{252} spectrum. Several experiments, based on this or similar schemes, have been reported.[22,23,35]

(2) Common Intercept Scheme

(hereafter referred to as CI)

In this scheme the pulse-height energy curves are taken to be a family of lines having a common intercept at V = 0 but with slopes increasing linearly with mass, i.e.,

$$a(A_1) = 0$$

$$b = b_o + b_1 (A_1 - 106)$$

This is the opposite extreme from the TP since it gives the maximum slopes and minimum intercepts (0); whereas the TP scheme has the minimum slope and maximum intercept. This calibration scheme is almost identical with that used by Viola and Sikkeland.[24]

(3) Parallel Line Scheme

(hereafter referred to as PL)

This scheme attempts to meet the requirement of the above constraints, at least approximately. It is assumed that the lines for all masses are parallel to the alpha line, i.e., the tendency of the I^{127} line to have a somewhat higher slope has been ignored.

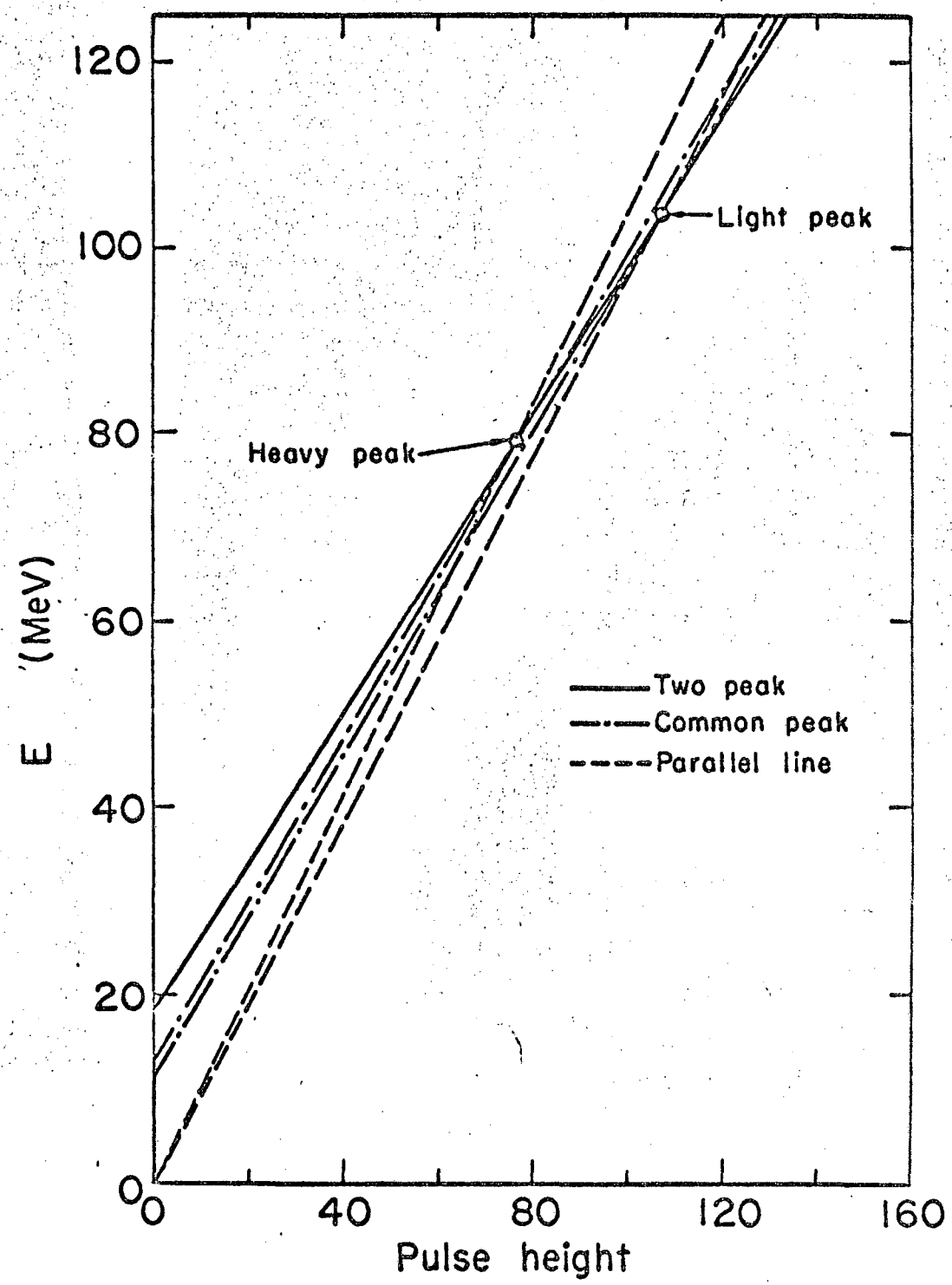

Figure 4. Graphical presentation of calibration schemes studied in detail. Heavy and light peaks of Cf^{252} are included for reference.

Further, the dependence of the intercept on mass has been taken to be linear:

$$a = a_o + a_1(A_1 - 106)$$

$$b = b_\alpha$$

The origin and basis for these approximations will be more apparent when the results are given.

The mathematical form of this scheme is identical to that used by Haines although in that work the slope of the calibration equation was determined by the $O^{16} + Au^{197}$ system.[16] This scheme is also close to that used by Britt et al.; however, these workers found that the displacements from the alpha line were constant, eliminating the need for any explicit A_1 dependence.[9,25]

Figure 4 illustrates graphically the above calibration schemes.

2. Choice of Variables

Fission-fragment pulse-height data in two-dimensions — i.e., the number of events having pulse heights V_1 and V_2, $N(V_1, V_2)$ — are usually transformed into one of two physically-significant representations: light-fragment energy and heavy-fragment energy, $N(E_L, E_H)$; or mass and total kinetic energy, $N(A_1, E_T)$. The latter is more commonly used; however, for this comparison the (E_L, E_H) representation has been chosen. This is because the relations to pulse height are simpler and because the effects of the two detectors used in the measurement are isolated as much as possible; but, at the same time, all of the time-of-flight data are utilized. In particular results will be discussed for the averages and standard deviations of the profiles of $N(E_L, E_H)$, viz. $N(E_L)$, E_H = constant and $N(E_H)$, E_L = constant. These averages and standard deviations, σ, are calculated:

$$\overline{E_L}(E_H) = \frac{\sum_i N((E_L)_i, E_H) \cdot (E_L)_i}{\sum_i N((E_L)_i, E_H)}$$

$$\sigma_L^2 = \overline{E_L^2(E_H)} - \overline{E_L(E_H)}^2$$

Similar definitions apply for $\overline{E}_H(E_L)$ and σ_H. The standard deviation (i.e., the square root of the variance) is a measure of the width of the distribution, as discussed in Section II C.

3. Choice of Time-of-Flight Values.

Both Whetstone[18] and Milton and Fraser[19] have remeasured Cf^{252} fission fragment velocities by the time-of-flight method. The results are not identical; however, Fig. 5 indicates that it makes little difference which set is chosen for the reference energies. The plot shows the differences, Δ_L and Δ_H, between the Whetstone and Milton-Fraser values.

The energy values differ by a constant amount; i.e., the shape of the $\overline{E_L}(E_H)$ and $\overline{E_H}(E_L)$ are the same, so that, if detector values are normalized at one point, the remainder of the curve should be reproduced. The divergence of the curves at low energies is not felt to be significant. The energies given in this work are relative to the Whetstone values.

4. Treatment of Neutrons

Time-of-flight measurements give fragment energies prior to the emission of neutrons; whereas a detector measures the energy of the fragment subsequent to neutron emission. Since the neutrons are usually assumed to be emitted isotropically from the fragments, on the average the fragment velocity, v_1, will not be appreciably changed; consequently the initial, E_1, and final, E_1^*, energies differ only because of the loss in mass due to the emission of υ_1 neutrons (See Appendix D):

$$E_1^* \approx 1/2\,(A_1 - \upsilon_1)\, v_1^2 = E_1\left(1 - \frac{\upsilon_1}{A_1}\right) \qquad (9)$$

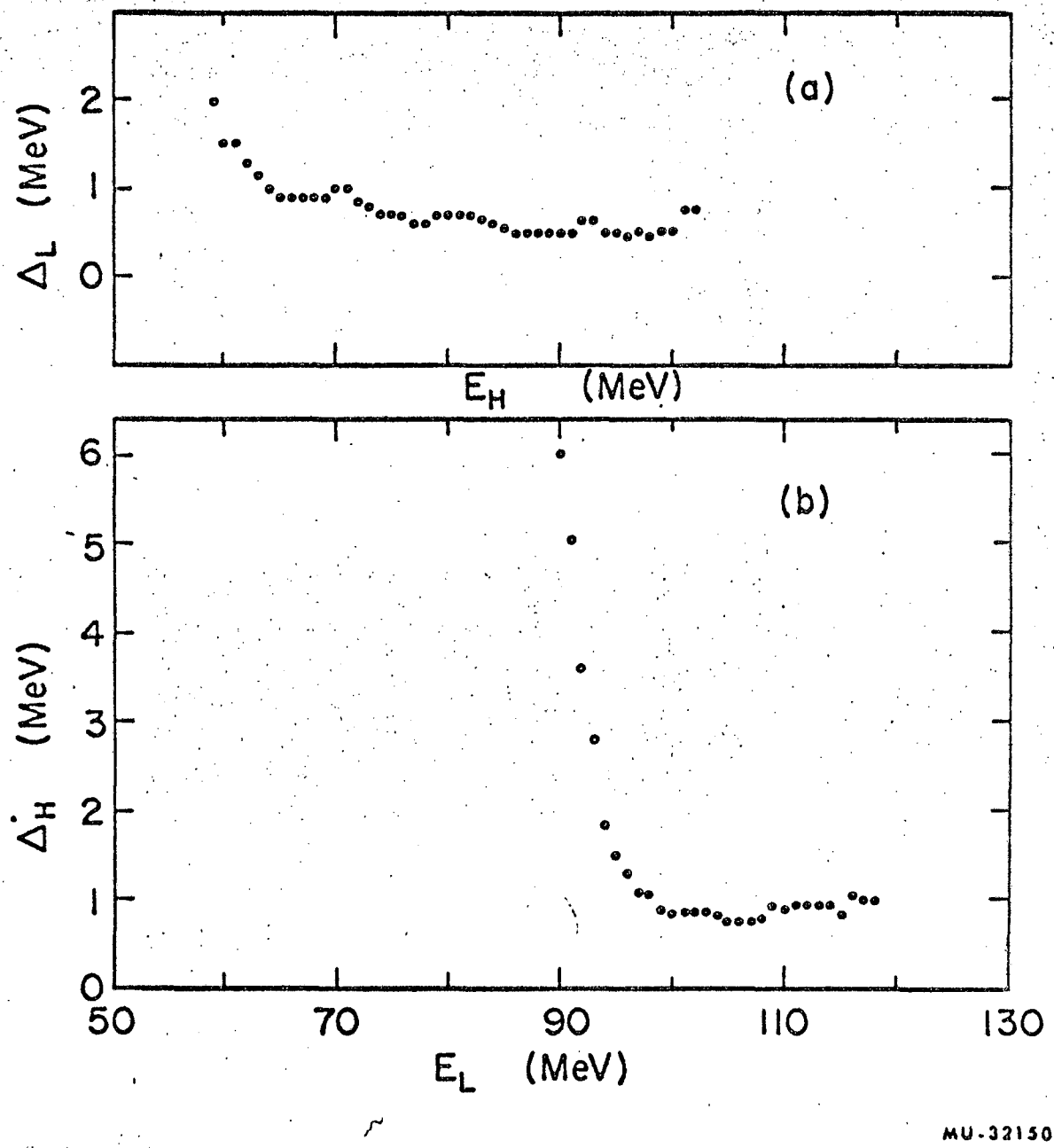

Figure 5. Plot of difference between Whetstone[18] and Milton and Fraser[19] Cf^{252} average energies. (a) Difference in coverage light fragment energy vs E_H. (b) Difference in average heavy energy vs E_I.

The final energies, calculated from the detector pulse heights, were converted to prompt energies on an event-by-event basis; i.e., for an observed (E_L^*, E_H^*), the corresponding prompt (E_L, E_H) were calculated by Eq. (9) using values for the average number of neutrons for a given mass, $\nu_1(A_1)$ taken from the work of Bowman, et al.[26,27] For a more detailed discussion of the effect of this type of neutron correction the work of Britt, Wegner and Whetstone should be consulted.[21] Similarly, the final overall average heavy and light fragment energies used to evaluate the coefficients of the calibration equations were calculated from Eq. (9) using values for the overall average initial energies and masses given by Whetstone[18] and overall $\bar{\nu}_1$ values given by Bowman et al.[27] These values are shown in Table II.

5. Results

It is more convenient to plot the differences between the detector and time-of-flight average energies rather than the values themselves; consequently the curves shown will be of $\Delta\overline{E_L}$ and $\Delta\overline{E_H}$ where, for example,

$$\Delta\overline{E_L} = \overline{E_L}(E_H)_{det} - \overline{E_L}(E_H)_{TOF} \qquad (10)$$

If there were perfect agreement between the two methods, then this curve would be zero at all points. The data are plotted in "fever chart" form in order to keep better track of the points for a given calibration scheme without being committed to drawing a smooth curve through the points. Results will be shown for one set of detectors; however, the conclusions drawn are based on results obtained from several sets of detectors which differed in type and resistivity. The results to be shown are quite typical; no effort has been made to select "best" results. The results shown are from 1700 ohm-cm guard-ring phosphorous-diffused detectors operated in the flat portion of the pulse-height bias curve at 92 V. Figure 6 shows plots of $\Delta\overline{E_L}$ and $\Delta\overline{E_H}$. Because the coefficients of the calibration equations were calculated using the known overall average heavy and light

Table II. Standard time-of-flight overall averages used in this work.

	Heavy	Light*
$\overline{E_1}$	79.87 MeV	105.52 MeV
$\overline{A_1}$	143.6	108.4
$\overline{\nu_1}$	1.68	1.97
$\overline{E_1^{\wedge}}$	78.8 MeV	103.6 MeV

*The average energy values differ slightly from those published in Ref. 18. The above were calculated by us from only a part of the original data of Ref. 18. This was obtained by private communication through the co-operation of Dr. S. L. Whetstone, Jr.

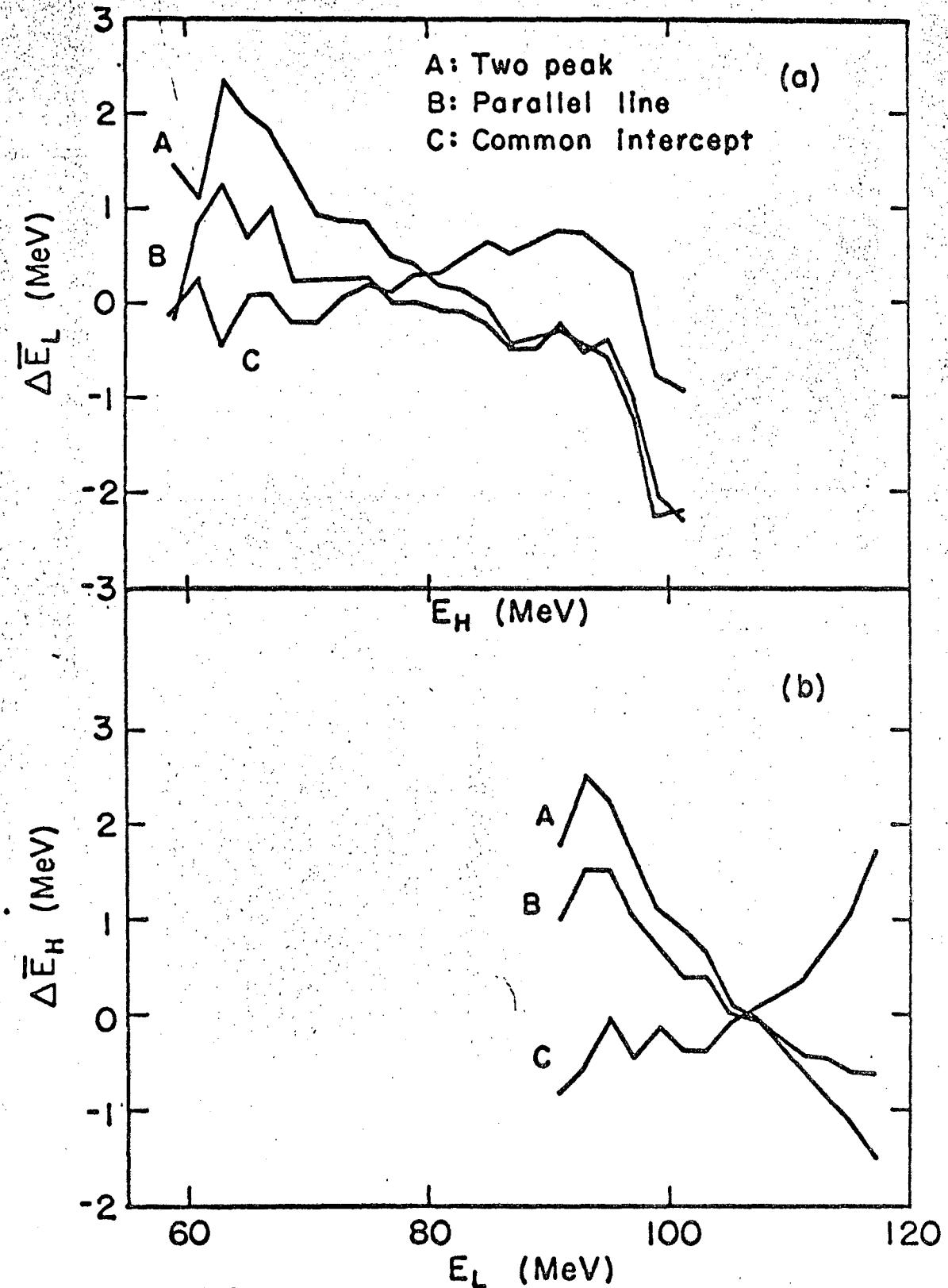

Fig. 6. Difference of Cf^{252} average energies measured by detector from those measured by time of flight for the calibration schemes considered.[18] Example shown is for 1700 ohm-om phosphorous-diffused guard-ring detector. (a) difference in average light energy vs E_H (b) difference in average heavy energy vs E_L.

MU-32158

energies, each curve is effectively normalized to the time-of-flight value (0) at one point. The $\overline{\Delta E_L}$ (E_H) curves shown in Fig. 6 all lie within ± 1 MeV of the zero line. The TP curve shows the greatest tendency to deviate; however, the agreement for all cases is satisfactory which is not surprising since the non-proportionality is smaller for light fragments. A much more pronounced deviation is shown by the $\overline{\Delta E_H}$ (E_L) curves in Fig. 6. In particular the TP curve shows little tendency to follow the time-of-flight curve and tends toward large positive values as E_L decreases. On the other hand the CI curve is slightly negative for low E_L and tends more positive for high E_L. The PL occupies an in-between position, as expected. On the basis of Fig. 6 alone, the TP calibration gives the poorest agreement with the time-of-flight data; however, no real distinction can be made between the CI and PL. In general, a good description of the average energies seems to require a high slope and small intercept in the calibration equation.

Figure 7 shows curves for σ_L (a function of E_H) and σ_H (a function of E_L) along with the time-of-flight curve. The error bars on the time-of-flight data represent the difference between the Milton-Fraser and Whetstone measurements. The most striking feature of these curves is that the order of agreement is reversed from that found for the averages in Fig. 6, i.e., the TP calibration gives the best agreement; whereas the CI curve deviates considerably from the time-of-flight curve. The PL curve again occupies an intermediate position. This is because the widths of the distributions are most strongly influenced by the slopes of the calibration lines which are largest for the CI and smallest for the TP; thus good agreement here requires small slopes and large intercepts, the opposite requirement from the averages. However, the widths from detector measurements are more affected by neutron emission than those from time-of-flight; thus, if a more exact neutron correction were made, the TP results may actually lie below the time-of-flight values with the PL values showing the best agreement. Such a tendency already exists in the σ_H curve of Fig. 7b.

28

One conclusion which can be drawn from the above analysis is that it is impractical to attempt to adjust the parameters in these calibrations

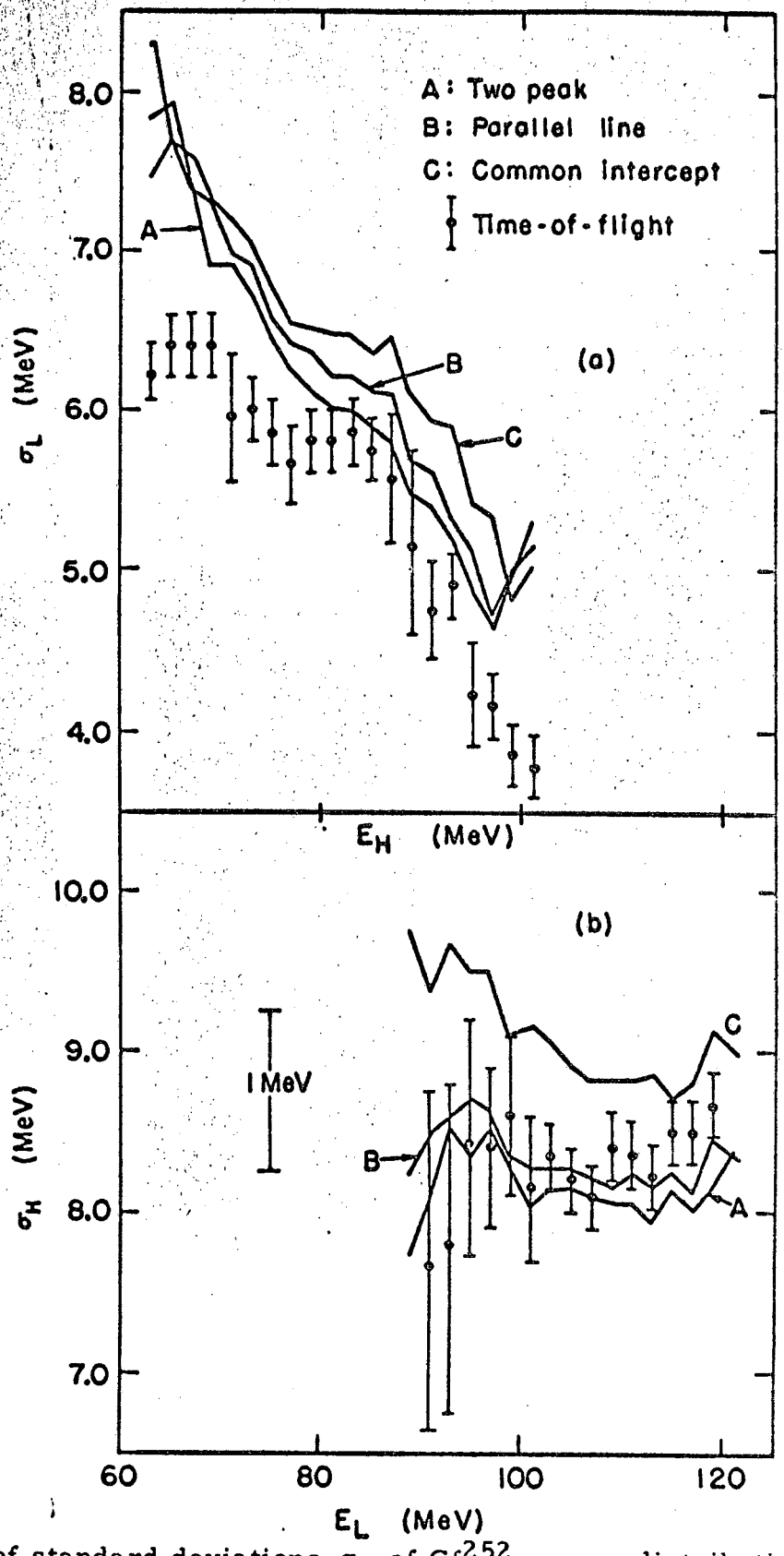

Fig. 7. Comparison of standard deviations, σ, of Cf^{252} energy distributions for the calibration schemes considered with time-of-flight results. (a) σ for light fragment distributions vs E_H. (b) σ for heavy fragment distributions vs E_L.

or to introduce new parameters in order to get a better "fit" to the time-of-flight results without the use of very complex schemes for which there is no basis at the present time. This is because, as long as a linear pulse-height energy relation for a given mass is required, the "best fit" to the averages requires large slopes and small intercepts; whereas the reverse is true for the widths. Consequently, it seems necessary to predetermine the coefficients. There are only three pieces of information which can be readily used to calculate a calibration equation for each detector: the average heavy and light fragment energies and the slope of the alpha line. Therefore we are limited to a three parameter equation and cannot reproduce exactly the type of mass dependence in the intercepts and slopes which is indicated by the Van de Graaff results.[20] Thus the PL scheme has been formulated as a compromise between the more extreme CI and TP schemes. This scheme is not completely satisfactory; however, it is sufficient for calculating energies from charged-particle-induced fission data which was the purpose of this investigation.

The effect of the above calibration schemes on fissioning systems other than Cf^{252} will be considered when these results are presented in Section IV.

One pleasing aspect of these comparisons has been the sensitivity to the various calibration schemes shown by the $\Delta\overline{E}$ and σ curves. At the beginning it was thought that, since all the schemes were normalized to the averages of the Cf peaks, all three might give an adequate representation of Cf and that no distinction could be made among the various schemes.

6. Comparison of Mass and Total Kinetic Energy Curves

The data in $N(E_1, E_2)$ form may be transformed into $N(A_H, E_T)$, where A_H is the heavy fragment mass and E_T is the total kinetic energy, by the usual equations:

$$E_T = E_L + E_H$$

$$A_H = \frac{E_L}{E_T} A$$

$$A_L = \frac{E_H}{E_T} A$$

$$A = A_1 + A_2$$

It should be emphasized that all the data have been used in the previous comparison; these results are merely looking at the data in another way.

Figure 8 shows the average total kinetic energy vs. mass curve for the TP and CI schemes. The PL has been omitted for clarity; it falls in between the TP and CI curves. The time-of-flight values in this case are from Fraser and Milton.[19] The general shape of the time-of-flight curve is reproduced fairly well; however, the detector curves are broadened and do not follow the dip at symmetric fission very well. As might be expected from the average energies, the CI calibration gives better agreement.

Figure 9 shows the total mass yield curve as measured by detectors and time-of-flight. The results of all the calibration schemes are contained in the heavy line, i.e., the mass-yield curve is quite insensitive to the calibration equation. This is explained by the fact that the effect of the above calibration schemes is to change the shape of the distributions along lines of constant mass across the (E_L, E_H) map; so that, to a first approximation, the number of events at a given mass is not changed.

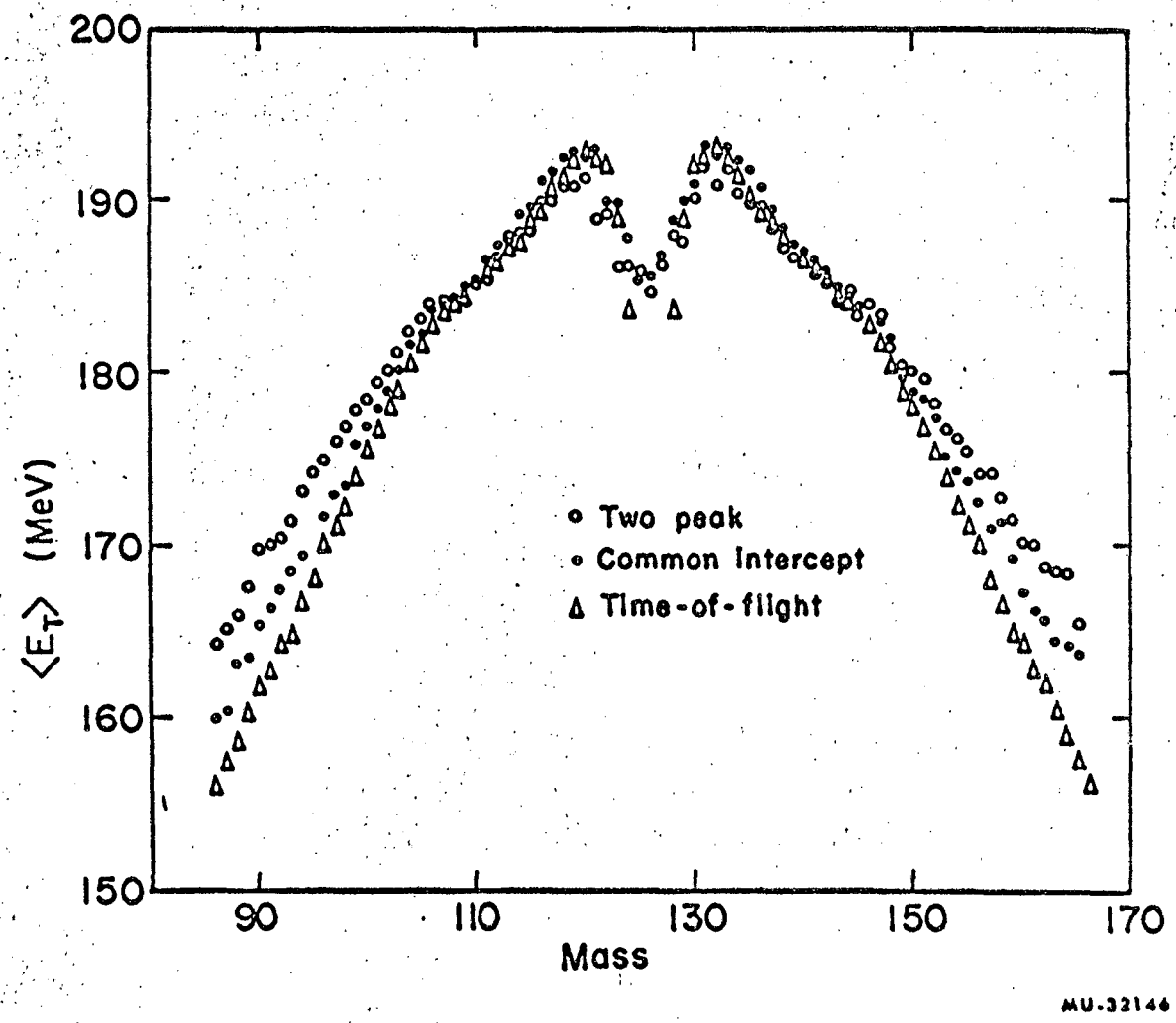

Figure 8. Average total kinetic energy for Cf^{252} vs fragment mass. Data shown for two of the calibration schemes considered and from time of flight data of Milton.

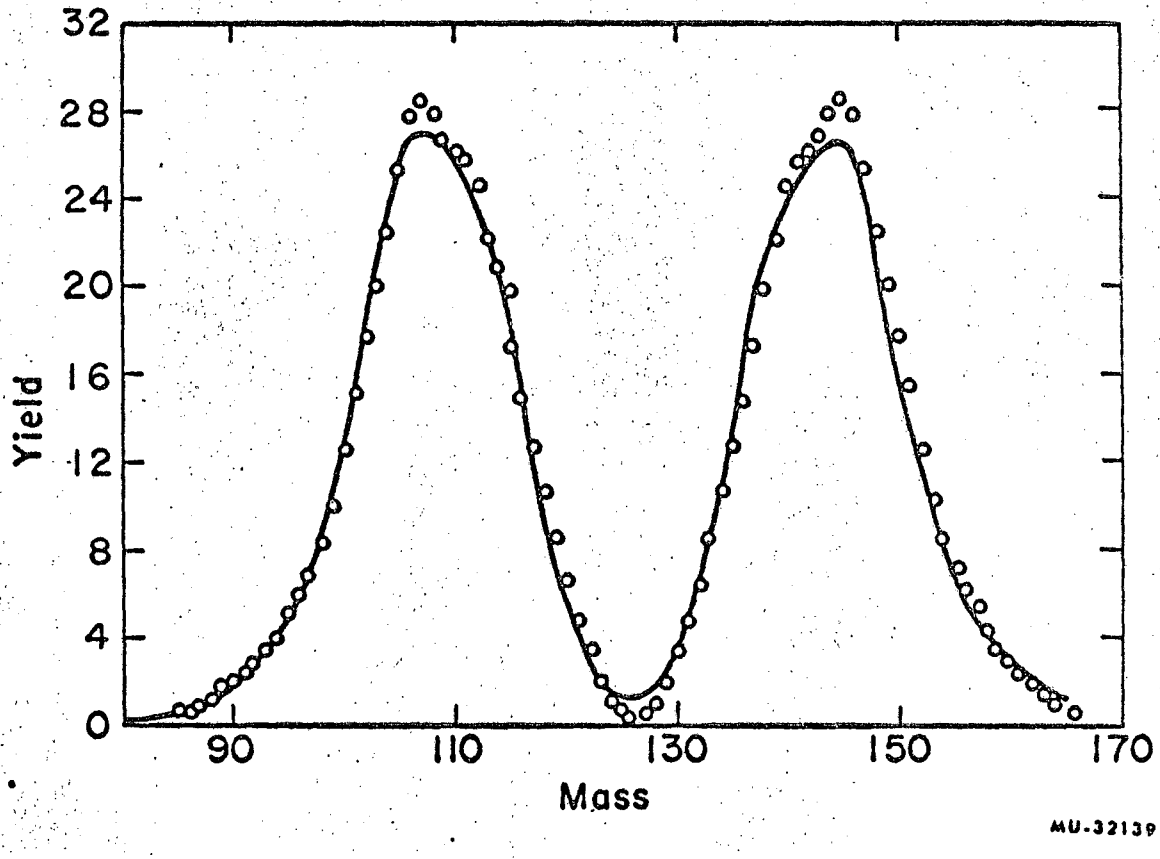

Figure 9. Overall mass-yield curve for Cf^{252}. All calibration schemes included by solid line; points are time-of-flight results.

IV. RESULTS AND DISCUSSION

The presentation and discussion of the results of these experiments will be organized in the following way two remaining experimental considerations, the effect of calibration uncertainties and the effect of the neutron corrections, will be illustrated. A systematic presentation of the results will then follow. Since fission data have a natural division depending on the x value of the fissioning nucleus, the Bi^{209} and Au^{197} data will be discussed separately and compared with quantitative liquid drop calculations available for this region of x. This will be followed by a more qualitative discussion of the Th^{232} and U^{238} data.

A. Effect of Calibration Uncertainties

Calibration errors become increasingly more significant as the fissioning nucleus becomes further removed from Cf^{252}. Consider, in particular, low x fission. For these cases the most probable mass split (symmetric) gives fragment masses close to the most probable light mass from Cf^{252}: however the pulse heights from these fragments are comparable to those of the heavy peak. The spread in the predicted values of the fragment energy is then the separation of the light fragment calibration lines at the pulse height of the heavy peak which Fig. 4 shows to be quite significant. This discrepancy will increase due to the divergence of the calibration lines as the most probable energy decreases (i.e., as x decreases).

This effect is illustrated quantitatively in Table III which compares the values for $\langle E_T^* \rangle$, the overall average of the total kinetic energy distribution after neutron emission, and $\mu_2\langle E_T^* \rangle$, the variance of this distribution, for the three calibration schemes discussed in Section III. The averages in this case are over all masses. Data are presented for a high x case, Th^{232} + 25.7 MeV alphas, and a low x case, Bi^{209} + 65.0 MeV alphas, for comparison. As was expected

Table III. Comparison of properties of the overall total kinetic energy distribution as calculated by three calibration schemes

System	Calibration Scheme					
	TP		PL		CI	
	$\langle E_T^* \rangle$ (MeV)	$\mu_2(E_T^*)$ $(MeV)^2$	$\langle E_T^* \rangle$ (MeV)	$\mu_2(E_T^*)$ $(MeV)^2$	$\langle E_T^* \rangle$ (MeV)	$\mu_2(E_T^*)$ $(MeV)^2$
Th^{232} + 25.7 MeV α	170.3	108	169.1	123	166.7	146
Bi^{209} + 65.0 MeV α	151.2	71	146.6	81	140.2	96

$\langle E_T^* \rangle$ is the overall average total kinetic energy uncorrected for neutrons. $\mu_2(E_T^*)$ is the variance of the overall total kinetic energy distribution and is also uncorrected for neutrons.

from Fig. 4, the TP scheme gives the highest $\langle E_T^* \rangle$ values and the CI the lowest, while the reverse is true for the variances. The difference in $\langle E_T^* \rangle$ for the three calibrations for Bi^{209} is 11 MeV; whereas it is only 3.6 MeV for Th^{232}. These numbers represent the maximum possible uncertainty due to calibration; thus, even for the case of Au^{197}, the PL scheme should give the true value to within ± 3 MeV. For the Th^{232} case the uncertainty is about ± 1 MeV which is somewhat smaller than the cumulative systematic error from other sources; whereas the reverse is true for the low x fission. It is felt that the PL scheme is adequate for the processing of these data; and all of the data to be presented subsequently will be from this scheme unless otherwise specifically mentioned. However, for data at still lower x (which is the direction of current interest) calibration errors will become still more important; and the adequacy of the PL scheme should be questioned.

The variances show a much wider spread; hence the uncertainties in the use of the PL scheme will be larger. These uncertainties are more difficult to estimate but are probably about ± 10 $(MeV)^2$.

Two further conclusions can be drawn. First, data from various experimenters should not be compared unless the effects of differences in calibration schemes and in Cf^{252} reference energies are taken into consideration. Secondly, because calibration errors are strongly dependent on x, systematics established by the self-consistent use of the same calibration do not necessarily have relative errors which are significantly smaller than the corresponding absolute errors.

Figures 10 and 11 indicate that the invariance of the total mass-yield curves to the nature of the calibration equation which was observed for Cf^{252} is maintained for the Bi^{209} and Th^{232} cases discussed above. This is significant because Britt and Whetstone[24] have shown that by a comparison of detector and time-of-flight overall mass-yield curves information on the average number of neutrons as a function of mass may be extracted. Since the taking of small differences is

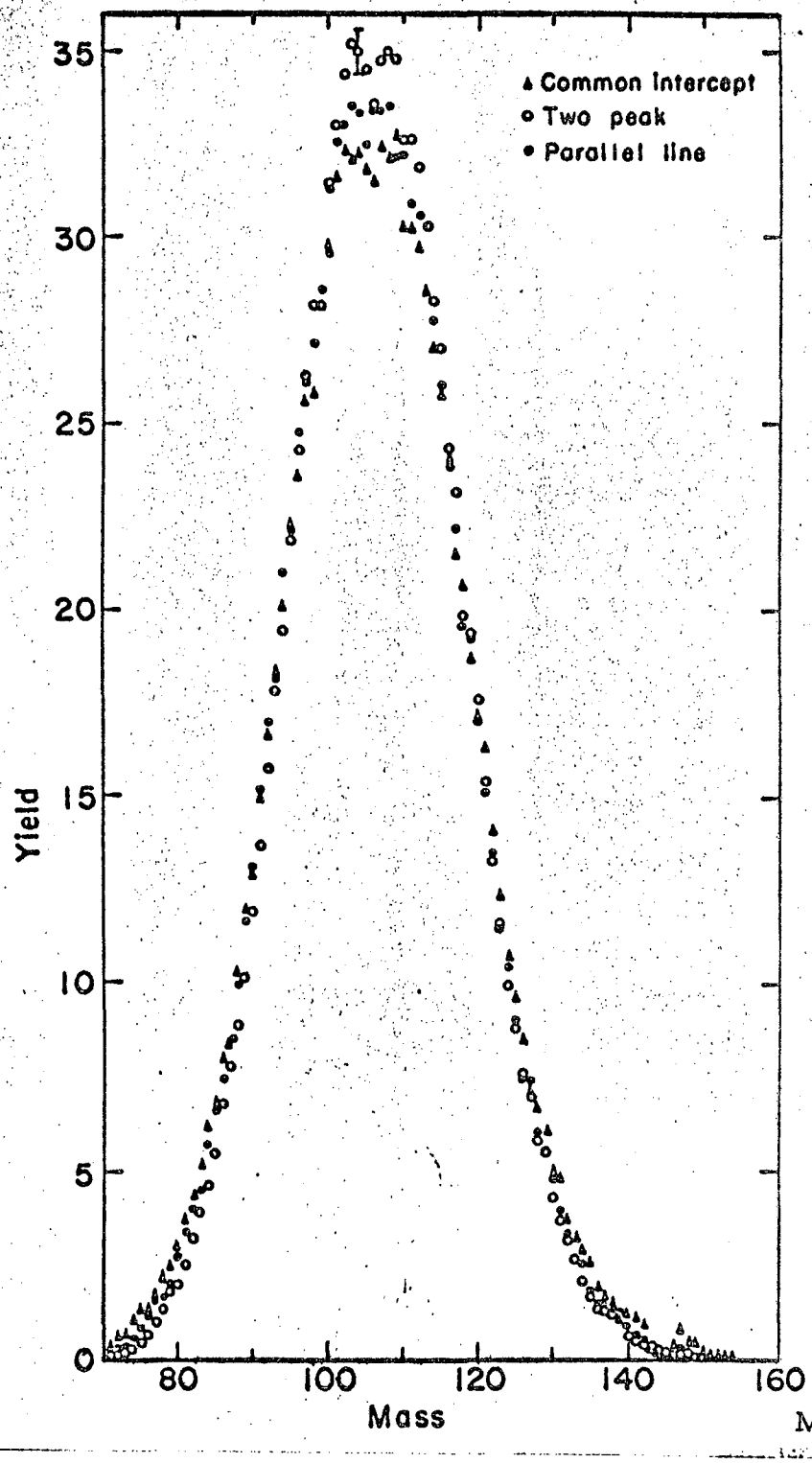

Figure 10. Overall mass-yield curve for Bi^{209} + 65 MeV alphas. Results shown for 3 calibration schemes.

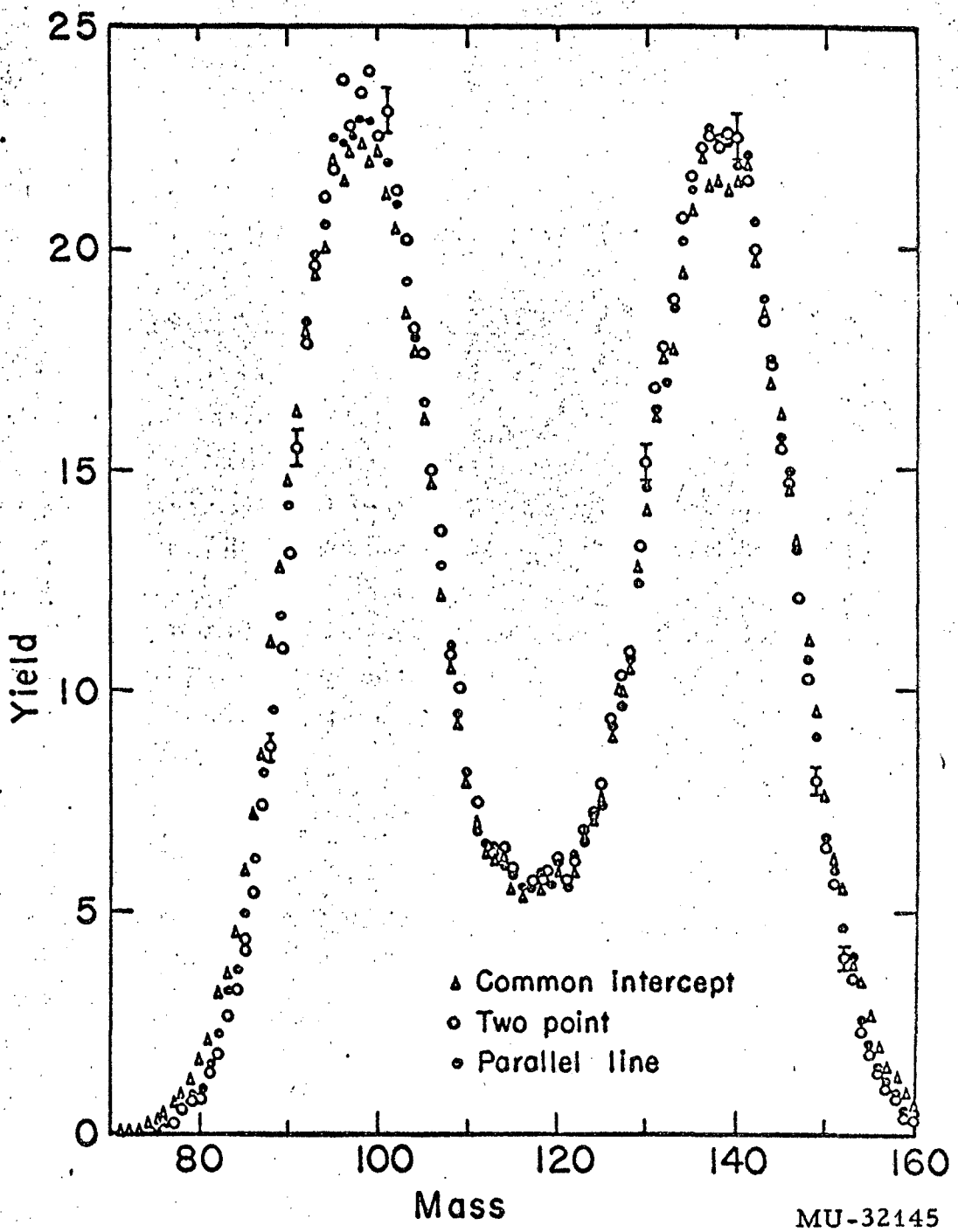

Figure 11. Overall mass-yield curve for Th^{232} + 25.7 MeV alphas. Results shown for 3 calibration schemes.

involved, calibration uncertainties could have potentially been very important.

Since there is more quantitative interest in the Bi data, the effect of calibration on the $\mu_2(E_T^*)$ and $\mu_2^*(A)$ curves for Bi^{209} (i.e., on the variances before neutron correction) are shown in Figs. 12 and 13. The differences for the high x data are similar and have no marked effect on the qualitative features which are of interest for these cases.

B. Effect of Neutron Corrections

The changes in the mass and total kinetic energy variances brought about by the neutron corrections given in Section II are illustrated for the case of Bi^{209} + 65 MeV alphas in Figs. 14 and 15. The effect on the $\mu_2(E_T)$ curve is, to first approximation, a downward shift; however there is some flattening of the curve since the correction is larger for the more asymmetric cases. The curves for the mass variances almost coincide; however this results from plotting the corrected mass variance vs. the average initial total kinetic energy $\langle E_T \rangle$. for the E_T^* at which the distribution was observed, where:

$$\langle E_T \rangle \cong E_T^* \left(1 + \frac{\nu T}{A}\right).$$

The resulting upward shift of the total kinetic energy scale coupled with the downward shift of the variance makes the initial and final curves almost conincide. Only neutron corrected results will be presented in the remainder of this paper unless otherwise specified.

C. Low x Results . . . . . Comparison with Predictions from the Liquid Drop Model

This section will present the experimental results in the form of moments of the $N(E_T, A_1)$ map and compare the results with recent calculations by Nix based on the liquid-drop model.[2,29] These calculations have their origin in the work of Cohen and Swiatecki on the

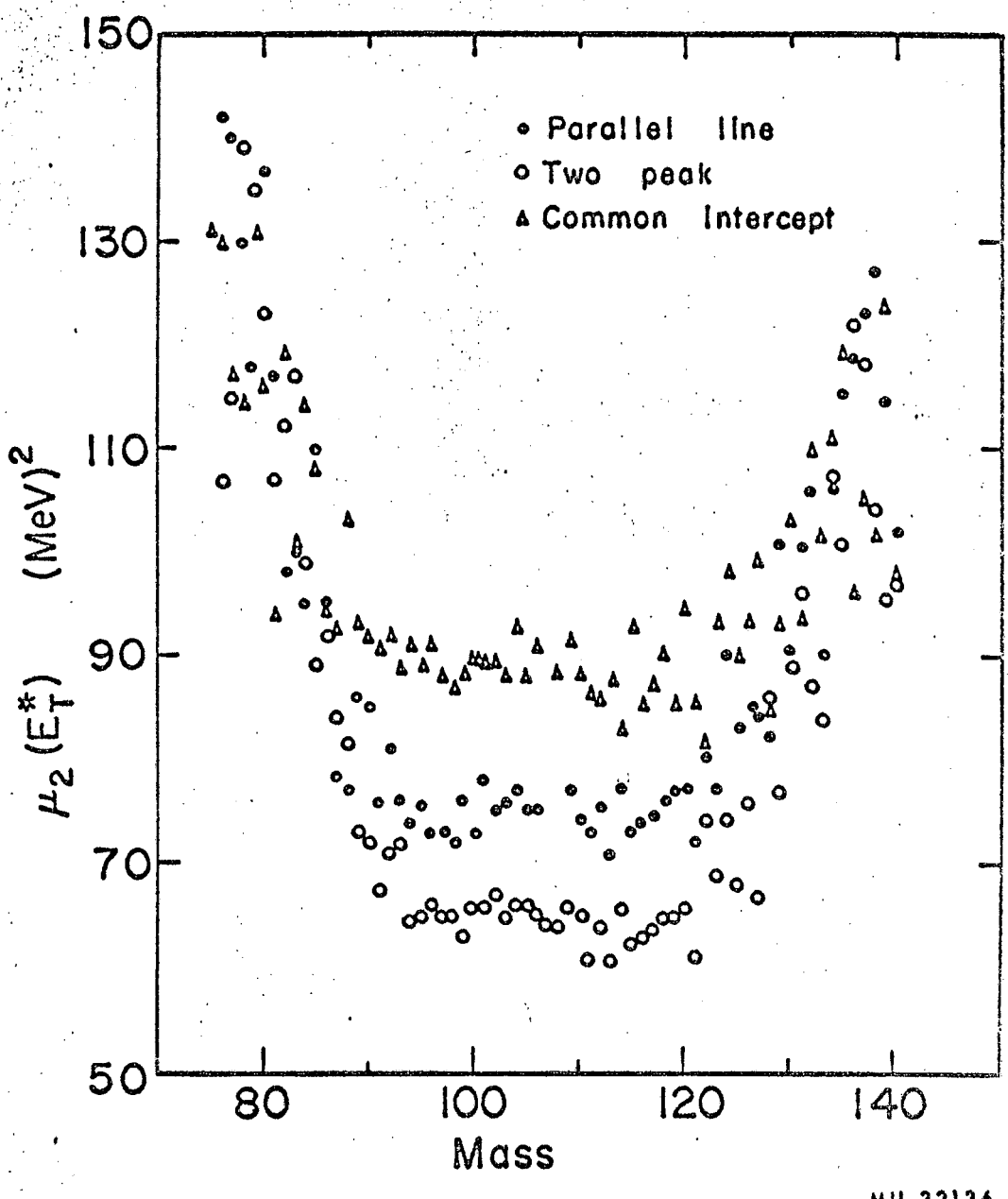

Figure 12. Comparison of variances of the total kinetic energy distributions for Bi^{209} + 65 MeV alphas as a function of mass for 3 calibration schemes. Data are not corrected for neutron emission.

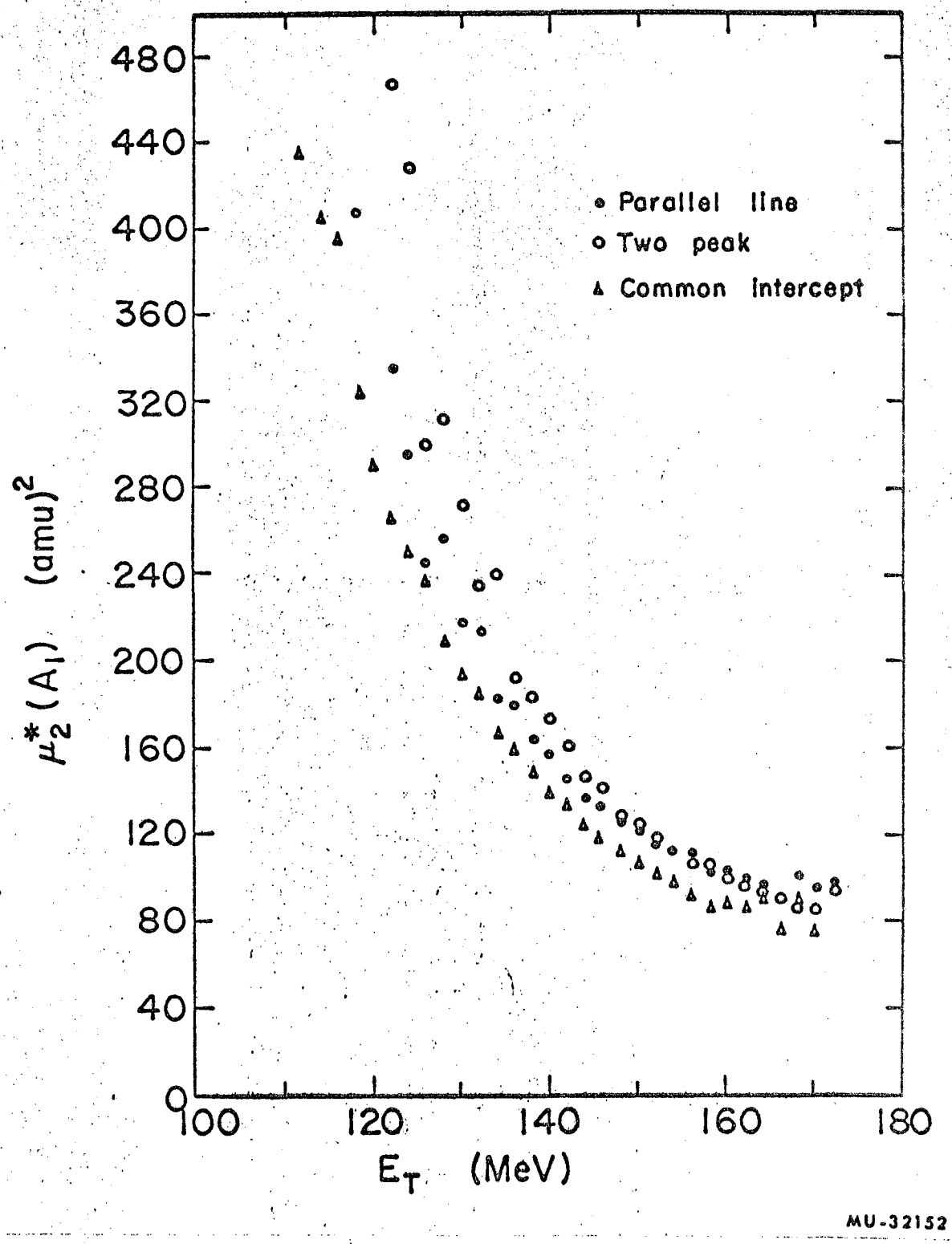

Figure 13. Comparison of variance of the mass distributions for Bi^{209} + 65 MeV alphas as a function of total kinetic energy for 3 calibration schemes. Data are not corrected for neutron emission.

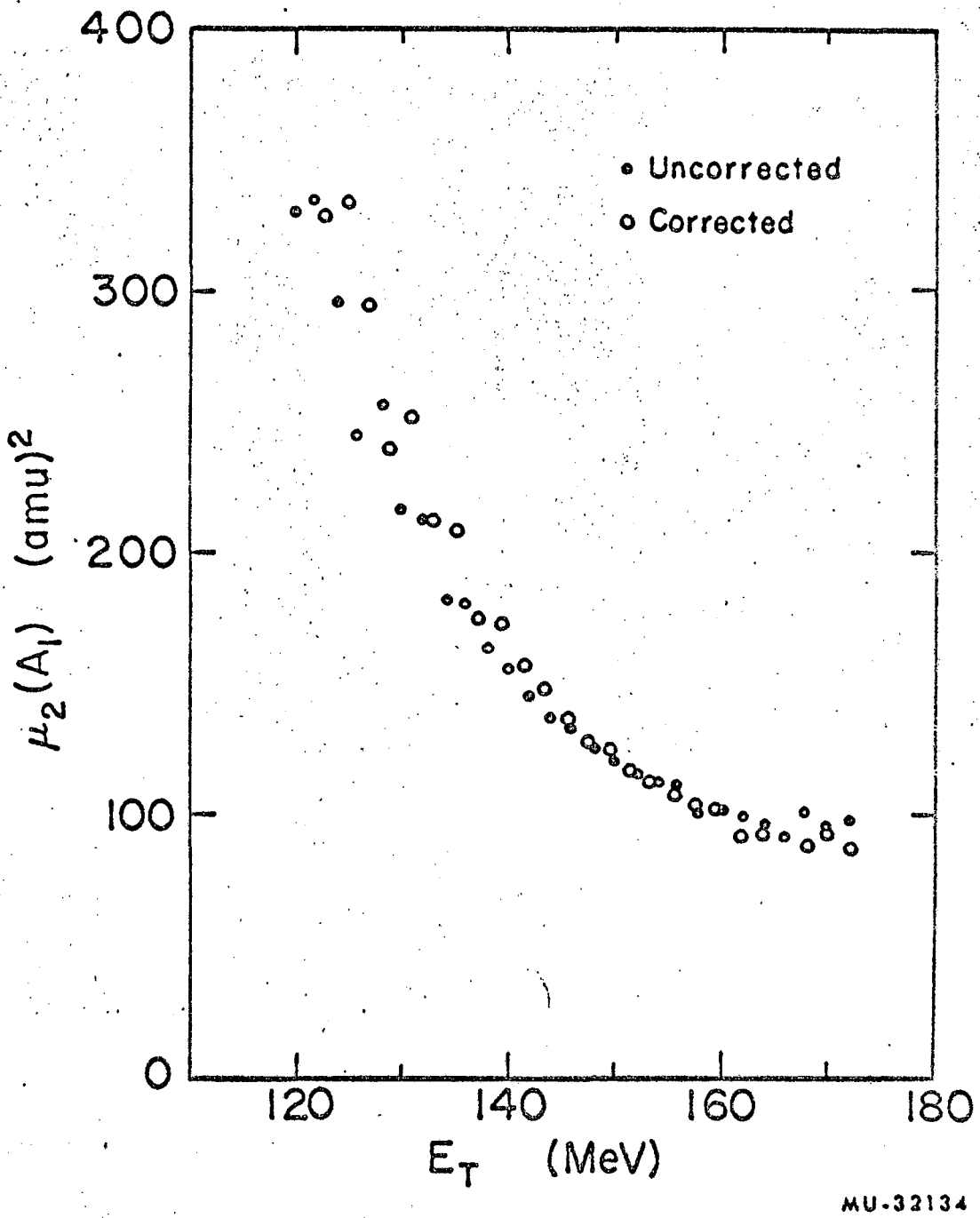

Figure 14. Comparison of neutron-corrected and uncorrected variances of total kinetic energy distributions as a function of mass for Bi^{209} + 65 MeV alphas.

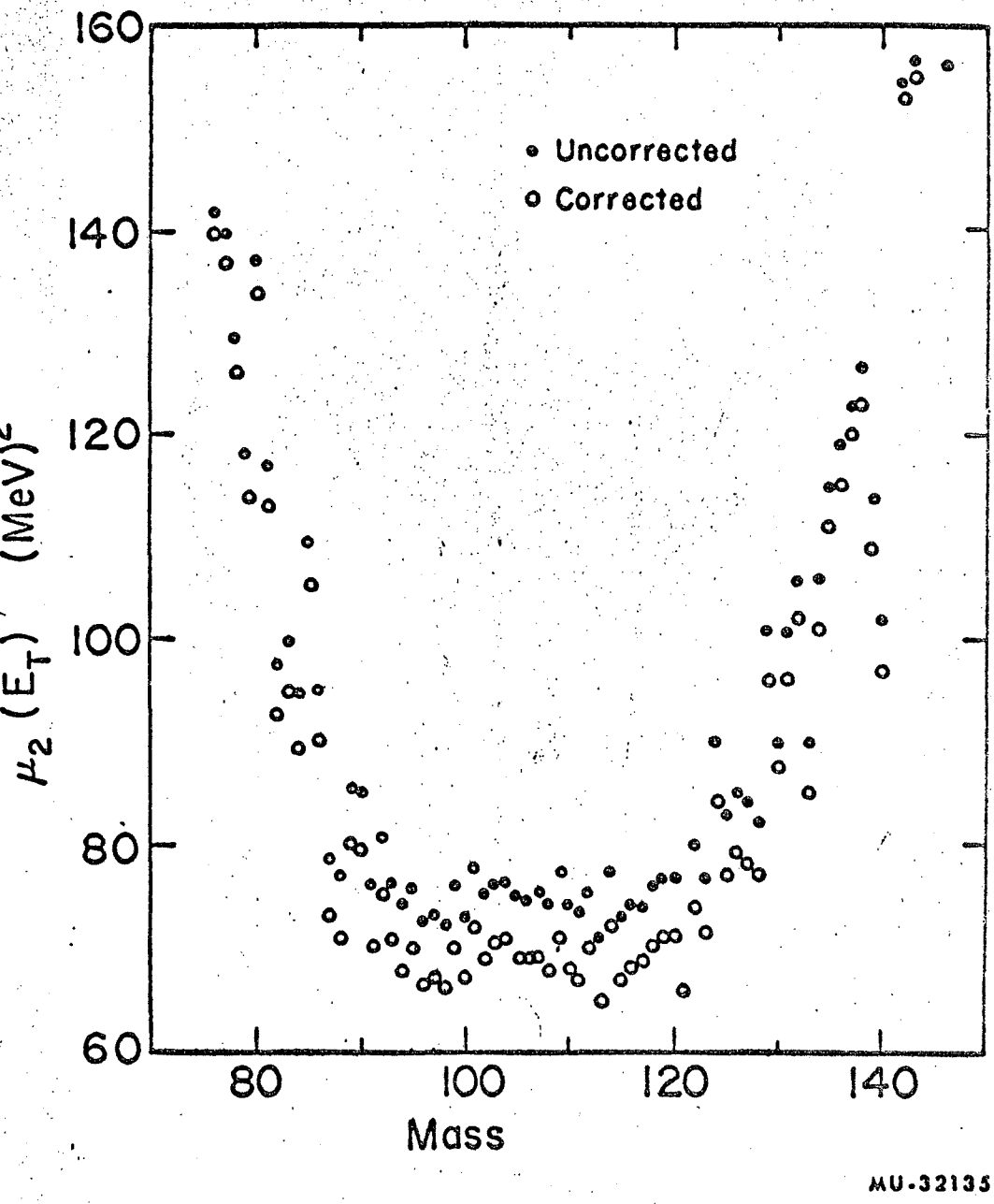

Figure 15. Commparison of neutron-corrected and uncorrected variances of mass distributions as function of total kinetic energy for Bi^{209} + 65 MeV alphas.

potential energy of a deformed uniformly-charged liquid drop. A principal result of this work has been the elucidation of saddle-point shapes as a function of x (the saddle-point shape is the critical shape in the deformation process leading to fission beyond which it is impossible to return to the initial shape). The important feature of these shapes is that below $x \cong 0.67$ the saddle point shape is quite necked-in resembling two spheroids connected by a thin neck; thus little additional deformation is necessary to cause the drop to scission. This implies that the fate of the fission event is almost completely determined at the saddle point. These simple features have led to the model used by Nix in which the fissioning nucleus is further idealized as two overlapping or separated spheroids. The co-ordinates used to describe the spheroids are shown in Fig. 16. For a given x the potential energy (the sum of the Coulomb and surface energy) is then calculated in terms of these co-ordinates. The potential energy calculations give saddle-point shapes which are symmetric tangent spheroids (i.e., the family of shapes specified by $q_1 = q_2 + q_3 = 2q_2$) up until about $x \cong 0.80$, where they change to overlapping spheroids and approach a sphere as x approaches 1.0. For $x \lesssim 0.67$ the saddle-point shapes from this model resemble the exact liquid drop shapes; thus the model is best suited for discussing fission in this region. However, for $0.67 \leqslant x \leqslant 0.80$, where the majority of the data on fission exist, the model is not expected to apply.

To calculate energy and mass distributions the dynamics of the deformed drop, as well as the statics, must be considered.[2] The fissioning nucleus at the saddle-point is assumed to be in statistical equilibrium. This allows the distributions in initial conditions (i.e., the probability of finding a given set of co-ordinates in the vicinity of the saddle-point) to be determined, using quantum mechanics whenever possible. For given sets of initial conditions at the saddle-point the classical equations of motion are solved, and the separation of the vibrating fragments is traced out to infinity. This allows the probability distributions in initial conditions to be transformed into the

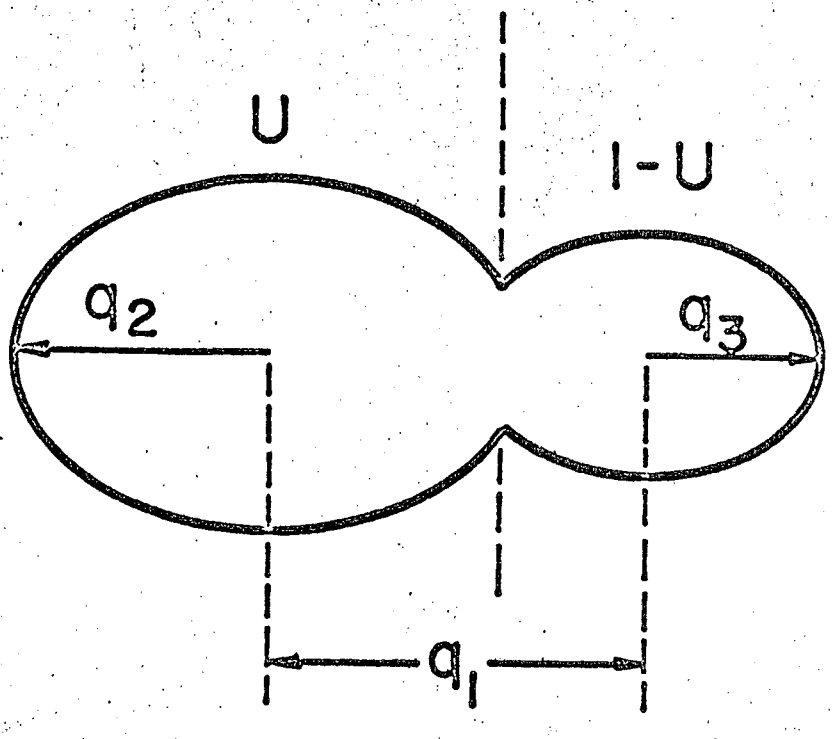

MU-32140

Figure 16. Co-ordinates used in spheroid model. q_1 is the separation of the centers of the spheroids. q_2 is the semi-major axis of the left-hand spheroid. q_3 is the semi-major axis of the right-hand spheroid. U is the fractional volume of the left-hand side of the drop.

probability $N(E_T, A_1)$ of observing a given fragment total kinetic energy E_T, and mass, A_1. The result can be represented approximately by

$$N(E_T,A_1) \cong \frac{E_0 F(E_T,A_1)}{A\, a\, \pi\sqrt{c_2 c_6}} \left(\frac{A_1 A_2}{(A/2)^2}\right) \frac{1}{E_T^2} \exp\left[\frac{(\frac{A_1}{A} - \frac{1}{2})^2}{c_6} - \frac{\left(\frac{E_0}{E_T}\frac{A_1 A_2}{(A/2)^2} - 1\right)^2}{a^2 c_2}\right]$$

$$A_2 = A - A_1$$

where A is the mass of the fissioning nucleus. Here E_0 is the total kinetic energy which results from starting the system off from the most probable initial condition (i.e., at the saddle-point). The calculable constant, a, can be physically related to the separation distance of two effective point charges having an interaction energy E_T. (See Ref. 2) In appropriate units E_0 and a depend only on x. The constant, c_2 and c_6, determine the widths of the distributions in the two initial conditions which are most important in determining the mass and total kinetic energy distributions. The distributions of initial conditions will broaden with temperature which, in turn, will cause a broadening of the observed mass and total kinetic energy distributions.[2] The factor, $F(E_T,A_1)$, has a rather complicated E_T and A_1 dependence but, in practice, has a value close to unity. A most appealing feature of these calculations is that none of the experimental data is used to determine the constants in Eq. (11); there are no adjustable parameters.

The above expression has been programmed for the LRL 7094 computer and the moments of the mass and total kinetic energy distributions calculated numerically using the same grid spacings as those used for the experimental data.

Figure 17 compares the experimental and theoretical curves for the average total kinetic energy, $\langle E_T \rangle$, as a function of mass. The error bars on the experimental points are statistical errors which are taken to be a measure of the relative error of one experimental point to

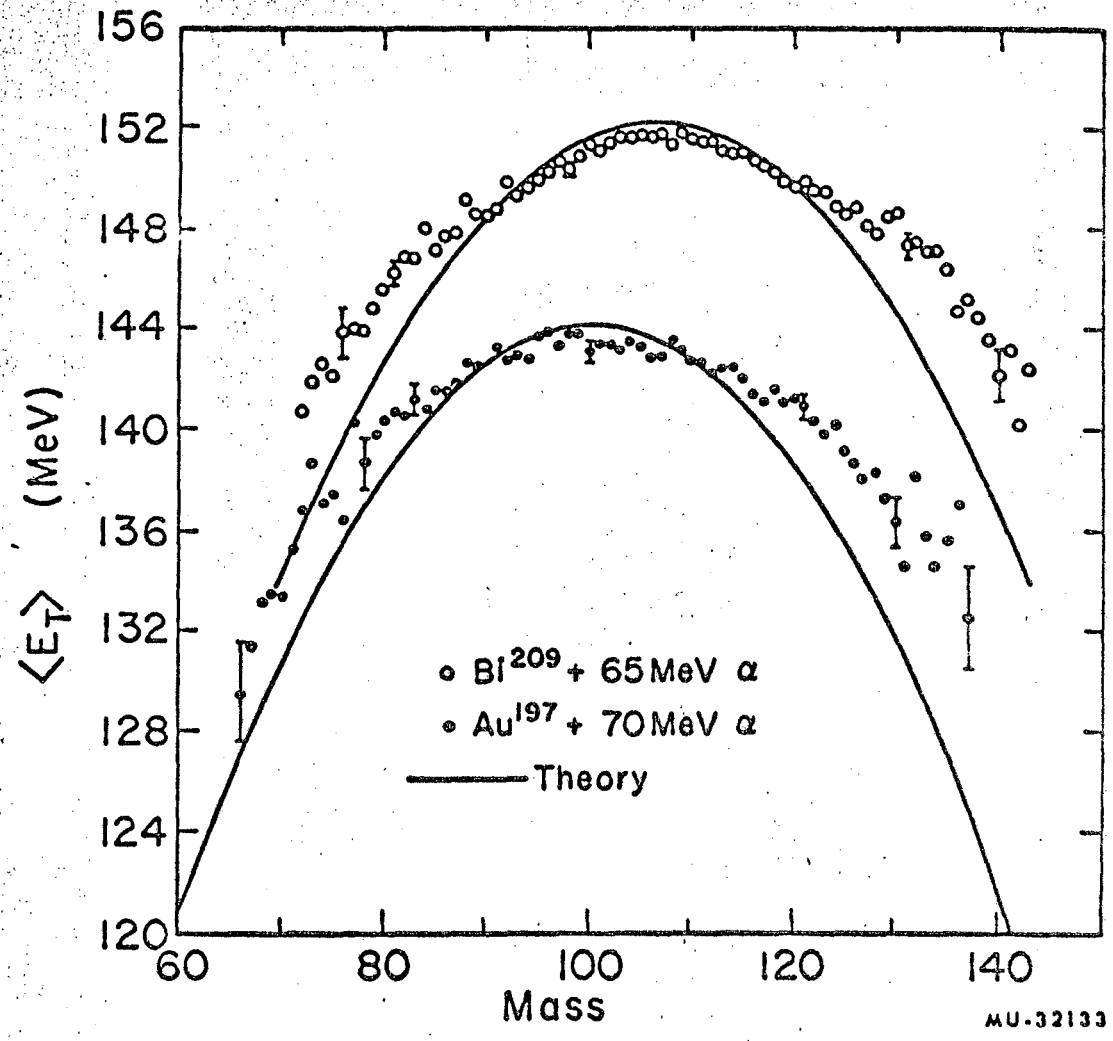

Figure 17. Comparison of theory (solid lines) and experiment (points) for the average total kinetic energy as a function of mass. Upper curves are Bi^{209} + 65 MeV alphas; lower are Au^{197} + 70 MeV alphas. The theoretical line is not normalized to the experimental points in any manner.

another. The total systematic error, including calibration and neutron correction uncertainties, is estimated as ± 4 MeV. Although the calculated curve drops off faster with increasing asymmetry, only for the extreme asymmetric events do the two curves lie outside the systematic error limits. However, the reproducibility of the deviation for both Au and Bi, which were completely independent measurements, indicates that it is probably real.

Figure 18 is a similar comparison for the variances of the total kinetic energy distributions, $\mu_2(E_T)$, as a function of mass. Again there is excellent agreement near symmetry; but here the experimental and theoretical curves show the opposite curvature with increasing asymmetry. Systematic error is estimated as ± 10 $(MeV)^2$, so the differences are significant.

In Fig. 18 the deviation of experimental points from the theoretical curve begins at masses 120-125 for both Bi and Au rather than at a constant mass ratio. This suggest that this deviation might be correlated with the doubly-closed shell at A = 132. Thus, at lower x, this argument predicts better agreement between experimental and theoretical $\mu_2(E_T)$ curves.

Figure 19 shows the variances of the mass distributions, $\mu_2(A_1)$, as a function of total kinetic energy, E_T. The overall shape of the experimental curves, particularly the rapid increase at low total kinetic energy, is well reproduced; however, the slopes of the two curves do not agree well. On the other hand systematic errors are estimated at ± 12 $(amu)^2$ which means that the deviation of the theoretical curve from the experimental points is less than experimental error for a range of total kinetic energy which includes roughly 80% of the observed events.

Table IV is a comparison between theoretical and experimental values for the overall averages and variances. Again, there is excellent agreement for all cases.

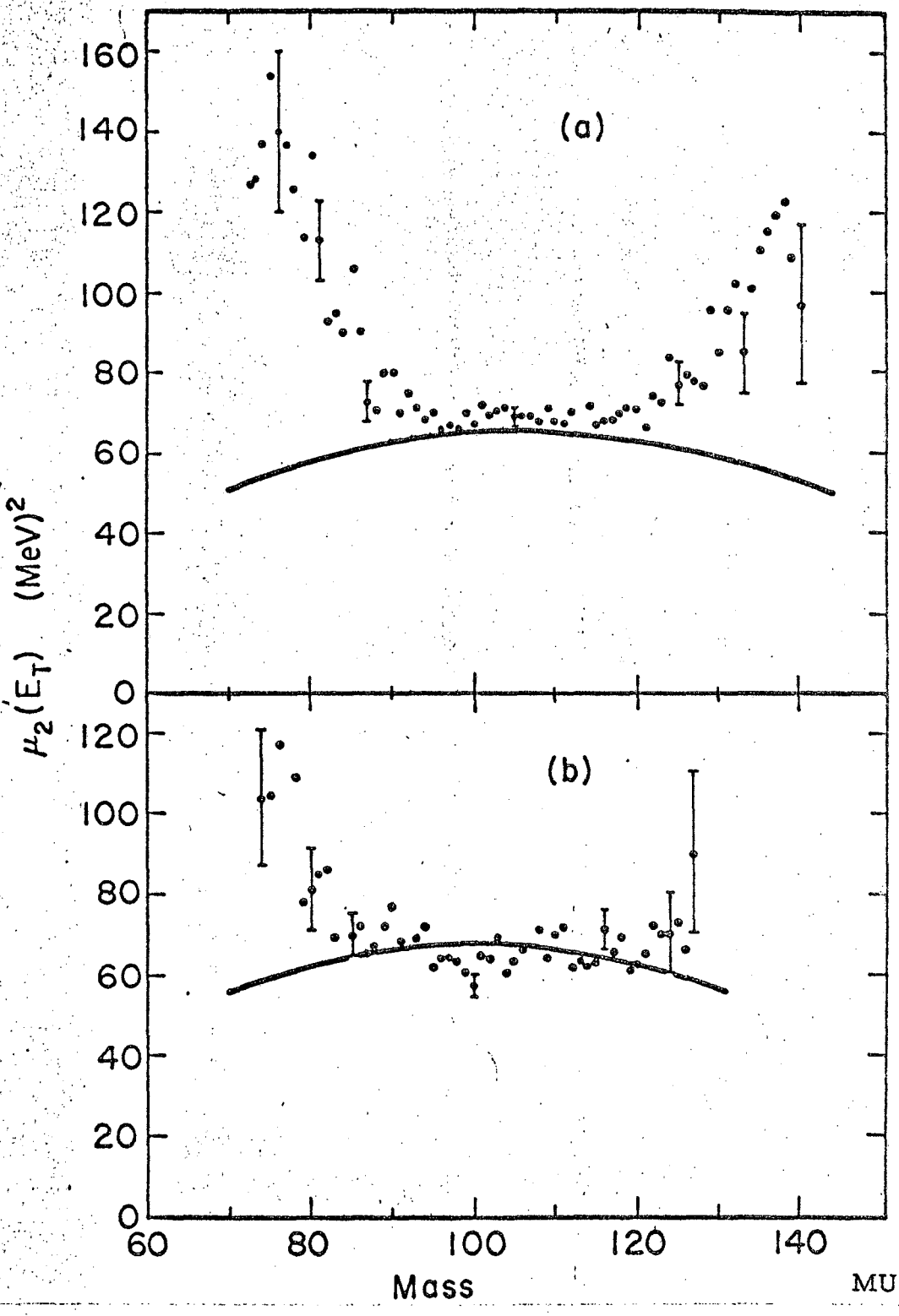

Figure 18. Comparison of theory (solid line) and experiment (points) for the variance of the total kinetic energy distribution as a function of mass for (a) Bi^{209} + 65 MeV alphas and (b) Au^{197} + 70 MeV alphas. The theoretical line is not normalized to the experimental points in any manner.

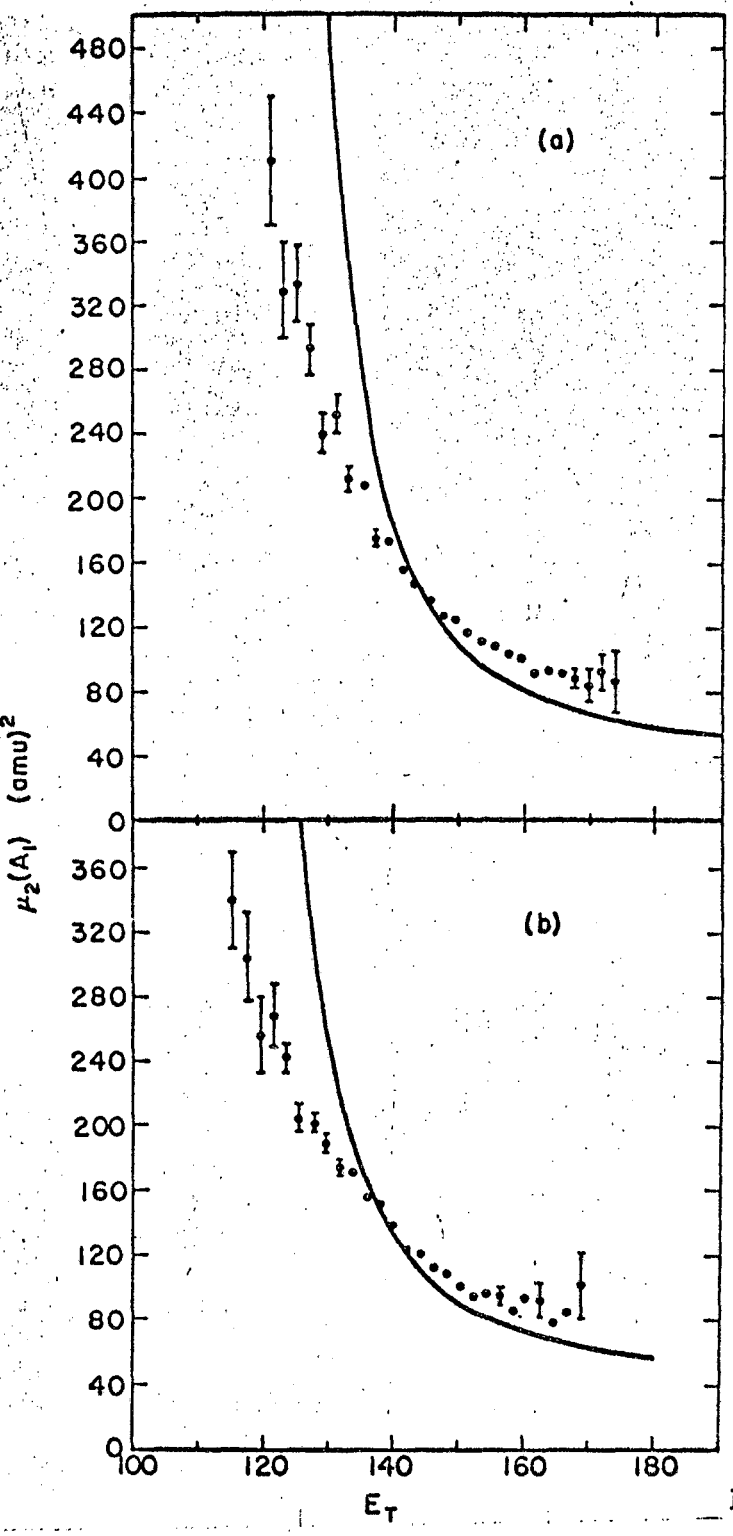

Figure 19. Comparison of theory (solid line) and experiment (points) for the variance of the mass distribution as a function of total kinetic energy for (a) Bi^{209} + 65 MeV alphas and (b) Au^{197} + 70 MeV alphas. The theoretical line is not normalized to the experimental points in any manner.

Table IV. Comparison of observed and predicted overall moments of the mass and total kinetic energy distributions for the low x cases.

	Bi^{209} + 65.0 MeV α		Au^{197} + 70.0 MeV α	
	Exp.	Theory	Exp.	Theory
$\langle E_T \rangle$	150.1 ± 4	150.4	142.1 ± 4	142.0
$\mu_2(E_T)$	74 ± 10	70.1	69 ± 10	74.3
$\mu_2(A_1)$	131 ± 12	126.3	137 ± 12	147.4

$\langle E_T \rangle$ is the overall average total kinetic energy corrected for neutrons. $\mu_2(E_T)$ and $\mu_2(A_1)$ are the neutron-corrected variances of the overall total kinetic energy and mass distributions respectively.

D. High x Results

For x above 0.67 the simple features of the saddle-point shapes which made possible the calculations discussed above no longer exist. In a narrow region of x the saddle-point shapes calculated by Cohen and Swiatecki change rapidly from shapes resembling two fragments connected by a thin neck to cylinder-like shapes which bear little resemblance to two fragments. The properties of these saddle-points do not necessarily determine completely the properties of the fragments, i.e., the saddle-point is no longer close to the scission point.

In a remarkable parallel the rather simple nature of the experimental fragment mass and energy distributions at low x become much more complex at high x.[9] This section will present these results and discuss them in the light of qualitative explanations which have been proposed concerning them. Similar results have been presented by other workers, however, the present work covers a larger range in bombardment energy; consequently this aspect of the data will be emphasized.

Of particular interest is the "two-mode" hypothesis which states that two independent mechanisms for fission can coexist within the same fissioning nucleus.[9,25,30,31,32,33] One mechanism, the "symmetric mode", is characterized by a predominantly symmetric mass distribution and lower total kinetic energy than the corresponding "asymmetric mode". Britt et al. have analyzed similar data in this region and find it consistent with the two-mode idea;[9,25] however, the idea has been questioned by others.[28,34] The point of view to be adopted here is that the two-mode hypothesis is not an alternative to or necessarily inconsistent with any theory of fission. In particular the hypothesis is vague about the physical processes which constitute the two modes; consequently it is difficult to make predictions based on the hypothesis. It will be valuable if it can organize a large body of experimental information into a consistent picture. Any theory of fission which can demonstrate that two independent coexisting mechanisms with the above properties are

possible, or, which could show why two mechanisms would appear to exist, would then automatically explain all data correlated by the hypothesis. The two-mode hypothesis has a disadvantage common to many phenomenological concepts in that it tends to absorb much of the experimental data in the formulation of the concept. One must then take care to distinguish explanations from definitions.

Table V shows the overall averages and variances of the total kinetic energy distributions studied. All limits of error are estimates of systematic errors. Also included are results from Britt and Whetstone[25] (detector) and Whetstone[8] (time-of-flight) for Th^{232} + alpha particles and from Fraser and Milton for U^{235} + thermal neutrons[10] which forms the same compound nucleus. In accordance with remarks made in Section A these detector results are comparable since they were obtained using what is felt to be a similar calibration scheme, and are based on the same Cf^{252} values. Work on Bi^{209} and Au^{197} + 43 MeV alphas has been reported by Vandenbosch et al.[35] and on Bi^{209} at 43 and U^{238} at 43 and 29 MeV by Unik et al.;[22] however, these are not comparable at present since they are based on different Cf^{252} values and a different calibration scheme. The values of $\langle E_T^* \rangle$ from the present experiments are about 3-3.5 MeV higher than those of Britt and Whetstone. This is too large to be accounted for by calibration uncertainties alone (compare Table III for Th^{232} + 25.7 MeV alphas) and is just outside the quoted limits of error for this experiment.

The $\langle E_T \rangle$ values obtained from detectors are significantly higher than those from time-of-flight measurements. This cannot be accounted for on the basis of uncertainties in the neutron correction used to obtain the detector values. No adequate explanation of this exists at the present time.

For these high x cases it is interesting to present the two-dimensional results in the form of mass profiles for various total kinetic energies. This is done in Fig. 20 for Th^{232} and in Fig. 21 for U^{238}. Results for three different bombardment energies are included. All curves are plotted in terms of normalized yield (to 200% by

Table V. Properties of the overall total kinetic energy distributions for high x cases.

System	$\langle E_T^* \rangle$	E_T	$\mu_2(E_T)$
$U^{235} + n_{th}$ (Milton and Fraser)	–	167.7	130
Th^{232} + 21.4 MeV α	170.6 ± 2.5	172.5 ± 3.2	116 ± 15
Th^{232} + 21.8 MeV α (Whetstone)	-	169.1	240
Th^{232} + 221.1 MeV α (Britt and Whetstone)	167.5	171.4	101
Th^{232} + 25.7 MeV α	169.1 ± 2.5	171.3 ± 3.2	121 ± 15
Th^{232} + 25.7 MeV α (Whetstone)	-	168.2	153
Th^{232} + 25.7 MeV α (Britt and Whetstone)	166.8	171.1	103
Th^{232} + 29.5 MeV α (Whetstone)	-	167.0	164
Th^{232} + 29.5 MeV α (Britt and Whetstone)	166.0	170.7	107
Th^{232} + 33.0 MeV α	167.6 ± 2.5	170.5 ± 3.5	124 ± 15
Th^{232} + 65.0 MeV α	162.6 ± 3.0	168.0 ± 4.5	154 ± 15
U^{238} + 25.7 α	172.9 ± 2.5	176.0 ± 3.2	139 ± 15
U^{238} + 33.0 α	170.9 ± 2.5	174.7 ± 3.5	143 ± 15
U^{238} + 65.0 α	166.7 ± 2.5	173. ± 4.0	141 ± 15

$\langle E_T^* \rangle$ and $\langle E_T \rangle$ are the overall average total kinetic energy uncorrected and corrected for neutrons, respectively. $\mu_2(E_T)$ is the neutron-corrected variance of the overall total kinetic energy distribution.

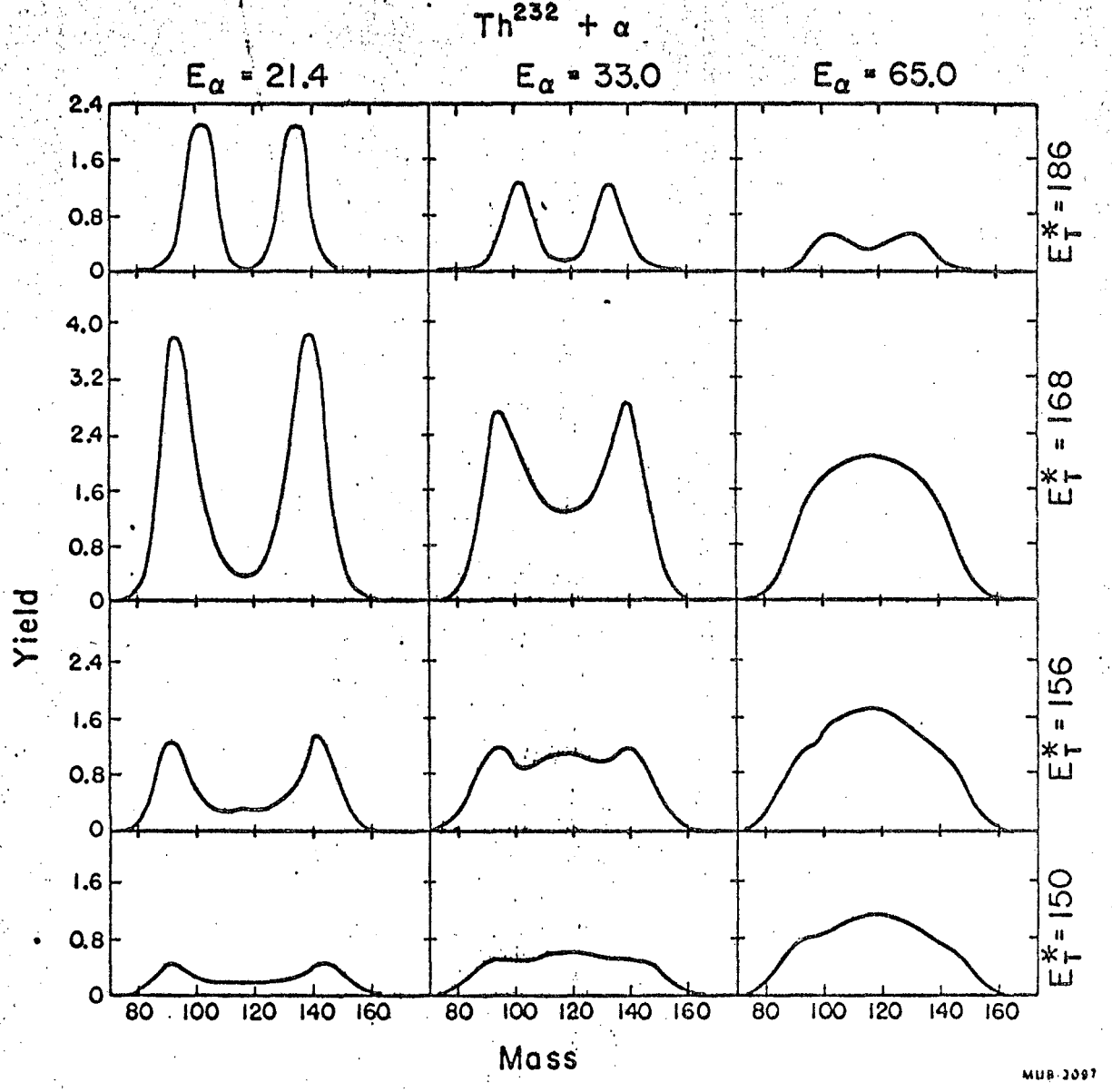

Figure 20. Mass profiles for various total kinetic energies E^* and bombardment energies E_α for Th^{232} + alphas. Total kinetic energies are not corrected for neutrons. Mass distributions are for range of ± 3 MeV from quoted E_T^* values. Yields are in percent per 3 cm where the total yield is normalized to 200%.

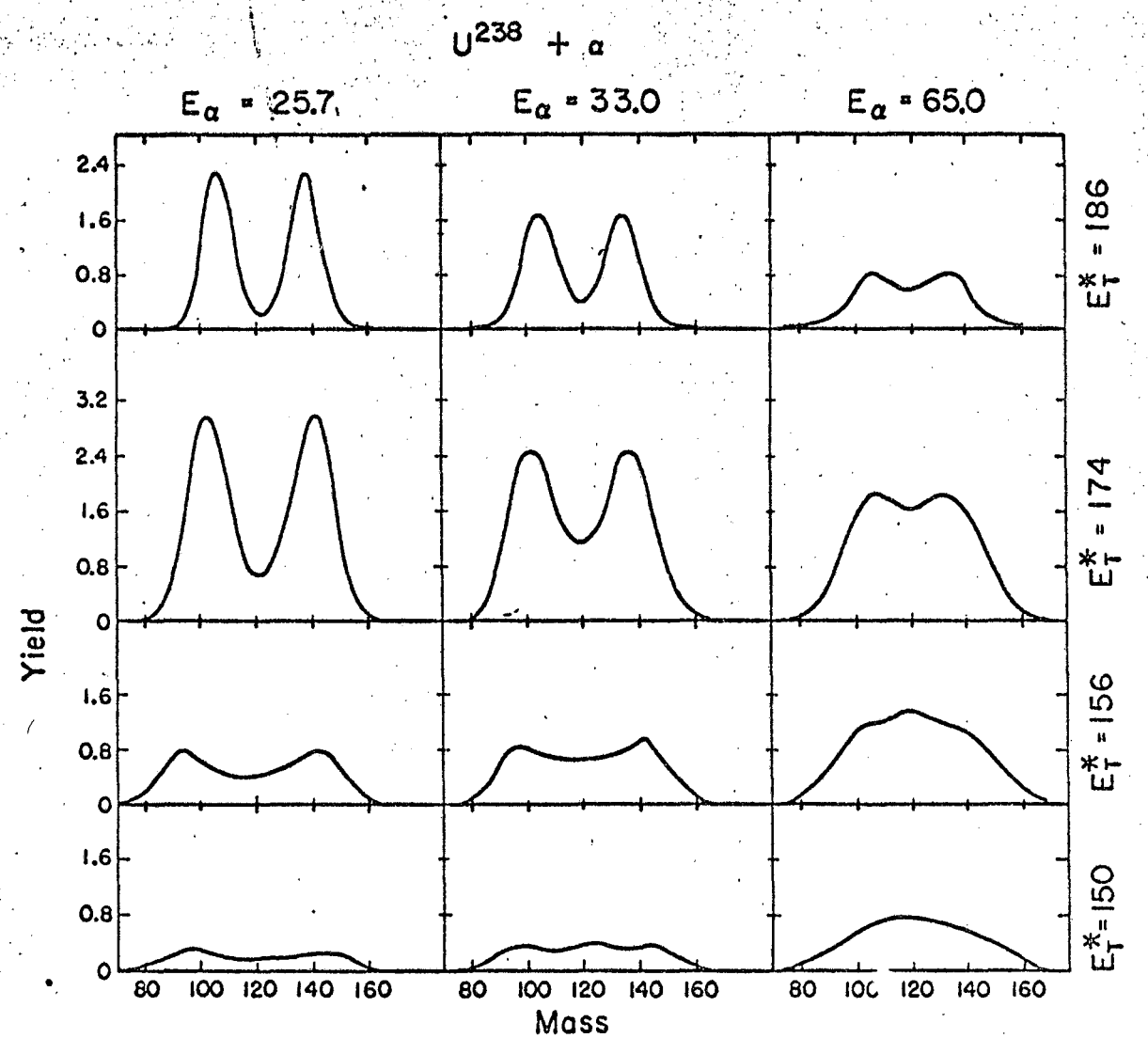

Figure 21. Mass profiles for various total kinetic energies E_T^* and bombardment energies E_α for U^{238} + alphas. Total kinetic energies are not corrected for neutrons. (Mass distributions are for range of ± 3 MeV around quoted E_T^* values. Yields are in percent per 3 amu where the total yield is normalized to 200%.)

convention); thus the relative heights and areas of the curves are comparable. All the important features of the data may be seen from these curves.

Note the tendency for the mass-yield curves to be triple peaked at low total kinetic energies and low bombarding energies. The Th^{232} distributions show a more pronounced effect than the U^{238} presumably due to the lower x value. These transform into asymmetric distributions (with increasing total kinetic energy and into symmetric distributions) with increasing bombardment energy. The increasing yield of the symmetric fission relative to the asymmetric as the bombarding energy is increased is clearly shown. There is a resemblance between these transitions from asymmetric to symmetric fission and the similar transition which occurs with decreasing x. The interpretation of this latter transition as the superposition of two distinct mass distributions has led to the revival of the two-mode hypothesis.[9,31] In the present case it would be possible to interpret the superposed symmetric and asymmetric distributions as being distributions at high and low excitation energy, respectively, since the probability of fission occuring after the emission of one or more neutrons is high.[36,37] This is especially true of the Th^{232} and, in particular, the increased asymmetry of the Th^{232} data relative to U^{238} at a given bombardment energy might be due to the larger probability for prefission neutron emission in the former. Note also the tendency of the asymmetric peaks to move closer together as the total kinetic energy increases.

We now turn to a more quantitative analysis of the data by the use of moments. Figures 22 and 23 show the average of the total kinetic energy distributions as a function of mass for the various bombardment energies studied. The "dip" at symmetric fission is now well established although there was considerable uncertainty as to their existence at one time. From preliminary work, the work of others in this region,[8,38] and the work of Haines and Thompson at high excitation energies[16,39] it was expected that the dip would vanish with increasing excitation energy. It is the manner in which the dip disappears that is of interest.

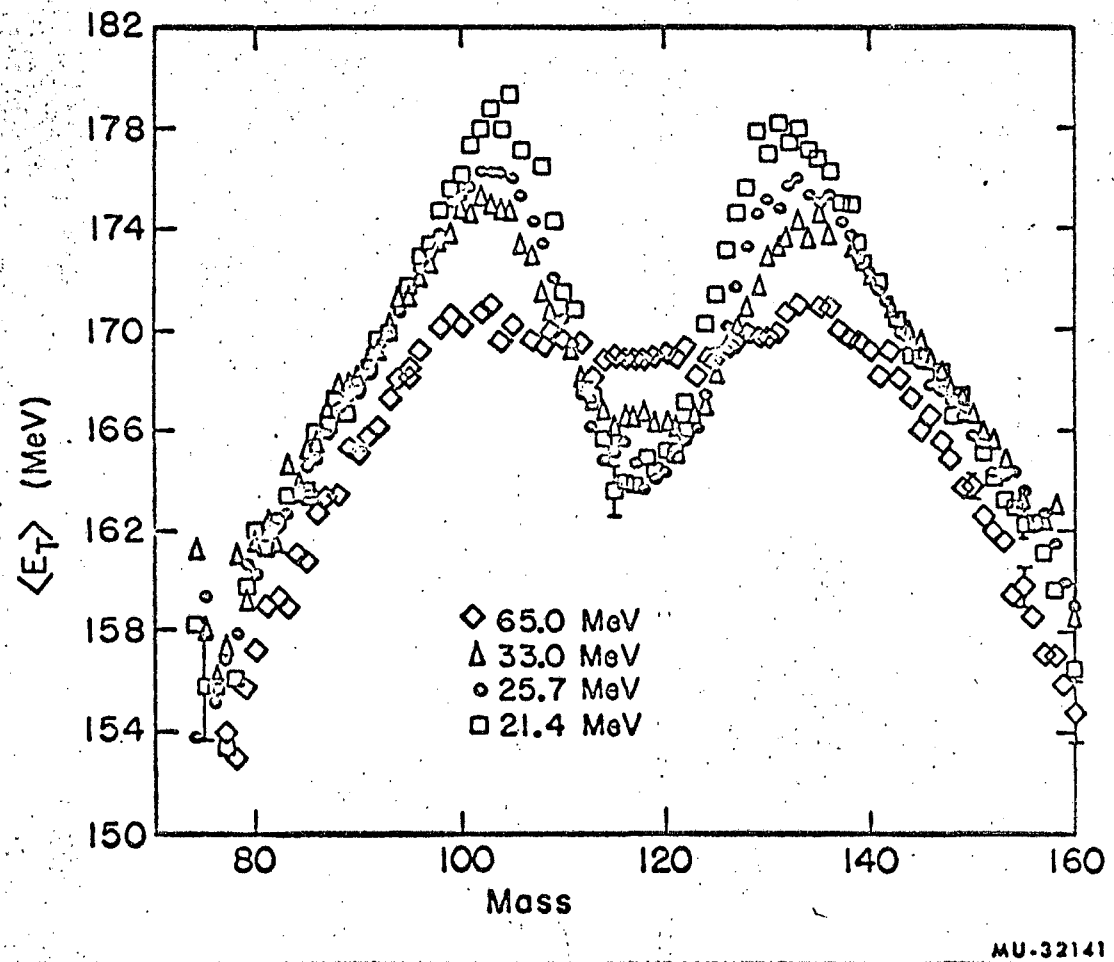

Figure 22. Average total kinetic energy as function of mass for Th^{232} + alphas at four different bombarding energies.

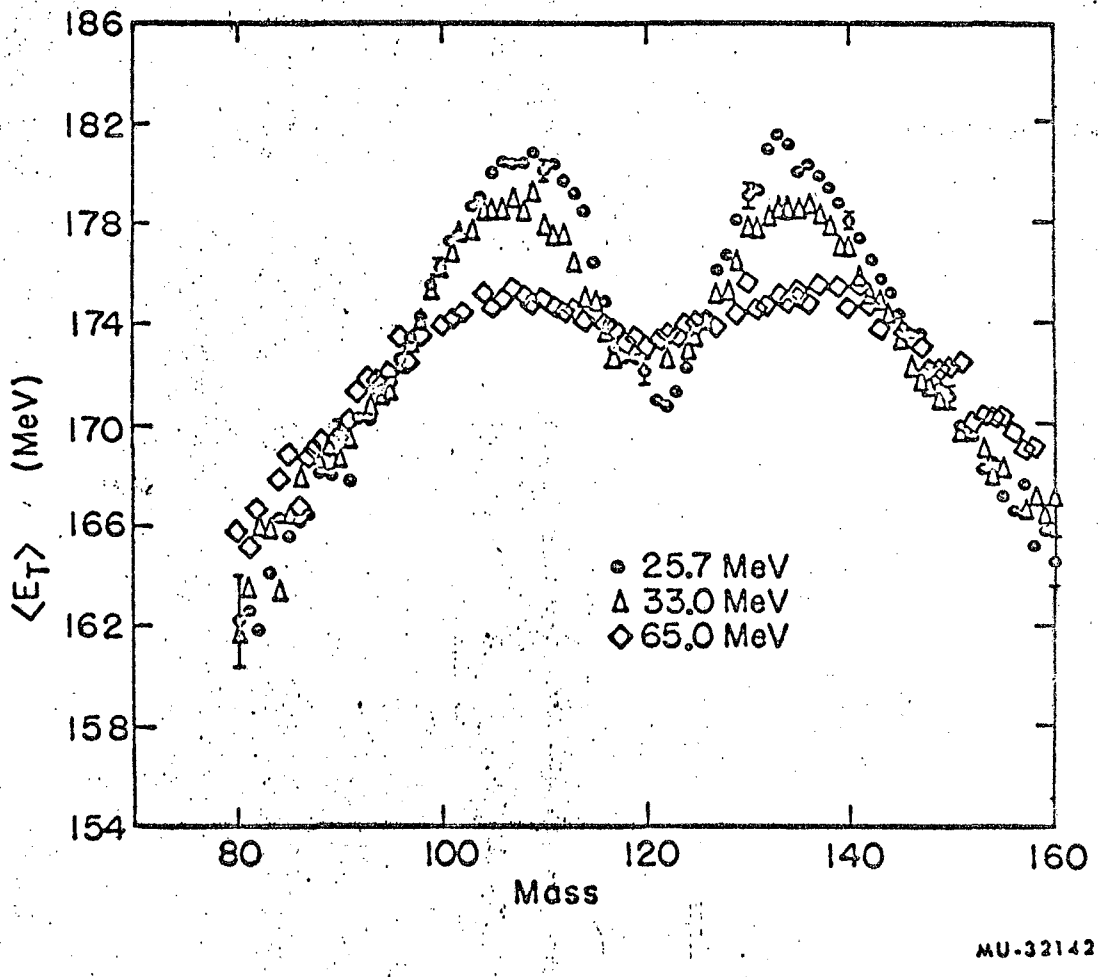

Figure 23. Average total kinetic energy as function of mass for U^{238} + alphas at three different bombarding energies.

What appears to happen is that the peak at about mass 133 decreases; whereas the valley at symmetric fission and the asymmetric wings stay relatively constant. The data of Britt and Whetstone show a similar trend.[25] This is what would be predicted by a two-mode hypothesis in which the E_T distribution for a given mass is viewed as a sum of the individual distributions from the symmetric and asymmetric modes and in which the symmetric mode grows in with increasing excitation energy. The total kinetic energy distributions for masses near A ≅ 132 then receive larger and larger contributions from the lower energy symmetric mode events. This causes the average total kinetic energy decrease in this mass region. This effect would have been difficult to reconcile with the present formulation of the hypothesis if the dip had disappeared as a consequence of an increase in the average total kinetic energy at symmetric fission. The Th^{232} curves are somewhat of an exception since $\langle E_T \rangle$ at symmetric fission is about 1.5-2 MeV higher for 33.0 MeV alphas and about 4 MeV higher for 65.0 MeV alphas than for the 21.4 and 25.7 MeV points. It is possible that this effect is not real since the 65 MeV data were taken under completely different experimental conditions (detector, target, etc.-- see Table I); whereas all the low energy data are from the same experiment. The relative error of the 65 MeV data to the remainder is thus no better than the absolute precision (± 3-4 MeV). But the 33.0 MeV curve remains significantly higher than the 25.7 and 21.4 curves if statistical errors are taken as a measure of the relative error for the low energy points.

A similar effect, although smaller and barely outside statistical error, is observed for U^{238}. There is no obvious reason why the Th and U cases should be different in this respect.

Vandenbosch has been able to qualitatively account for the dip in $\langle E_T \rangle$ vs mass curve by assuming that the effects which determine the ground state shape of the fragment remain important at the scission point.[34] Thus, at symmetry for the Th^{232} + alpha system, both of the fragments are "soft" toward deformation reflecting a predicted tendency of the fragments in their ground states to be deformed. The Coulomb

repulsion of the deformed fragments is smaller due to their increased separation; hence the average total kinetic energy is lower. When one of the fragments has a mass close to a closed shell (e.g., A $\cong$ 132), this fragment tends to assume a spherical shape which decreases the separation distance and increases the kinetic energy. On this model the dip is not associated with symmetric fission per se but rather with the mass range 112-120, and the peak is associated with the region about 132. The $\langle E_T \rangle$ curves then has three parts:

(1) a basic monotonically decreasing curve which would be obtained by some constant scission-point shape model, e.g., two tangent spheroids.

Superimposed on this is:

(2) the dip in the region of A $\cong$ 112-120

(3) a "bulge" due to the closed shell at A $\cong$ 132

$\langle E_T \rangle$ curves which show a dip have been reported for nuclei ranging from Fm^{254} to Ac^{228} and in each case the maximum in the curve occurs for A $\cong$ 130-135.[8,9,10,23,25] However, the dip tends to follow symmetry rather than the 112-120 mass region. Both of these trends can be seen by a comparison of Figs. 22 and 23. As the excitation energy is increased, one would expect the influence of the ground state properties of the fragments to be less important, i.e., the shell effects tend to "wash out". The decrease of the bulge near mass 133 is consistent with this view, but the tendency of $\langle E_T \rangle$ at symmetric fission to stay constant is not unless one assumes that the rate of "washing out" is different for the two mass regions. The relative position of the Th^{232} + 65 MeV curve does give some credibility to the latter statement. All in all, the case for a bulge in the $\langle E_T \rangle$ curve at A $\cong$ 132 being due to a shell effect is strong; however, the analogous case for the dip is on much weaker ground.

Figures 24 and 25 show the variances of the total kinetic energy distributions as a function of mass. The shape of these curves is consistent with the two-mode hypothesis because, with increasing asymmetry, the superposition of a displaced distribution from the asymmetric

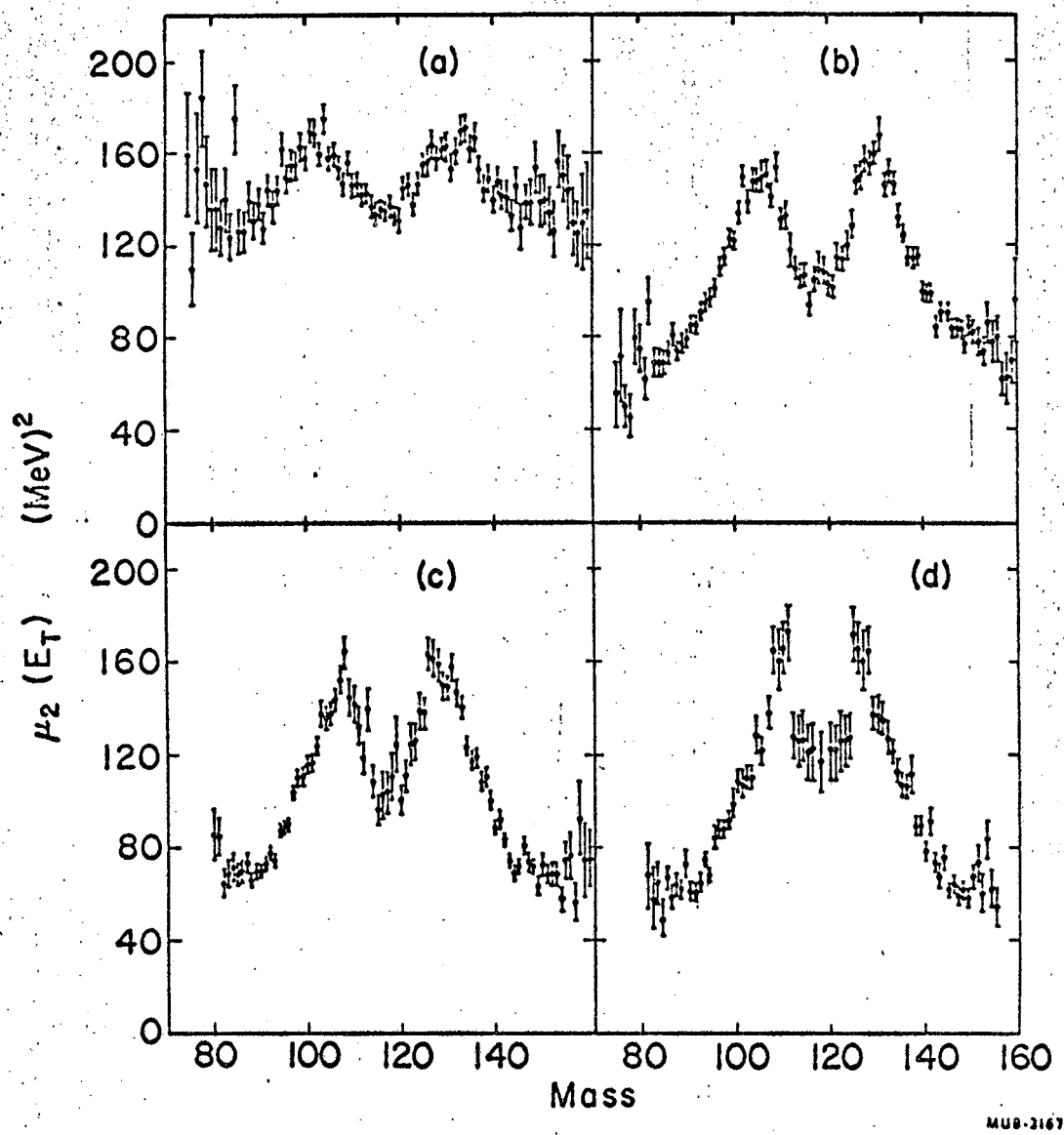

Figure 24. Variances of total kinetic energy distributions as a function of mass for Th^{232} + alphas at four different bombarding energies: (a) 65.0 MeV, (b) 33.0 MeV, (c) 25.7 MeV, (d) 21.4 MeV. The points in the region from mass 117 to 129 for the 21.4 MeV curve have been folded to improve statistics.

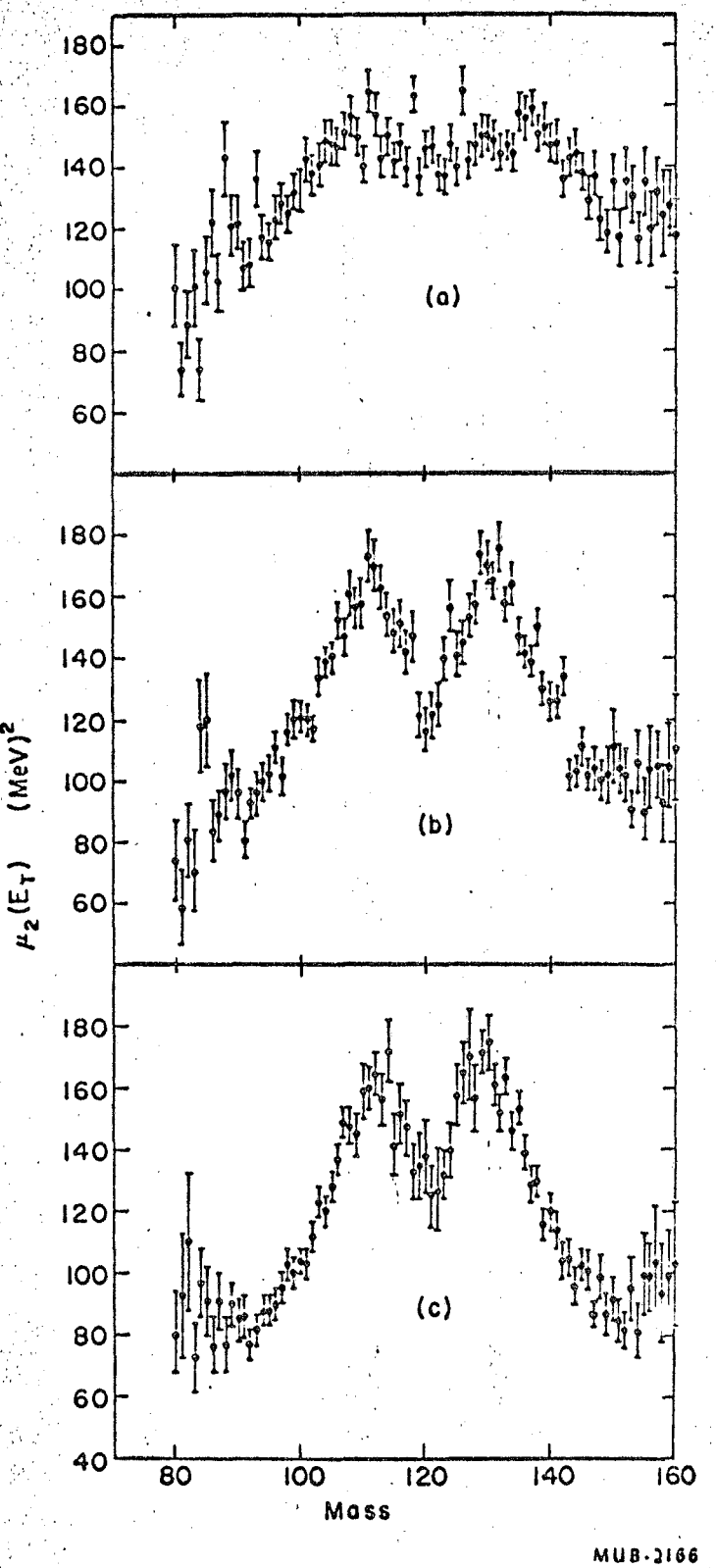

Figure 25. Variances of total kinetic energy distributions as a function of mass for U^{238} + alphas at three different bombarding energies: (a) 25.7 MeV, (b) 33.0 MeV, and (c) 65.0 MeV.

mode —— combined with a decreasing yield of the symmetric mode —— has a broadening effect on the overall distribution. Britt et al. have made a detailed analysis of similar curves including an attempt to draw quantitative conclusions concerning the properties of the modes.[9] Repetition of such an analysis on the present results would serve no useful purpose. The only prediction which the two-mode hypothesis can make on the effect of increasing excitation energy is that the variances should increase at those masses where the contribution of the symmetric mode is becoming increasingly more significant. However, this prediction is nullified because, in general, the distributions are expected to broaden with increasing temperature.

Several features of these curves are, nevertheless, worthy of comment. (1) The maxima in the variance curves occur about 3-5 mass units lower than those in the average total kinetic energy curves. (2) The maxima in the variance curves tend to shift to higher masses with increasing bombardment energy. A somewhat smaller effect can be seen in Figs. 22 and 23. (3) The dip again appears to be correlated with symmetric fission and tends to die out with increasing bombardment energy; however, the manner in which this occurs is more complex than for the averages. What appears to happen is

(a) the asymmetric wings (around $A_1 \cong 150$) tend to rise steadily;

(b) the maxima tend to stay about constant;

(c) the dip at symmetric fission remains roughly constant for the low energy points, but show a significant rise at 65 MeV.

(There is actually a decrease in the variance at symmetric fission between $E_\alpha = 21.4$ and $E_\alpha = 25.7$ for Th^{232} and between $E_\alpha = 25.7$ and $E_\alpha = 33.0$ for U^{238} however, it is not outside statistical error.) Neutron emission before fission would counteract the tendency of the variance to increase with increasing bombardment energy; however, one would expect this effect to be more important for the more asymmetric fission. This suggests that at least (c) above is not due to this effect.

The overall mass yield curves shown in Figs. 26 and 27 are actually a by-product of the more detailed information obtained in a two-dimensional

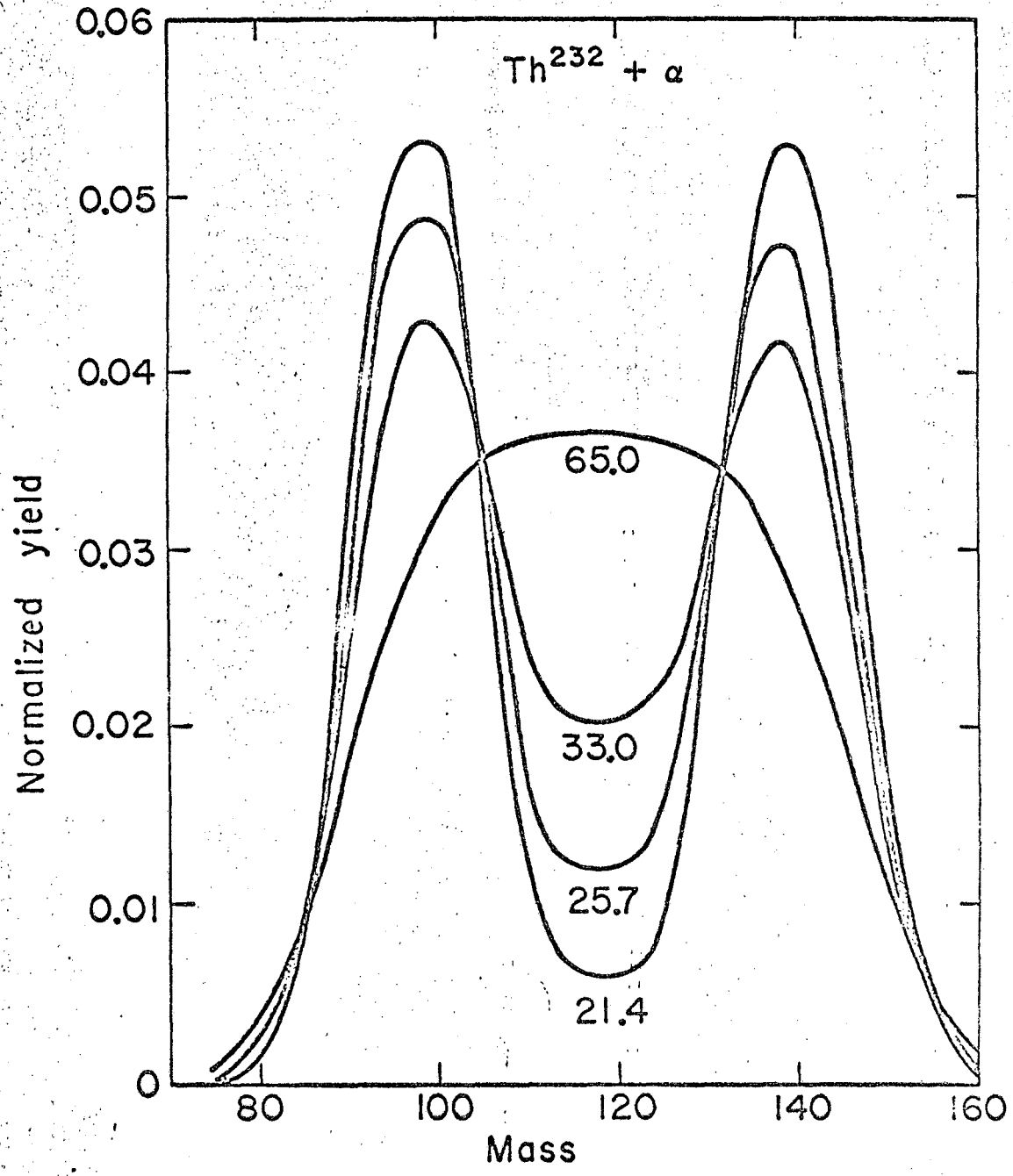

Figure 26. Mass yield curves for Th^{232} + alphas showing transition from asymmetric to symmetric fission. Yields are normalized to total of 200%.

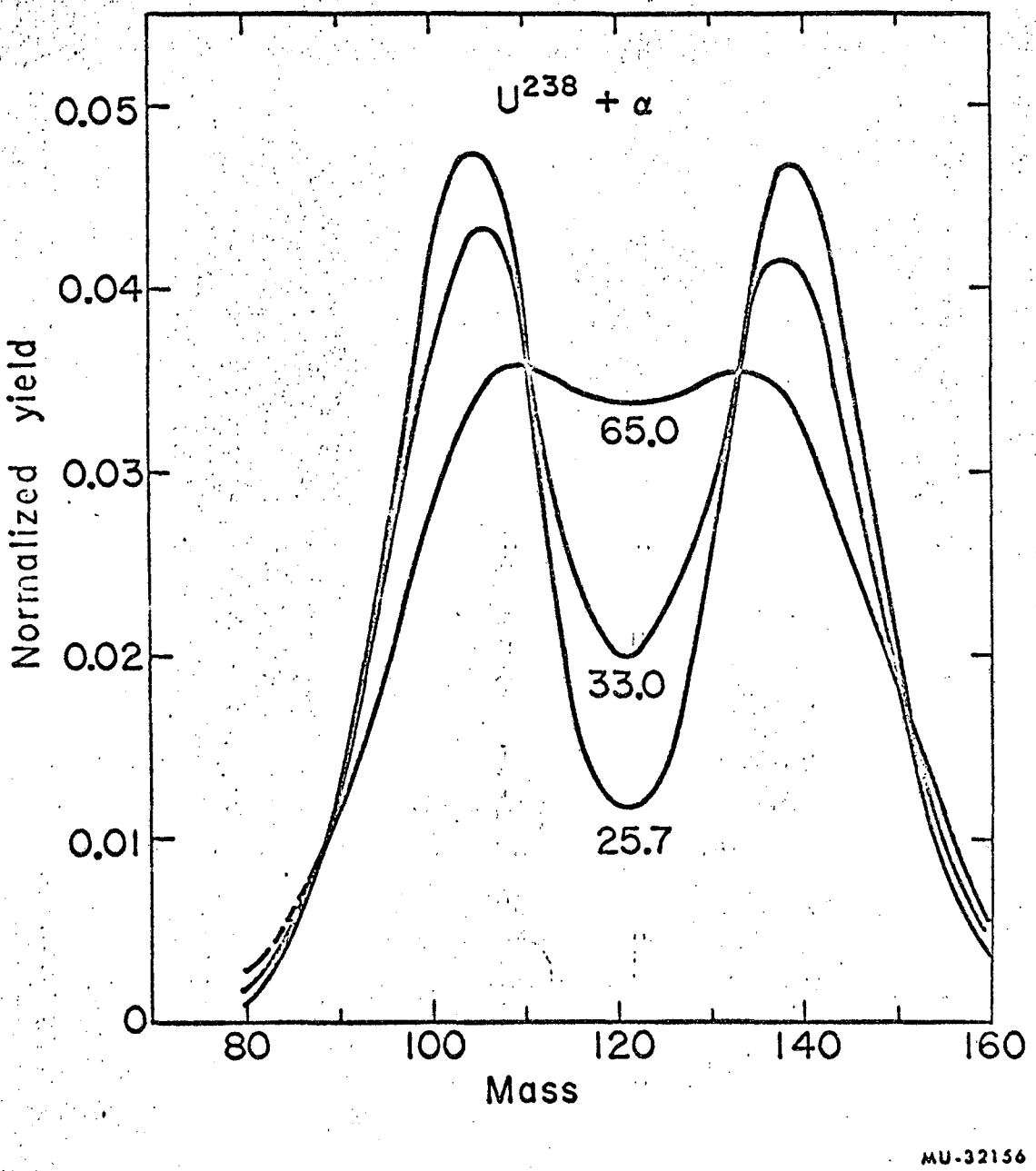

Figure 27. Mass yield curves for U^{238} + alphas showing transition from asymmetric to symmetric fission. Yields are normalized to total of 200%.

experiment; however, there is still considerable interest in these curves. Further these distributions are least subject to calibration errors. Such curves do not possess the mass resolution of mass spectrometric or radiochemical measurements; but, on the other hand, there are no missing mass regions and the relative error of one part of the curve to another is small which may not be true in radiochemical work. The net result is that the overall shape of the mass yield curves and the transition from asymmetric to symmetric fission is better demonstrated by experiments of the type described in this work.

Figure 28 illustrates some properties of the mass distributions as a function of total kinetic energy. For the case of 21.4 MeV alphas + Th^{232} the fission is predominantly asymmetric and one wants to present the properties of the individual asymmetric peaks. However, the strong variation of the yield at symmetric fission with total kinetic energy causes significant changes in the calculated statistical moments which are not necessarily related to the properties of the heavy peak itself. Thus Figs. 28a and 28b give the most probable heavy mass and the half-width at half-maximum measured on the high mass side of the heavy peak. The mass distributions were folded for the purpose of this calculation. For comparison Fig. 28c is a plot of $(\mu_2^*(A))^{1/2}/2$ for 65 MeV alphas + Th^{232} which is of comparable magnitude to the above half-width. In this case the variance was calculated over all masses since the fission is predominantly symmetric. A monotonic decrease in the width of the mass distributions with increasing total kinetic energy is something which all fissioning systems seem to have in common (compare Fig. 19) although there are individual differences in slope and curvature. This similarity supports the interpretation of such curves made by Haines and Thompson which states that these curves reflect the approximately-parabolic shape of the average energy release curve taken as a function of mass.[39] High total kinetic energies can only be obtained from a more restricted range of mass splits; consequently the widths of these mass distributions are smaller. Such a thermodynamic explanation should hold at any x and is consistent with the experimental data.

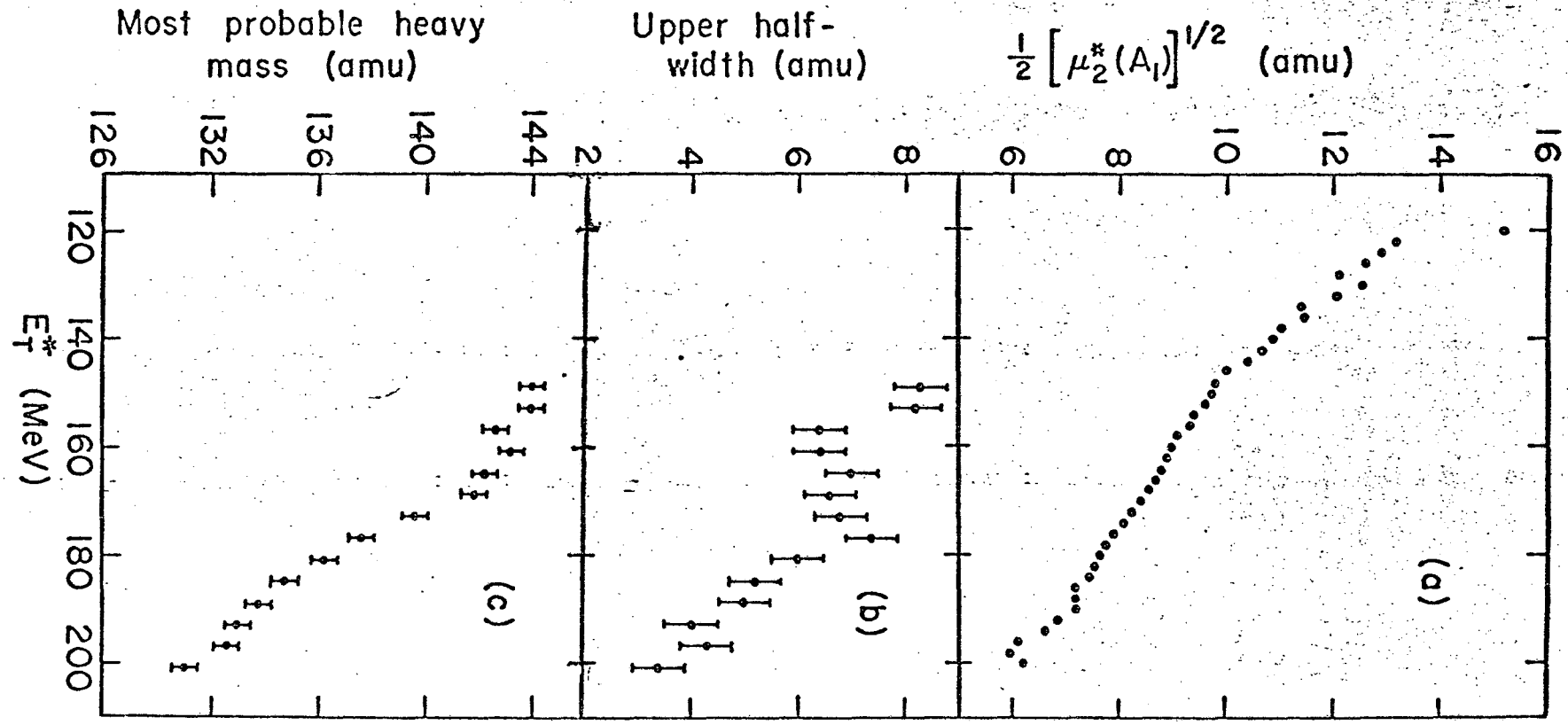

Fig. 28. Properties of the mass distributions as a function of total kinetic energy for Th^{232} + alphas. Data are not corrected for neutrons (a) most probable heavy mass for E_α = 21.4 MeV, (b) upper (high mass) half-width at half maximum for 21.4 MeV alphas, (c) $1/2\,(\mu_2^*(A_1))^{1/2}$ for 65 MeV alphas. This is equivalent to a fourth-width at $1/2\,(\mu_2^*(A_1))^{1/2}$ half-maximum for a predominately symmetric mass distribution.

MU-32149

The heavy peak also shows a monotonic decrease with increasing total kinetic energy, i.e., the two asymmetric peaks move closer together as was noted in the discussion on Figs. 20 and 21. One should realize, however, that this trend is implicit in the data that have already been presented. Given that the average total kinetic energy is a decreasing function of the heavy mass, it is inevitable that the average mass will be a decreasing function of total kinetic energy unless the two-dimensional $N(A_H, E_T)$ distribution is very irregular.

In the light of Fig. 28a recall the oft-quoted result that the heavy peak of the overall mass distribution tends to stay constant for all fissioning nuclei (see Figs. 26 and 27). Obviously this is only true on the average, because, as a function of total kinetic energy, the heavy mass peak varies by about 15 mass units.

V. CONCLUSION

The most satisfying aspect of this work has been the comparison of the low x data with the theoretical liquid drop predictions. The rather good agreement between the experimental and theoretical results gives one reason to believe that the liquid drop model of fission may be capable of accounting for at least the main features of low x fission. It is important for the progress of fission theory to decide this point. This calls for a considerable experimental effort in order to obtain data over as wide a range in x (below 0.67) and excitation energy as possible. At the present time medium-energy fixed-frequency cyclotrons are available which can produce excitation energies in the range from 20-100 MeV. At the higher energies the fission cross sections for the heavier rare-earth elements should be high enough to enable mass-energy measurements to be carried out.

In addition to mass-energy measurements it may also be possible to provide experimental values for fission barriers to compare with the liquid drop predictions by utilizing the ability of certain materials, such as mica, to preferentially register fission-fragment tracks.[40] This technique may allow measurement of the very small fission cross sections for elements perhaps as far down as silver.

Although the present liquid-drop theory is capable of predicting the distribution in the vibrational energy of the separating fragments, the corresponding experimental measurements of the neutrons resulting from the deexcitation of the vibrating fragments does not seen feasible in the near future in the low x region; thus mass, kinetic energy, and threshold measurements will have to provide the immediate test of the theory.

Efforts should also be made to improve the overall precision of fission energy measurements. Improved precision would allow the reliable measurement of differences between experimental and theoretical curves which may be significant in determining the influence of shell effects on nuclear fission.

ACKNOWLEDGMENTS

The completion of this work was only possible through the cooperation of many other persons. I wish to express my deepest appreciation to:

Dr. Stanley G. Thompson for continual help and encouragment through the many ups and downs of this work.

Dr. Wladyslaw J. Swiatecki and Mr. J. Rayford Nix for many hours of patient tutoring on the theoretical aspects of this work, and for the use of their work prior to publication.

Franz Plasil, Harry R. Bowman, Llad Phillips, Dr. Eldon L. Haines, Dr. Reinhard Brandt, Dr. John Alexander, and Dr. Torbjørn Sikkeland for help with the experiments and numerous discussions of this work.

Professor Glenn T. Seaborg for his interest in the early phases of this work.

Leonard E. Gibson and Sam Nolan for always having the proper capacitor to keep the electronics running and to George Simonof and Michiyuki Nakamura for help with the multidimensional analyzer.

Hermann Grunder and the crew of the 88-inch cyclotron for help in setting up the bombardments, John Meneghetti and the accelerator technicians for splendid mechanical work on short notice, and to John Wood and the crew of the old 60-inch cyclotron for help in the early phases of this work.

H. C. Britt and S. L. Whetstone, Jr., J. C. D. Milton and J. S. Fraser, H. W. Schmitt, et al. and W. M. Gibson for use of data prior to publication and for useful discussions.

Mrs. Jean Rees for plotting, calculating, and advice on administrative matters.

My wife, Eileen, for typing, plotting, and forbearance during the period of this work.

The National Science Foundation and The General Electric Foundation for financial support.

This work was performed under the auspices of the U. S. Atomic Energy Commission.

APPENDIX A

Details of the Electronic System

A block diagram of the electronic system is shown in Fig. A1. The Goldsworthy Model VI linear system was operated in the double-differentiating mode using rise times in the 0.2-1.0 μsec. range.[12] In order to improve stability: (1) the variable preamplifier feedback capacitor was set at its maximum value (13 pF). With this setting the preamplifier will become completely charge sensitive (i.e., output pulse height independent of detector capacitance) at a detector capacitance of about 250 pF or less. (2) The bias supply resistor was decreased from 22 to 0.5 megohms. This reduces the effect of any changes in detector leakage current. Linearity checks on the whole system were made prior to each run.

Coincidence gate widths were set at 0.3-0.4 μsec. and a delay curve using Cf^{252} fission fragments was taken prior to each run to insure that the entire coincidence system was functioning properly.

The basic features of the multi-dimensional analyzer, designed and built by M. Nakamura and G. S. Simonof, are schematically shown in Fig. A2.[14] The analyzer utilizes pulse stretchers to receive and hold the input pulses until they can be analyzed sequentially by a single analog to digital converter (ADC). A Technical Measurement Corporation 256 channel pulse height analyzer was modified to provide the ADC and the buffer memory. The memory, which previously held 2^8 channels by 2^{18} events, was altered such that two pulse heights up to 256 channels could be stored in the location previously occupied by the number of events for a single channel. The pulse heights from successive events are then stored in turn along what was previously the channel axis. When the capacity of the memeory (1024/n where n is the number of dimensions which must be an even number) is reached, the memory is dumped onto magnetic tape. A most useful feature is that the analyzer is capable of reading back its own tapes to give the singles

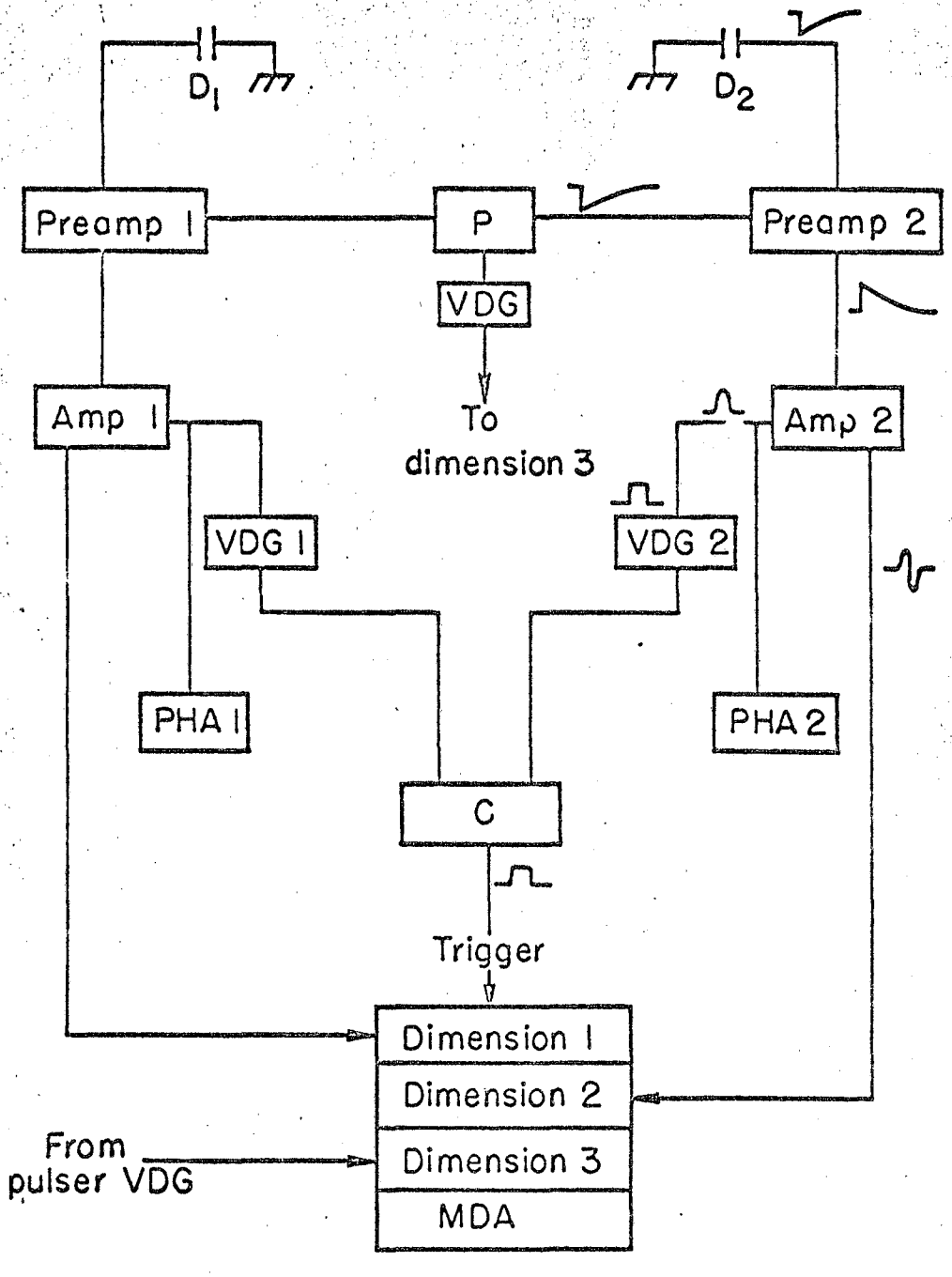

Figure A1. Block diagram of electronics (d)semiconductor detectors; (PRE) preamplifiers; (AMP) linear amplifiers; (VDG) variable delay and gates; (PHA) monitor pulse height analyzers; (c) slow coincidence unit; (MDA) multi-dimensional analyzer; (P) pulse generator.

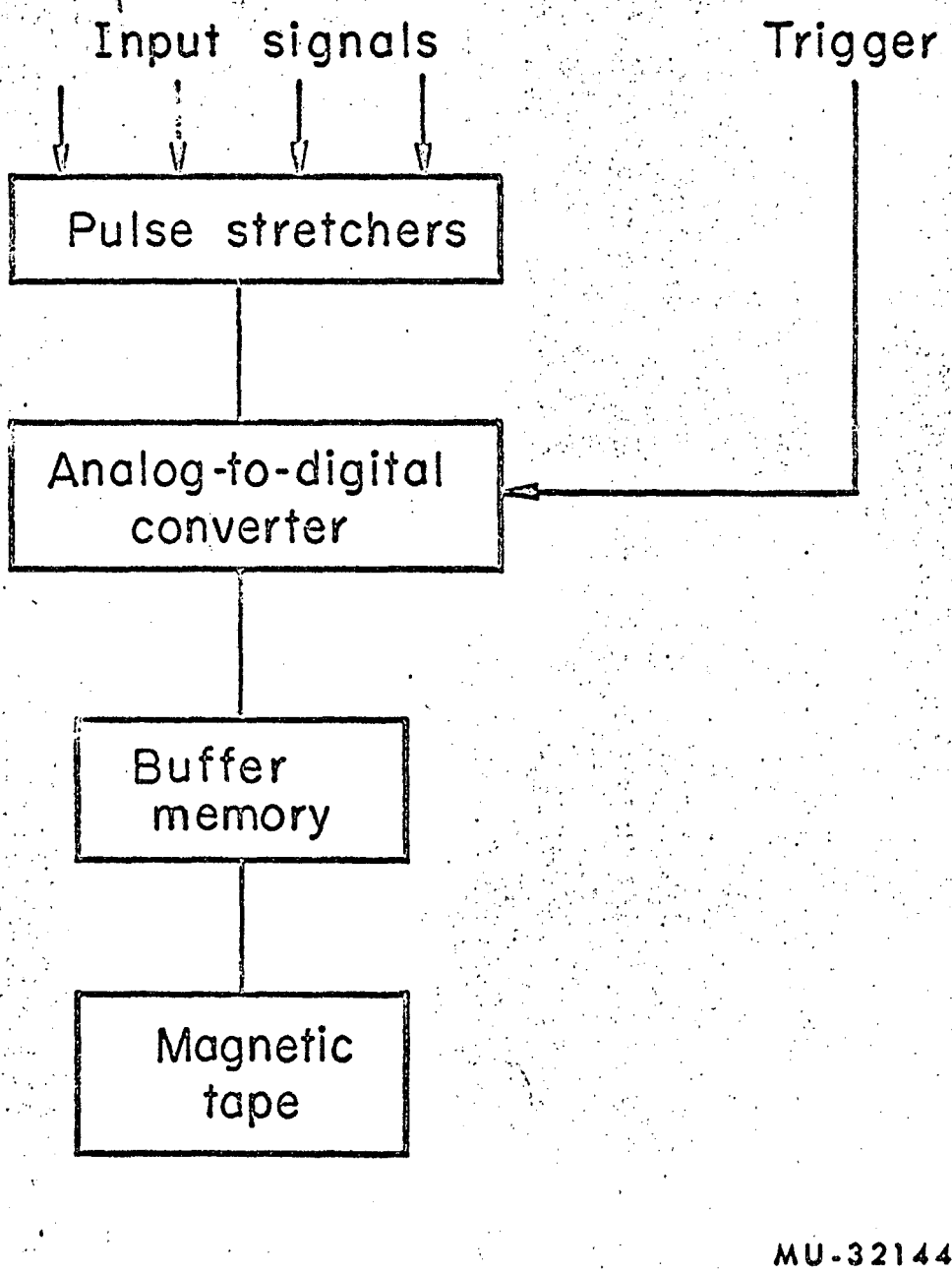

Figure A2. Basic features of the multi-dimensional analyzer.

distributions in each of the dimensions which are a valuable check on what has been written onto tape.

The Au^{197} + 70 MeV α measurement was made in collaboration with F. Plasil using a somewhat different electronics including a faster coincidence system. These electronics will be described in a later report.[41]

APPENDIX B

Symmetry Properties of the Mass-Total Kinetic Energy Distributions

If the two-dimensional data are not folded, the required symmetry properties of the distributions provide a valuable check on systematic errors which are not the same for each detector, e.g., difference in detector resolution, errors in the backing foil thickness correction, etc. Some of these properties are:

(1) the singles energy distributions in each dimension should be identical.

(2) the moments of the total kinetic energy distributions taken as a function of mass should have reflection symmetry about symmetric fission.

(3) the mass distributions, both overall and as a function of total kinetic energy, should have reflection symmetry.

(4) the average mass of mass distributions for predominantly symmetric fission should be half the mass of the fissioning nucleus. This should be true for the overall mass distribution and at each total kinetic energy. (Also all other odd moments would be expected to be 0.)

(5) for mass distributions analyzed in terms of heavy and light peaks all the moments of the light fragment distribution (including the zeroth, the number of events) should agree with those of the heavy fragment for both the overall distributions and at each total kinetic energy.

If deviations from these conditions occur in a random manner, statistical errors are becoming significant. If the deviations occur smoothly, systematic errors are indicated.

Neutron yield will vary with both fragment mass and total kinetic energy; thus data uncorrected or improperly corrected would be expected to show systematic deviations from the above conditions. If one were very confident that other effects were under control, such deviations might possibly be used to obtain information on neutrons.

Item (1) is particularly useful since these distributions depend only on the pulse heights in a single detector; hence deviations are more easily interpreted. Shifts in these distributions of about 1 MeV were not uncommon; the worst case was 2 MeV. It is important to match these distributions, even if this must be done arbitrarily, since a significant dispersion in the resulting total kinetic energy distributions will result if they are not. In these experiments it was found that using the angle of the uncollimated detector rather than the collimated to calculate the center-of-mass correction usually would bring the deviating cases into line. Errors from this source have been included in the estimated systematic errors in the average values.

APPENDIX C

Calculation of ν_T

By combining the experimental mass-total kinetic energy information with values for the energy release in fission, $\langle E_R \rangle$, calculated using a program written by Milton, it was possible to estimate ν_T.[42] A value for $\nu_T(A)$ for each mass split was calculated at the average total kinetic energy for that mass. (Note that this is not necessarily the same as the value of ν_T at a given mass averaged over the total kinetic energy.)

$$\nu_T(A_1) = \frac{\langle E_R(A_1)\rangle + \langle E_x\rangle - \langle E_T(A_1)\rangle - \langle E_\gamma\rangle}{\langle B_n(A_1)\rangle + \langle E_n\rangle} \qquad (C1)$$

$\langle E_T\rangle$ is the average initial total kinetic energy for the mass split, i.e., values prior to neutron emission should be used. As a first approximation to ν_T, ν_T', was estimated using the empirical formula of Leachman.

$$\nu_T' = \nu_{T_0} + 0.12\,\langle E_x\rangle \qquad (C2)$$

where ν_{T_0} is ν_T for spontaneous fission of the compound nucleus and $\langle E_x\rangle$ is the average excitation energy of the fissioning nucleus.[43] Values for ν_{T_0} were taken from Hyde.[49] This value of ν_T' and the observed $\langle E_T^*(A)\rangle$ were used in Eq. (5a) in the text to calculate $\langle E_T(A_1)\rangle$. To be precise one should iterate a second time; however, this was not done since the resulting change in ν_T is about ± 0.3; whereas the final value for ν_T certainly cannot be trusted to better than ± 0.5. $\langle B_n(A_1)\rangle$ is the average neutron binding energy which is also calculated by Milton's program.[42] $\langle E_n\rangle$, the average neutron kinetic energy, was calculated:

$$\langle E_n \rangle = 4/3\ T_m = 4/3 \sqrt{\frac{8x\langle E_x' \rangle}{A}} \qquad (C3)$$

T_m is the mean temperature of the fission fragments.[45] $\langle E_x' \rangle$ is the average value of the total fragment excitation energy which will vary with mass; however, the crude approximation, $\langle E_x' \rangle \approx \langle E_x \rangle$, was used which makes $\langle E_n \rangle$ a constant. A is the total mass of the fissioning nucleus. $\langle E_\gamma \rangle$ is the average total energy carried off by γ rays. It was assumed that this should reflect primarily the properties of the fragments rather than the fissioning nucleus; thus the experimental value of 8.2 MeV measured for Cf^{252} was used.[44] In calculating $\langle E_x \rangle$ an attempt was made to take pre-fission neutron emission into account for the U^{238} and Th^{232} calculations. This was done by using the fission branching ratios given by Thomas, Harvey and Seaborg[42] for U^{238} and by Warhanek, Vandenbosch and Huizenga[41] for Th^{232}. It was assumed that the branching ratios were independent of excitation energy; but the fact that the nucleus has only a few chances to fission at low bombarding energy was considered. In particular the third chance fission for the system Th^{232} + 25.7 MeV was considered to be enhanced since there is a high probability for the de-excited nucleus to end up with an excitation energy between the fission barrier and the neutron binding energy. The fission of Au and Bi was assumed to be all first chance.

The final values for ν_T, obtained by averaging $\nu_T(A)$ over the observed mass distribution, are shown along with values for $\langle E_x \rangle$ in Table CI. One interesting result of the calculations of $\nu_T(A)$ is that for Bi the total kinetic energy is typically about 5 MeV larger than the energy release at all masses and for Au this difference is increased to 15-20 MeV, i.e., $\langle E_T \rangle$ is dropping off slower than $\langle E_R \rangle$ with decreasing x. Thus it appears that as x decreases, more and more of the deformation energy of the fragments at the saddle-point is appearing as total kinetic energy rather than in the form of neutrons.

Table CI. Calculated values for the average total number of neutrons emitted in fission, N_T, and the average excitation energy of the fissioning nucleus $\langle E_x \rangle$

Target	E_α	$\langle E_x \rangle$	ν_T
Au^{197}	70.0	67.2	6.0
Bi^{209}	65.0	54.4	5.1
Th^{232}	21.4	12.9	2.6
Th^{232}	25.7	13.6	3.0
Th^{232}	33.0	17.9	4.1
Th^{232}	65.0	49.7	7.8
U^{238}	25.7	16.2	4.4
U^{238}	33.0	20.7	5.3
U^{238}	65.0	51.7	9.3

APPENDIX D

Derivations of Neutron Correction Formulae

The method used in deriving these corrections is basically that used by Haines[16] and by Terrell.[28] The final equations given here differ somewhat from those of Haines primarily because higher order terms, which have a noticeable effect on the results, are retained.

Let $E_{1\nu}$ and $A_{1\nu}$ be the energy and mass of a fragment after the emission of ν neutrons (i.e., $A_{1\nu} = A_1 - \nu$). For the case of one neutron of energy E_{1n} emitted at an angle of θ_1 in the center-of-mass system of the moving fragment, vector analysis gives:

$$E_{11} = \frac{A_{11}}{A_1} E_1 + \frac{M}{A_{11}} E_{1n} - 2\left(\frac{M E_{1n} E_1}{A_1}\right)^{1/2} \cos\theta_1 \qquad (D1)$$

where M is the neutron mass. Similarly the energies before and after the emission of the νth neutron are related

$$E_{1\nu} = \frac{A_{1\nu}}{A_{1\nu-1}} E_{1\nu-1} + \frac{M}{A_{1\nu}} E_{1\nu n} - 2\left(\frac{M E_{1\nu n} E_{1\nu-1}}{A_{1\nu-1}}\right)^{1/2} \cos\theta_{1\nu} \qquad (D2)$$

where $\theta_{1\nu}$ is the angle at which the νth neutron is emitted. Equation (D2) is the basic equation from which these derivations will proceed.

The standard assumptions of isotropic emission of the neutrons in the center-of-mass system, and the assumption that no correlation between fragment kinetic energy, neutron kinetic energy and angle exists, will be made, e.g.,

$$\langle \cos\theta_{1\nu} \rangle = 0$$
$$\langle \cos^2\theta_{1\nu} \rangle = 1/3$$
$$\langle E_1 E_{1n} \rangle = \langle E_1 \rangle \langle E_{1n} \rangle \text{ etc.}$$

The exact calculation of these corrections requires knowing $\nu_1 (E_T, A_1)$, the average number of neutrons for a given mass and total kinetic energy; however, with the exception of Cf^{252}, such information is not available for any fissioning system. To obtain explicit expressions it is then necessary to assume $\langle \nu_1 f (E_{T1} A_1) \rangle = \langle \nu_1 \rangle \langle f(E_T A_1) \rangle$ where $f(E_T, A_1)$ is any function of mass and/or total kinetic energy. More explicitly, in deriving corrections to the total kinetic energy distributions for a given mass it is necessary to assume that ν_1 is independent of total kinetic energy, and in deriving corrections to the mass distributions for a given total kinetic energy it is necessary to assume that ν_1 is independent of mass. Thus it is inconsistent to allow ν_1 to be a function of mass in the total kinetic energy correction and allow ν_1 to depend on total kinetic energy in the correction to the mass distributions although some information might be obtained on $\langle \nu_1 (A_1) \rangle$ and $\langle \nu_1 (E_T) \rangle$ individually i.e., on the additional averages of $\nu_1 (A_1, E_T)$ over E_T and A_1 respectively.[25,53] Consequently, it was assumed, removing the brackets, that $\nu_1 = \nu_2 = \frac{\nu_T}{2} = \text{const.}$ (ν_T is the total number of neutrons emitted by both fragments.)

1. Correction to the average total kinetic energy for a given mass.

The measured total kinetic energy, E_T^*, is

$$E_T^* = E_{1\nu} + E_{2\nu} \qquad \text{(a)}$$

$$\langle E_T^* \rangle = \langle E_{1\nu} \rangle + \langle E_{2\nu} \rangle \qquad \text{(b)} \qquad \text{(D3)}$$

where the averages are taken with the mass held constant and where ν neutrons are assumed to be emitted from both fragment 1 and fragment 2. Equation (D2) is a recursion relation; and, by successive application, it is possible to express $\langle E_{1\nu} \rangle$ in terms of $\langle E_1 \rangle$. The terms of order M/A_1 which occur are found to be negligible and the final reduction gives

$$\langle E_T^* \rangle = \frac{A_{1\nu}}{A_1} \langle E_1 \rangle + \frac{A_{2\nu}}{A_2} \langle E_2 \rangle = \langle E_T \rangle \left(1 - \frac{\nu A_2}{A_1 A} - \frac{\nu A_1}{A_2 A}\right) \tag{D4}$$

2. Correction to the variance of the total kinetic energy distribution for a given mass.

By squaring and averaging (D3a) and subtracting from the square of (D3b) we obtain, for a constant mass,

$$\mu_2(E_T^*) = \mu_2(E_{1\nu}) + \mu_2(E_{2\nu}) + 2 \{\langle E_{1\nu} E_{2\nu} \rangle - \langle E_{1\nu} \rangle \langle E_{2\nu} \rangle\} \tag{D5}$$

As in section (1) $E_{1\nu}$ may, by successive application of (D2), be expressed in terms of E_1 retaining only terms of order M/A_1. The resulting equation is averaged, than squared and subtracted from the corresponding expression obtained by squaring, then averaging. This gives:

$$N_2(E_{1\nu}) = \left(\frac{A_{1\nu}}{A_1}\right)^2 \mu_2 (E_1) + \frac{4}{3} M \frac{\langle E_1 \rangle \langle E_n \rangle}{A_1} \sum_{i=1}^{\nu} \frac{A_{1\nu}^2}{A_{ii}^2} \tag{D6}$$

Eq. (D6) has also assumed no correlation between the kinetic energies of successive neutrons emitted from the same fragment. Eq. (D6) may

be simplified and expressed in terms of E_T by using:

$$\text{(a)}\quad \mu_2(E_1) = \left(\frac{A_2}{A}\right)^2 \mu_2(E_T) \tag{D7}$$

$$\text{(b)}\quad \langle E_1 \rangle = \frac{A_2}{A} \langle E_T \rangle$$

$$\text{(c)}\quad \sum_{i=1}^{\nu} \frac{A_{1\nu}^2}{A_{1i}^2} \cong \frac{A_{1\nu}^2}{A_1^2} \left(\nu + \frac{(\nu+1)}{A} + \cdots\right)$$

In an identical manner the products in the third term in Eq. (D5) may be evaluated. This result, combined with Eqs. (D6) and (D7), is substituted into Eq. (D5) to give

$$\mu_2(E_T^*) \cong \mu_2(E_T)\left(1 - \frac{\nu A_2}{A_1 A} - \frac{\nu A_1}{A_2 A}\right)^2 + \frac{4\nu}{3} \frac{M}{A} \langle E_T \rangle \langle E_n \rangle \left[\frac{A_1}{A_2} + \frac{A_2}{A_1}\right] + \cdots \tag{D8}$$

where only the 1st order term from (D7c) has been retained. Note that the ν term obtained from (D7c) is dimensionless. The statement that the correction for ν neutrons omitted is just ν times that for 1 neutron is true to first order but not in general. Solving for $\mu_2(E_T)$ gives Eq. (5b) in the main text. For the variance of the overall total kinetic energy distribution averaged over all masses, $\mu_2^1(E_T)$, an analogus equation (although not strictly correct) was used:

$$\mu_2^1(E_T) = \left[\mu_2^1(E_T^*) - \frac{4}{3} \nu_T \frac{M}{A} \langle E_T \rangle \langle E_n \rangle\right] \left(1 - \frac{\nu_T}{A}\right)^{-2}$$

3. Correction to mass variance for a given total kinetic energy.

"Masses" have been calculated from the observed energies by:

$$A_2'' \simeq \frac{E_{1\nu}\, A}{E_{1\nu} + E_{2\nu}} \tag{D9}$$

where the primes are used to distinguish A_2'' from A_2. The difference between A_2 and A_2'' is not large; so that the corrections to the kinetic energy distributions could be calculated holding A_2 constant but applied to distributions for a constant A_2''. The difference E_T^* and E_T is larger, thus the correction for the mass variance calculated along lines of constant E_T^* cannot be assumed to be the same as that calculated along a line of constant E_T i.e., whereas

$$\mu_2(A_2'') = \frac{A^2}{E_T^{*2}}\, \mu_2(E_{i\nu}) \equiv \mu_2^*(A_2)$$

$$\mu_2(A_2) \neq \frac{A^2}{E_T^2}\, \mu_2(E_1) \tag{D10}$$

It will be necessary to carry the calculation of $\mu_2(E_1^*)$ to second order in the small dimensionless parameters ν/A, M/A, $\frac{\langle E_{1\nu}\rangle}{\langle E_T^*\rangle}$, and $\frac{\mu_2(A_2)}{A^2}$. Considerable calculation can be saved if it is recognized that any second order term appearing in $\langle E_{1\nu}\rangle^2$ (which is subtracted from an equivalent term in $\langle E_{1\nu}^2\rangle$) is really third order since the subtraction will introduce a $\mu_2(A_2)/A^2$ term. Thus only second order terms which do not subtract need be considered.

The derivation will only be carried out for mass distributions taken symmetrically rather than distributions analyzed asymmetrically in terms of heavy and light fragment distributions. Thus:

$$\langle \frac{A_1}{A} \rangle = \langle \frac{A_2}{A} \rangle = \frac{1}{2}$$

$$\mu_2(A_1) = \mu_2(A_2) = \langle (\frac{A_1}{A})^2 \rangle - \frac{1}{4} \qquad \text{(D11)}$$

The problem is then to calculate $\mu_2(E_1^*)$ in terms of $\mu_2(A_2)$ holding E_T^* constant. This is done by reducing (D2) until $E_{1\nu}$ is a function of E_1, then writing E_1 as a function of E_T and A_2:

$$E_1 = \frac{A_2}{A} E_T(E_T^*, A_2)$$

where E_T is then written as a function of E_T^* and A_2

$$E_T \cong E_T^* \left[1 + \frac{\nu A_2}{A,A} + \frac{\nu A_1}{A_2 A} - 2 \left(\frac{M E_{1n} A_2}{A E_T^* A_1}\right)^{1/2} \sum_{i=1}^{\nu} \cos\theta_{1i} \right. \qquad \text{(D12)}$$

$$\left. - 2 \left(\frac{M E_{2n} A_1}{A E_T^* A_2}\right)^{1/2} \sum_{j=1}^{\nu} \cos\theta_{2j} \right] + \text{2nd order terms which subtract}$$

$$+ \text{higher order terms}$$

These relations are then inserted into the $E_{1\nu}$ expression and $\langle E_{1\nu} \rangle^2$ and $\langle E_{1\nu}^2 \rangle$ are calculated. The quantity $\langle \frac{A}{A_1} \rangle$ appears frequently in the calculation, and is expanded:

$$\langle \frac{A}{A_1} \rangle \cong 8 \langle (\frac{A_1}{A})^2 \rangle + \text{----} \; .$$

It is also assumed that there is no correlation between the angles of emission of successive neutrons, i.e.,

$$\langle \cos\theta_{1i} \quad \cos\theta_{1j} \rangle = 0 \tag{D14}$$

$$\langle (\sum_{i=1}^{\nu} \cos\theta_{1i})^2 \rangle = \frac{1}{3} \quad \nu$$

(Note that the ν term which arises from this source is dimensionless) Despite all the above simplification a considerable amount of calculation is necessary to give the final result:

$$\mu_2^* (A_2) = \mu_2(A_2) \left(1 - \frac{4\nu}{A}\right) + 2\nu \, MA \, \frac{\langle E_n \rangle}{E_T^*} \tag{D15}$$

Solving for $\mu_2 (A_2)$ and using $\nu_T = 2\nu$, the result given in Eq. (5c) in the text is obtained. Note that to the order of approximation in this derivation (first order in $\frac{\nu}{A}$) the correction for ν neutrons is again ν times the correction for 1 neutron. An analogus equation was used for the overall mass variance, $\mu_2' (A_2)$ averaged over all total kinetic energy:

$$\mu_2' (A_2) = \left[\mu_2'^* (A_2) - \nu_T \, MA \, \frac{\langle E_n \rangle}{\langle E_T^* \rangle} \right] \left(1 - \frac{2\nu_T}{A}\right)^{-1}$$

APPENDIX E

Detector Properties and Operating Conditions

For fission fragment energy measurements it is desirable to have a large electric field in order to maximize the charge collection but, at the same time, have a small depletion layer in order to minimize background. This implies a low resistivity detector. Beyond this the choice of operating conditions for the detectors used in these experiments was strongly influenced by what was thought to be the processes causing the non-proportionality. The following section will be organized in terms of these processes and certain detector parameters associated with them. Analysis of the experiments on the response of semiconductor detectors to fission fragments indicates that at least three different processes can contribute to the non-proportionality between pulse height and energy.[20,46,47,48] All of these processes have been investigated by other workers; the purpose of this section is merely to define those experimental conditions which could conceivably influence the final results in order to make any comparison of experimental results, present and future more significant.

1. Bias (Field) Dependent Incomplete Charge Collection Efficiency

The pulse height from a semiconductor detector is bias dependent even after compensation is made for any change in pulse height due to changes in detector capacitance.[46,47] The pulse height rises sharply at first, then levels off; and, eventually shows a saturation effect. These results imply that a large electric field must be established within the depletion layer in order to obtain the maximum charge collection efficiency. (The "flattening-out" of the pulse height does not, however, mean that the charge collection efficiency is 100%; it only says that we have attained the maximum possible amount of charge from the detector.)

Miller and Gibson have examined several possible origins for this effect and concluded that recombination of electrons and holes on recombination centers is theoretically the most probable mechanism for the incomplete charge collection.[46]

Figure E1 shows sample curves of pulse height vs. $\sqrt{B}/\rho$ which is proportional to the maximum electric field. (B is the detector bias in volts and ρ is the resistivity in ohm-cm.) Pulse height is plotted as V/V_s where V_s is the pulse height at saturation. Figure E1 shows that, even for a given resistivity, other factors besides the electric field determine the position of the plateau. In particular large area detectors seem to require a larger bias to achieve saturation. This is unfortunate since it is difficult to hold a high bias on large area detectors and since such detectors are necessary for many experiments. It has been particularly difficult to achieve saturation with large area surface barriers. The curve for the large 140 ohm-cm. detector is typically what one observes. Success with large area diffused-junction detectors is mainly due to the guard-ring structure which allows a much larger bias to be used than is possible with a simple diode.[49] It appears that minimizing detector area may be just as important as low detector resistivity in choosing a detector for fission fragments.

The necessity to apply a bias which results in a depletion layer several times larger than the range of fission fragments is unfortunate since it increase the pulse height of longer range particles thus creating a larger background.

The pulses from a detector which is not operated on the plateau tend to show a variation in rise times as viewed from the output of a preamplifier. Such a variation is not observed when the detector is operated on the plateau; consequently such observations may constitute a rapid means of correctly adjusting detector bias. Certainly a detector which shows an observable variation in rise time is not on the plateau but whether the converse is true has not been thoroughly investigated.

Unless otherwise specifically specified all measurements were made while operating on the plateau of the pulse-height bias curve.

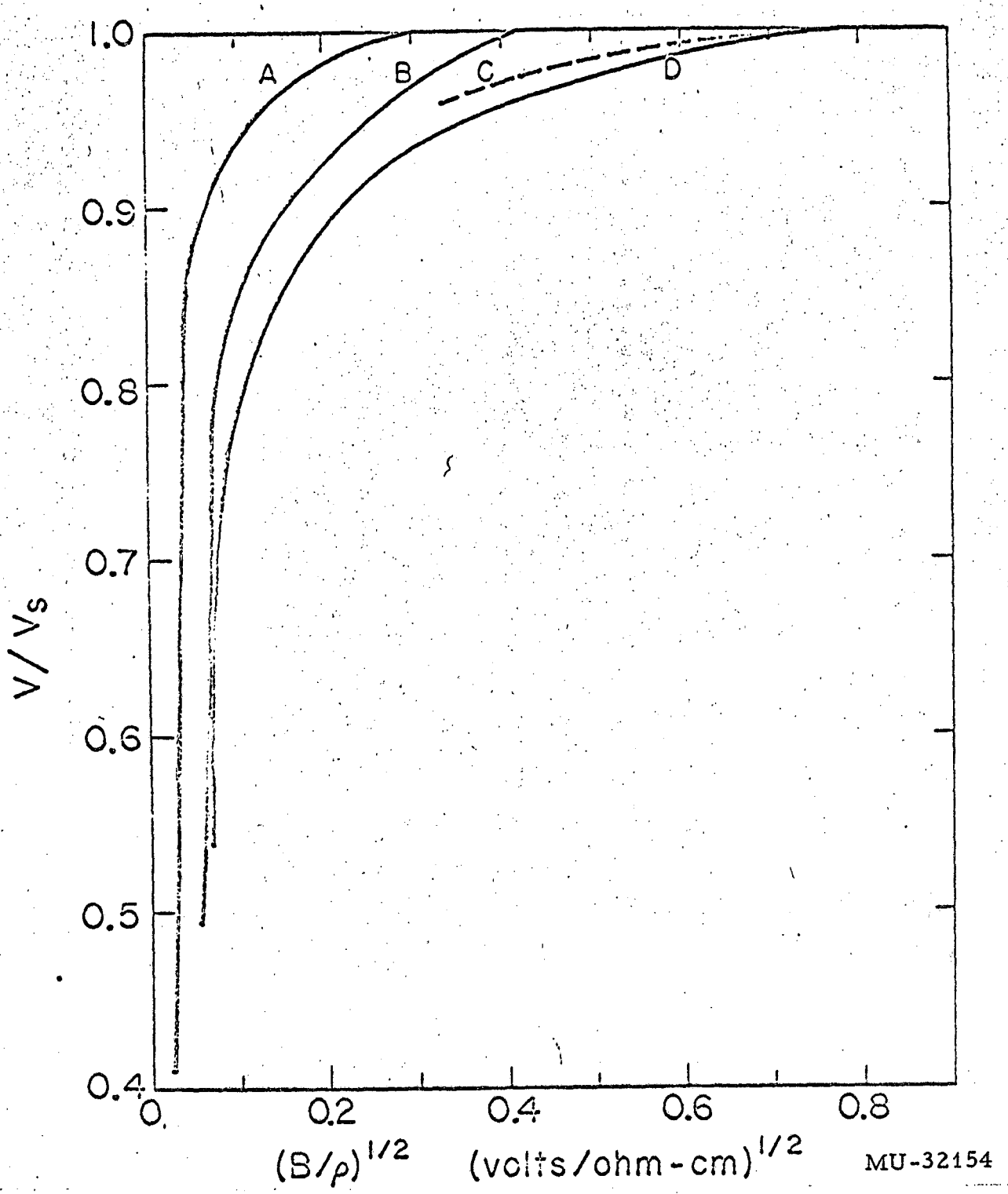

Fig. E1. Plots of pulse height, for Cf^{252} peaks expressed as a fraction of its saturation value, vs $\sqrt{B/\rho}$ which is proportional to the maximum electric field. Heavy and light peaks fall approximately on one curve. (a) 1700 ohm-cm phosphorous-diffused guard-ring. (b) 140 ohm-om surface barrier, 16 mm^2 area. (c) 140 ohm-om surface barrier, 1100 mm^2 area. (d) 200 ohm-om phosphorous-diffused guard-rng. Detectors (a) and (c) not made from same Si. bar.

2. The "Angle Effect"

Experiments with well collimated sources of fission fragments indicate that the detector pulse height is dependent on the incidence angle of the fragments. This is expected since, in a surface barrier detector, the gold front contact is a source of energy loss which will not contribute to the output voltage pulse, and, in a diffused-junction detector, the "window" is just the undepleted region of the P-N junction near the surface. This energy loss, ΔE_a, was obtained by measuring the shift in pulse height for fission fragments entering at 60° compared to those entering normal to the detector surface. The energy loss is given by $\Delta E_a = b\,\Delta c$ where Δc is the shift in pulse height and b is the energy per channel of the electronic system. The value of b will depend upon the choice of calibration scheme, consequently the values of ΔE_a will be ambiguous to this extent. Table E1 gives some measured values for several detectors for the heavy and light peak of Cf^{252}. The values in Table E1 are calculated with a calibration equation based on the two peaks of Cf^{252}. If a slope calculated on the basis of an extrapolated alpha line were used, the values of ΔE would be about 5% lower. The source-detector distance was 4 inches which gave a maximum spread of $\pm 5^\circ$ in the incidence angle for the largest detector used. Peaks were determined using both a local-averaging method devised by F. Plasil[50] and a Caussian-fitting program obtained from the Los Alamos Scientific Laboratory.[51] The resulting energy losses from the two methods agree to within ± 0.2 MeV. The values listed in Table E1 are from the local-averaging method.

It can be argued that the above measurement really does not measure a window thickness since the charge collection efficiency would be expected to be higher when the column of ionization created by the impinging fragment is oriented obliquely to the electric field lines than when the ionization column is parallel to the field lines. From this point of view the measured energy loss, ΔE_a, is the difference between the energy loss due to the window, ΔE_w, and the gain in energy due to oblique incidence, ΔE_0. However, the discussion in Section 1

Table EI. Measured angle effects for several detectors.

Det.	Type	Resistivity (ohm-cm)	Bias (volts)	ΔE_a Light peak	Heavy peak
6	Diffused-junction guard ring	200	100	$2.2^{+1.0}_{-0.2}$	$2.6^{+1.0}_{-0.2}$
5	Diffused-junction guard ring	200	40*	2.1 ± 0.3	2.4 ± 0.3
2	Diffused-junction guard ring	1700	100	2.3 ± 0.2	2.1 ± 0.2
1	Surface barrier ORTEC	300	100	0.2 ± 0.2	0.6 ± 0.2
2	Surface barrier ORTEC	300	100	0.3 ± 0.2	0.6 ± 0.2

*Not operated on plateau of pulse-height bias curve.

can be taken to mean that recombination (or any other effect which has its origin in the shielding of the center of the ionization column from the electric field) is expected to be field dependent; thus the independence of pulse height and bias is to be taken as an indication that such effects have been eliminated. However, the data in Table E1 are not consistent with these ideas because what little is known of fission fragment range-energy relations indicates that the light peak of Cf^{252} will lose more energy in a thin absorber than the heavy peak.[15] This qualitative behavior has been observed many times in measurements of target and backing foil thicknesses. With one exception, the energy losses for the heavy peak are larger than those for the light peak. This suggests that ΔE_0 for the light peak is larger than that for the heavy peak. Since very little is understood about recombination effects, there is no definite prediction as to how ΔE_0 should depend on energy and mass. The above results are reasonable if ΔE_0 is assumed to be an increasing function of the maximum ionization density (i.e., maximum dE/dx). Note that these results do not contradict the observation that the heavy peak is more displaced from an alpha calibration line since there is a third contribution to this deviation which is yet to be discussed. From this point of view the smaller values of ΔE_a for the surface barriers can either be due to a smaller ΔE_w or a larger ΔE_0. ΔE_w was expected to be larger for the diffused junction detectors than for the surface barriers since the diffusions were carried out at 900°C. for 1 hour, which is a relatively long exposure. However, the differences in the ΔE_a values are larger than was expected which suggests that ΔE_0 may be larger for the surface barriers.

Although these results suggest that some sort of field-independent recombination effect may exist, too few data are presented here for any definite conclusion. In particular better knowledge of fission-fragment range-energy relations may prove the above statements invalid; further a small positive slope in the pulse-height bias curve in the region where the measurements were made cannot be ruled out. A more complete study of this effect as a function of bias, resistivity, detector size,

fabrication technique, etc., which is outside the scope of this work, would be more definitive and quite interesting.

3. Residual Pulse Height Defect

The discussion in Sections 1 and 2 indicate that even if a detector were operated on the plateau of the pulse-height bias curve and the existence of a window were quantitatively taken into consideration, the detector pulse height would still be less than expected from an extrapolated alpha line. This resulting deviation, δ, has been called, for lack of a better name, the "residual pulse height defect."

$$\delta = E_f - \Delta E_w - b_\alpha V_f$$

where E_f = true fission fragment energy

ΔE_w = energy loss in window

b_α = slope of extrapolated alpha calibration line

V_f = fission fragment pulse height

Since the measurements in Section 2 cannot be unambiguously identified with ΔE_w, it is not possible to get quantitative values for δ. However, the measured ΔE_a is a lower limit for ΔE_w; consequently some upper limits for δ, δ_{max}, can be calculated using ΔE_a in place of ΔE_w in the above equation. These are shown in Table EII for the heavy and light peaks of Cf^{252}.

The experiments of Schmitt et al.[20] nicely illustrate this effect. If an "angle correction" is made on the curves shown in Fig. 2, the Br^{79-81} line then coincides with the alpha line and the I^{127} line, which previously had a slightly positive slope with respect to the alpha line, is now parallel to it but still displaced. Qualitatively similar results were obtained with a large number of detectors. The magnitudes of those displacements are consistent with the δ_{max} values given in Table EII although the latter are somewhat larger.

Table EII. Values of δ_{max} for several detectors for Cf^{252}.

Det.	Type	Resistivity (ohm-cm)	Bias (volts)	δ_{max} (MeV) Heavy	Light
6	Diffused junction guard ring	200	100	5.9	3.6
5	Diffused junction guard ring	200	40*	7.0	4.2
2	Diffused junction guard ring	1700	100	5.1	2.5
1	Surface barrier ORTEC	300	100	8.5	5.3
2	Surface barrier ORTEC	300	100	8.9	6.2

*Not operated on plateau of pulse-height bias curve.

These results suggest that the residual pulse height defect is a function of mass (and/or charge) only. A possible mechanism for this effect would be the non-ionizing nuclear collisions that are the energy loss mechanism for fission fragments at the end of their range when they become neutrally charged.[52] The resulting energy loss would depend only on some critical velocity at which the fragment became neutral which, in turn, would depend only on the charge and mass of the fragment and the stopping material and would be independent of the initial fragment energy. Detector type, resistivity, and fabrication technique would then only slightly influence the magnitude of the effect, if at all. However, in view of the discussion in Section 2, it is still not possible to rule out recombination-type effects.

4. Conditions Associated with Detector Resolution

The requirements for the resolution of a semiconductor detector for fission work need not be strict. Detectors that are unsuitable for alpha particle spectroscopy may make excellent fission detectors. The work of Schmitt et al.[20] has shown that, for monoenergetic Br^{79-81} and I^{127} ions, the full width at half maximum is about 1 MeV. In the present work detector resolution was judged primarily by the peak-to-peak and the light peak-to-valley ratios of the Cf^{252} pulse height spectrum. The values of these ratios for the singles energy spectrum measured by time of flight are 1.37 and 3.11 respectively;[18] however, these values refer to the energy spectrum prior to neutron emission, whereas a semiconductor detector observes the fragments after neutron emission. When a rough correction is made for the change in shape of the spectrum due to neutron emission, one obtains 1.34 and 2.70 which are the appropriate values for comparison with a detector pulse height spectrum. In practice it is not uncommon to find peak-to-valley ratios of 2.70 or higher; however, peak-to-peak ratios usually run about 1.26 to 1.31. It should be emphasized that only approximate agreement with the standard values is expected in view of the non-proportionality.

In some cases a poor detector may be discovered by watching the noise level. These detectors show sudden bursts of noise lasting up to several seconds. The noise level during these bursts is several times the quiescent noise level which, in some cases, is quite low. Such detectors usually give a poor pulse height spectrum; however, observing the noise is much less time-consuming. The bursts are probably associated with microscopic breakdown or "channeling" at the detector surface.[54] Channeling is also indicated by a sloping or "ohmic" current-bias curve instead of the flat curve expected from a diode. This behavior has not been observed in guard ring detectors.

In order to obtain the maximum resolution, the detectors were always operated with their edges covered and in darkness. It was observed that for a certain type of fluorescent lighting it was possible to have two completely-resolved fission spectra registering simultaneously on the pulse height analyzer due to 60-cycle pickup from the lights. Care was also taken never to expose the detector to air with an applied bias.

APPENDIX F

The Possibility of an Exact Solution to the Detector Calibration Problem.

This could be done by a simultaneous measurement of v_1, v_2, V_1, V_2, where v is a velocity and V a pulse height. The velocity measurements themselves are sufficient to calculate the masses and energies of the fragments; thus the following transformation can be performed using known values for $\nu_1 (A_1, E_T)$ for Cf^{252}

$$N(v_1, v_2, V_1, V_2) \rightarrow N_1 (E_1, A_1', V_1) \text{ and } N_2 (E_2 A_2', V_2)$$

where the N refer to numbers of events, and the A' refer to the masses after neutron emission. N_1 and N_2 are exactly what is needed to establish the pulse-height energy relation, since by averaging over V for a given E and A: $V_1 (E_1, A_1)$ and $V_2 (E_2, A_2)$ may be calculated.

REFERENCES

1. S. Cohen and W. J. Swiatecki, The Deformation Energy of a Charged Drop: Part V: Results of Electronic Computer Studies, UCRL-10450 August 1962.
2. J. R. Nix, Estimates of Fission-Fragment Kinetic-Energy Distributions on the Basis of the Liquid-Drop Model, UCRL-10695, April 1963.
3. S. Cohen and W. J. Swiatecki, Ann. Phys. 19, 67 (1962).
4. Reference here is to The Statistical Theory of Fission. See, for example, P. Fong, Phys. Rev. 102, 434 (1956) and Bull. Am. Phys. Soc. II, 8, 385 (1963).
5. E. K. Hyde, A Review of Nuclear Fission. Part II. Fission Phenomena at Moderate and High Energy, UCRL-9065, February 1960.
6. S. Katcoff, J. A. Miskel, and C. W. Stanley, Phys. Rev. 74, 631 (1948).
7. J. C. D. Milton and J. S. Fraser, Phys. Rev. 111, 877, 1958.
8. S. L. Whetstone, Coincident Time-of-Flight Measurements of the Velocities of Fission Fragments from Changed-Particle-Induced Fission (to be published).
9. H. C. Britt, H. E. Wegner, and J. Gursky, Phys. Rev. 129, 2239 (1963).
10. J. C. D. Milton and J. S. Fraser, Can. J. Phys. 40, 1626, 1962.
11. T. Sikkeland, E. L. Haines, and V. E. Viola, Phys. Rev. 125, 1350 (1962).
12. William W. Goldworthy, Model VI Linear Amplifier System and Preamplifier, UCRL-9816, August 1961.
13. Lawrence Radiation Laboratory Counting Handbook, UCRL-3307 Rev., January 1959, Files CC3 and CC10.
14. M. Nakamura and G. S. Simonof, A Multiporameter Pulse-Height Recording System, UCRL-10874, April 1963.
15. J. M. Alexander and M. F. Gazdik, Phys. Rev. 120, 874 (1960).
16. E. L. Haines, Mass-Energy Relations on the Fission of Highly Excited Heavy Nuclei, (Ph.D. Thesis), UCRL-10342, June 1962.

17. T. D. Thomas, and W. M. Gibson, Transformations of Two-Dimensional Data, Princeton-Pennsylvania Accelerator, PPAD 473E, October 1962.
18. S. L. Whetstone, Phys. Rev. 131, 1232 (1963).
19. J. C. D. Milton and J. S. Fraser, Atomic Energy of Canada, Ltd, private communication.
20. H. W. Schmitt, F. J. Walter, J. H. Neiler, C. D. Moak, W. M. Gibson, and T. D. Thomas, Response of Silicon Solid-State Detectors to Heavy Ions and Fission Fragments, in Physics Division Annual Report, ORNL-3425, p. 130.
21. H. C. Britt, H. E. Wegner, and S. L. Whetstone (to be published in Nucl. Instr. and Meth.).
22. J. Unik, G. L. Bate, and J. R. Huizenga, Bull. Am. Phys. Soc., Series II, 7, 303 (1962)
23. R. Brandt, Spontaneous Fission of Some Heavy Isotopes, (Ph.D. Thesis) UCRL-10481 September 1962.
24. V. E. Viola, Jr. and T. Sikkeland, Phys. Rev. 130, 2044, 1963.
25. H. C. Britt and S. L. Whetstone, (to be published).
26. H. R. Bowman, S. G. Thompson, J. C. D. Milton, and W. J. Swiatecki, Phys. Rev. 126, 2120 (1962).
27. H. R. Bowman, J. C. D. Milton, S. G. Thompson, and W. J. Swiatecki, Phys. Rev. 129, 2133 (1963).
28. J. Terrell, Phys. Rev. 127, 880 (1962).
29. J. R. Nix, Lawrence Radiation Laboratory, private communication.
30. A. Turkevich and J. B. Niday, Phys. Rev. 84, 52 (1951).
31. A. W. Fairhall, R. C. Jensen, and E.F. Neuzil in Proceedings of the Second United Nations International Conference on the Peaceful Uses of Atomic Energy (United Nations, Geneva, 1958) Vol. 15, p. 452.
32. H. B. Levy, H. G. Hicks, W. E. Nervik, P. C. Stevenson, J. B. Niday and J. C. Armstrong, Jr., Phys. Rev. 124, 544 (1961) and H. G. Hicks, H. B. Levy, W. E. Nervik, P. C. Stevenson, J. B. Niday, and J. C. Armstrong, Jr., Phys. Rev. 126, 700 (1962).

33. G. E. Gordon, Massachusetts Institute of Technology, (unpublished work).

34. R. Vandenbosch, (to be published).

35. R. Vandenbosch and J. R. Huizenga, Phys. Rev. 127, 212 (1962).

36. R. Vandenbosch, H. Warhanek, and J. R. Huizenga, Phys. Rev. 124, 846 (1961).

37. T. D. Thomas, B. G. Harvey, and G. T. Seaborg, in Proceedings of the Second United Nation International Conference on the Peaceful Uses of Atomic Energy (United Nations, Geneva, 1958), Vol. 15. p. 292.

38. J. M. Alexander, M. F. Gazdik and S. Wasif, Kinetic Energy Release in 23 MeV Deuteron Fission of U^{238}, UCRL-10193, May 1961.

39. E. L. Haines and S. G. Thompson, (to be published in Phys. Rev.).

40. P. B. Price and R. M. Walker, Phys. Letters, 3, 113 (1962).

41. F. Plasil, Lawrence Radiation Laboratory, to be published.

42. J. C. D. Milton, Fission Energy Tables and an Application to Nuclear Charge Division, UCRL-9883 Rev. January.

43. R. B. Leachman, in Proceedings of the Second International Conference on the Peaceful Uses of Atomic Energy, (United Nations, Geneva, 1958) Vol. 15 p. 229.

44. E. K. Hyde, A Review of Nuclear Fission. Part I. Fission Phenomena at Low Energy, UCRL-9036 Rev., April 1962.

45. J. M. B. Lang and K. J. Le Couteur, Proc. Phys. Soc. (London) A 65, 592 (1954).

46. G. L. Miller and W. M. Gibson, Charge Collection in Semiconductor Particle Detectors, in Nuclear Electronics, Vol. I, International Atomic Energy Agency, (Vienna, 1962), p. 477.

47. H. C. Britt and H. E. Wegner. Rev. Sci. Inst. 34, 274 (1963).

48. J. Colard and J. Gal, Nucl. Inst. and Meth. 16, 195 (1962).

49. F. S. Goulding and W. L. Hansen, Leakage Currant in Semiconductor Radiation Detectors and Its Influence on EnergyResolution Characteristics, UCRL-9436, November 1960.

50. F. Plasil, Lawrence Radiation Laboratory, private communication.

51. P. McWilliams, W. S. Hall, and H. E. Wegner, Rev. Sci. Inst. 33, 70 (1962).

52. J. Lindhard and V. Nielsen, Phys. Letters 2, 209 (1962).

53. J. A. McHugh, Mass-Spectrometric Study of Fission from the U^{236} Compound Nucleus at Moderate Excitations, (Ph.D. Thesis), UCRL-10673, February 1963.

54. W. M. Gibson, Bell Telephone Laboratories, private communication.